BAŞKENT UNIVERSITY
INSTITUTE OF SCIENCE
DEPARTMENT OF MOLECULAR BIOLOGY AND GENETICS
MASTER OF SCIENCE IN
MOLECULAR BIOLOGY AND GENETICS

COLLAGEN/KERATIN/ALGINATE BASED HYDROGEL DELIVERING MICRO-RNA TO MODULATE THE ANGIOGENIC PROPERTIES ON HUMAN UMBILICAL VEIN ENDOTHELIAL CELLS (HUVECs)

BY

YASEMİN PAZARÇEVİREN

MASTER OF SCIENCE THESIS

ANKARA-2024

BAŞKENT UNIVERSITY
INSTITUTE OF SCIENCE
DEPARTMENT OF MOLECULAR BIOLOGY AND GENETICS
MASTER OF SCIENCE IN
MOLECULAR BIOLOGY AND GENETICS

COLLAGEN/KERATIN/ALGINATE BASED HYDROGEL DELIVERING MICRO-RNA TO MODULATE THE ANGIOGENIC PROPERTIES ON HUMAN UMBILICAL VEIN ENDOTHELIAL CELLS (HUVECs)

BY

YASEMİN PAZARÇEVİREN

MASTER OF SCIENCE THESIS

ADVISOR
ASSIST. PROF. DR. ÖZGE ERDEMLİ

CO-ADVISOR
ASSIST. PROF. DR. BAŞAK KANDEMİR

ANKARA-2024

BAŞKENT UNIVERSITY
INSTITUTE OF SCIENCE

This study, which was prepared by Yasemin PAZARÇEVİREN, for the program of Master of Science with Thesis (English), has been approved in partial fulfillment of the requirements for the degree of MASTER OF SCIENCE in MOLECULAR BIOLOGY AND GENETICS Department by the following committee.

Date of Thesis Defense: 30/01/ 2024

Thesis Title: Collagen/Keratin/Alginate-Based Hydrogel Delivering Micro-RNA to Modulate the Angiogenic Properties on Human Umbilical Vein Endothelial Cells (HUVECs)

Examining Committee Members	**Signature**
Assist. Prof. Dr. Bengi YILMAZ, University of Health Sciences	……..
Assist. Prof. Dr. Özge ERDEMLİ, Başkent University	……..
Assist. Prof. Dr. Aliye Ezgi GÜLEÇ TAŞKIRAN, Başkent University	……..

APPROVAL
Prof. Dr. Ömer Faruk ELALDI
Director, Institute of Science
Date: … / … / ……..

BAŞKENT UNIVERSITY

INSTITUTE OF SCIENCE

YÜKSEK LİSANS / DOKTORA TEZ ÇALIŞMASI ORİJİNALLİK RAPORU

Tarih: 18 / 03 / 2024

Öğrencinin Adı, Soyadı : Yasemin PAZARÇEVİREN

Öğrencinin Numarası : 22020074

Anabilim Dalı : Moleküler Biyoloji ve Genetik

Programı : Moleküler Biyoloji ve Genetik Tezli Yüksek Lisans (İngilizce)

Danışmanın Unvanı/Adı, Soyadı : Dr. Öğr. Üyesi Özge Erdemli

Tez Başlığı : Collagen/Keratin/Alginate-Based Hydrogel Delivering Micro-RNA to Modulate the Angiogenic Properties on Human Umbilical Vein Endothelial Cells (HUVECs)

Yukarıda başlığı belirtilen Yüksek Lisans tez çalışmamın; Giriş, Ana Bölümler ve Sonuç Bölümünden oluşan, toplam 74 sayfalık kısmına ilişkin, 18 / 03 / 2024 tarihinde tez danışmanım tarafından Turnitin adlı intihal tespit programından aşağıda belirtilen filtrelemeler uygulanarak alınmış olan orijinallik raporuna göre, tezimin benzerlik oranı % 10'dur. Uygulanan filtrelemeler:

1. Kaynakça hariç
2. Alıntılar hariç
3. Beş (5) kelimeden daha az örtüşme içeren metin kısımları hariç,

"Başkent Üniversitesi Enstitüleri Tez Çalışması Orijinallik Raporu Alınması ve Kullanılması Usul ve Esaslarını" inceledim ve bu uygulama esaslarında belirtilen azami benzerlik oranlarına tez çalışmamın herhangi bir intihal içermediğini; aksinin tespit edileceği muhtemel durumda doğabilecek her türlü hukuki sorumluluğu kabul ettiğimi ve yukarıda vermiş olduğum bilgilerin doğru olduğunu beyan ederim.

Öğrenci İmzası:…….

ONAY

Tarih: 18 / 03 / 2024

Öğrenci Danışmanı Unvan, Adı, Soyadı, İmza:

Dr. Özge ERDEMLİ

…….

To my beloved family and precious friends

Yasemin PAZARÇEVİREN

Ankara – 2024

ACKNOWLEDGEMENTS

I would like to express my deepest gratitude to my respected supervisor Dr. Özge Erdemli and co-advisor Dr. Başak Kandemir for their guidance, support, patience, criticism, and valuable suggestions during my study and in preparing my thesis.

During my thesis study, some valuable people supported me and gave me insights throughout my study. To those, Prof. Dr. Ayşen Tezcaner, Prof. Dr. Özlem Darcansoy, Dr. Bengi Yılmaz, Dr. Aydın Tahmasebifar.

The most special and sincerest appreciation and thankfulness belongs to my loved husband, Ahmet Engin Pazarçeviren for his support, assistance, and valuable contributions, for being an excellent partner in every aspect, my light, and my role model both as an amazing human and a dedicated scientist.

I must speak of the enormous support and love that I received from my family and my dearest parents, Fatma Esin Özgül and Ahmet Tekin Özgül.
I am happy to have wonderful beloved friends, Sema Akbaba, Milad Fathi, Gülhan Işık Ertop, Kağan Ertop, Mustafa Bahadır Güner, Hilal Üstüner, Eren Küçük. Ekin Varlı, Ali Cemil Şen.

I also wish to mention my dear friends and all my lab-mates Öykü Irmak Dikkatli, Efe Mıhçı, Rümeysa Işıl Özdemir, Buse Öncel, Batuhan Ünal, Oğuzhan Yaprak, Kaan Yıldırım for their loving, fun, supportive, collaborative friendship and fellowship.
I would like to thank Başkent University and TENMAK-BOREN for the support and facilities that they have provided during my study.

ABSTRACT

Yasemin PAZARÇEVİREN

COLLAGEN/KERATIN/ALGINATE BASED HYDROGEL DELIVERING MICRO-RNA TO MODULATE THE ANGIOGENIC PROPERTIES ON HUMAN UMBILICAL VEIN ENDOTHELIAL CELLS (HUVECs)

Başkent University Institute of Science

Department of Molecular Biology and Genetics

2024

In the last years, the integration of genome editors and regulatory ribonucleic acids (RNAs) with biomaterials has gained attention, especially in the field of therapeutics and personalized medicine. This thesis study aimed to develop a functional, biocompatible, and micro-RNA carrying hydrogel based on collagen, keratin, and alginate for the modulation of angiogenesis. For this purpose, firstly keratin and collagen were isolated from waste human hair and bovine Achilles tendon, respectively. For both isolated proteins, all the characteristic peaks of keratin and collagen were observed by Fourier transform infrared spectroscopy (FT-IR). Two major bands were observed in human hair keratin samples at approximately 45 kDa and 63 kDa, while collagen samples gave four bands at around 300 kDa, 245 kDa, 135 kDa, and 100 kDa on SDS-PAGE. Col/Ker/Alg hydrogels with different ratios were prepared and their chemical, microstructural properties, percent porosity, *in vitro* hydrolytic degradation behavior, water uptake properties, *in vitro* protein release behaviors, and biocompatibility were characterized to optimize the hydrogels for the preparation of PEI:miR-21 plasmid complex loaded hydrogels for subsequent investigations. The hydrogel group consisting of 1% w/v of each component showed the highest swelling rate and porosity percentage (80.89%), the lowest degradation rate (only 15.19% at the end of 21 days), and better biocompatibility. The miR-21 expression vector was loaded onto this hydrogel group to be used as a gene-activated matrix (GAM) to observe the effects on HUVECs. To observe the effects of the complex and hydrogels on HUVECs, fluorescent microscopy, confocal laser scanning microscopy (CSLM), and RT-qPCR for gene expression analysis were conducted. miR-21, pro-angiogenic factor *VEGFA*, direct targets of miR-21 and *PTEN*, *SPRY1*, and *SPRY2 we*re examined. *In vitro* studies revealed that hydrogels and over-expression of miR-21 were not toxic on cells and provided a successful transient

transfection of HUVECs by observing green fluorescent protein (GFP) reporter. The migration of HUVECs into the hydrogel and the transfection was observed by CSLM and the GFP fluorescence signal increased from day 1 to day 4. Gene expression results for miR-21 were higher in the transfected groups (TCP control and PEI: plasmid loaded hydrogels) as expected. *PTEN*, *SPRY1*, and *SPRY2* gene expression decreased in transfected groups since they are the direct targets of miR-21, yet *VEGFA* gene expression increased in those groups compared to the negative controls. In addition, regular tubular sprouting as seen in angiogenesis was not observed in any experimental groups.

KEYWORDS: Collagen, Keratin, Hydrogel, miR-21, HUVEC

ÖZET

Yasemin PAZARÇEVİREN

İNSAN GÖBEK DAMARI ENDOTTEL HÜCRELERİ (HUVEC'ler) ÜZERİNDEKİ ANJİYOJENİK ÖZELLİKLERİ MODÜLE ETMEK İÇİN MİKRO-RNA TAŞIYAN KOLAJEN/KERATİN/ALJİNAT BAZLI HİDROJEL

Başkent Üniversitesi Fen Bilimleri Enstitüsü

Moleküler Biyoloji ve Genetik Anabilim Dalı

2024

Son yıllarda genom düzenleyicilerin ve düzenleyici ribonükleik asitlerin (RNA'ların) biyomateryallerle entegrasyonu, özellikle terapötik ve kişiselleştirilmiş tıp alanında ilgi görmüştür. Bu tez çalışmasının amacı, anjiyogenezin modülasyonu için kolajen, keratin ve aljinat bazlı, fonksiyonel, biyouyumlu ve mikro-RNA taşıyan bir hidrojel geliştirmektir. Bu amaçla öncelikle atık insan saçı örneklerinden keratin ve sığır Aşil tendonundan kolajen izole edildi. Her iki izole edilmiş protein için, keratin ve kolajenin tüm karakteristik zirveleri Fourier dönüşümü kızılötesi spektroskopisi (FT-IR) ile gözlemlendi. İnsan saçı keratin numunelerinde yaklaşık 45 kDa ve 63 kDa'da iki ana bant gözlenirken, kolajen numuneleri SDS-PAGE'de yaklaşık 300 kDa, 245 kDa, 135 kDa ve 100 kDa'da dört bant verdi. Farklı oranlarda Col/Ker/Alg hidrojelleri hazırlanmış ve bunların kimyasal, mikroyapısal özellikleri, gözeneklilik yüzdesi, *in vitro* hidrolitik bozunma davranışı, şişme özellikleri*, in vitro* protein salım davranışları ve biyouyumluluğu, hidrojellerin PEI:plasmid yüklenmesine hazırlanması için optimize edilmesi amacıyla sonraki araştırmalar için karakterize edilmiştir. Her bileşenden ağ/hac olarak %1'inden oluşan hidrojel grubu en yüksek şişme oranı ve gözeneklilik yüzdesini (%80,89), en düşük bozunma oranını (21 gün sonunda sadece %15,19) ve daha iyi biyouyumluluğu gösterdi. miR-21 ekspresyon vektörü, HUVEC'ler üzerindeki etkileri gözlemlenmek amacıyla genle aktifleştirilen bir matris (GAM) olarak kullanılmak üzere bu hidrojel grubuna yüklendi. Kompleksin ve hidrojellerin HUVEC'ler üzerindeki etkilerini gözlemlemek için floresan mikroskobu, konfokal lazer tarama mikroskobu, gen ekspresyonu analizi için RT-qPCR gerçekleştirildi. miR-21, pro-anjiyogenik faktör *VEGFA*, miR-2'in doğrudan hedefleri, *PTEN*, *SPRY1* ve *SPRY2* [30] ifadeleri incelenmiştir. *In vitro* çalışmalar, hidrojellerin ve miR-21'in aşırı ekspresyonunun hücreler üzerinde toksik olmadığını ve yeşil

floresan protein (GFP) raportörünü gözlemleyerek HUVEC'lerin başarılı bir geçici transfeksiyonunu sağladığını ortaya çıkardı. HUVEC'lerin hidrojele göçü ve transfeksiyonu CSLM ile gözlemlendi ve GFP floresans sinyali 1. günden 4. güne arttı. miR-21 için gen ifadesi sonuçları transfekte edilmiş gruplarda (TCP kontrolü ve PEI:plazmid yüklü hidrojeller) daha yüksekti. *PTEN*, *SPRY1* ve *SPRY2* gen ekspresyonu transfekte edilmiş gruplarda miR-21'in doğrudan hedefleri oldukları için azaldı, ancak *VEGFA* gen ekspresyonu bu gruplarda negatif kontrollere göre arttı. Ayrıca hiçbir deney grubunda anjiyogenezde görüldüğü gibi düzenli tübüler filizlenme gözlenmedi.

ANAHTAR KELİMELER: Kolajen, Keratin, Hidrojel, miR-21, HUVEC

TABLE OF CONTENTS

LIST OF TABLES

Page

LIST OF FIGURES

Page

LIST OF SYMBOLS AND ABBREVIATIONS

3D	Three Dimensional
APS	Ammonium persulfate
BCA	Bicinchoninic acid assay
C/K/A	Collagen/Keratin/Alginate
CRISPR	Clustered Regularly Interspaced Short Palindromic Repeats
CSLM	Confocal Scanning Laser Microscopy
DAPI	4′,6-diamidino-2-phenylindole
DMEM	Dulbecco's Modified Eagle Medium
ECM	Extracellular Matrix
EDC	1-Ethyl-3-(3-dimethyl aminopropyl)carbodiimide
EDTA	Ethylenediamine tetraacetic acid
FBS	Fetal Bovine Serum
FT-IR	Fourier Transform Infrared
GFP	Green Fluorescent Protein
HUVEC	Human Umbilical Vein Endothelial Cell
KBr Disc	Potassium bromide Disc
miRNA	micro RNA
miR-21	micro RNA 21
NHS	N-Hydroxysuccinimide
PBS	Phosphate Buffered Saline
RT	Room Temperature
SDS-PAGE	Sodium Dodecyl Sulfate Polyacrylamide Gel Electrophoresis
SEM	Scanning Electron Microscopy
TCP	Tissue Culture Plate
TEMED	N, N, N', N'-Tetra methyl ethylene diamine
UV	Ultraviolet

1. INTRODUCTION

Aging, diseases, traumas, and congenital defects are widespread main reasons that impair organs and tissues, leading to their removal or causing patient discomfort, and even mortality. In recent years, important developments have been made in transplantation techniques, presenting promising solutions for addressing compromised tissue and organs. However, despite the initial success of transplants, complications including inflammation and necrosis have been encountered, frequently attributed to rejection by the immune system. These limitations led the medical community to explore alternative approaches, ultimately giving rise to the field of regenerative medicine.

Regenerative medicine is defined as the utilization of stem and mature cells, biomaterials, and cellular signals to facilitate tissue healing, renewal, and substitution [1]. Cell-based therapies, mostly used as an approach to regenerative medicine, encounter challenges such as low survival rates, issues with differentiation and cellular aging, as well as limited integration with target tissues, as indicated in the literature [2]. These identified shortcomings point out the importance of tissue engineering applications.

Tissue engineering has undergone significant advancements in recent years, driven by improvements in cellular programming [3], advanced biomaterials [4], genome editing technologies [5, 6], and/or nanoparticle delivery systems [7]. Tissue-engineered scaffolds have demonstrated significant potential both in clinics and in basic scientific research related to tissue regeneration. In tissue engineering, tissue scaffolds are constructed to mimic the native extracellular matrix (ECM) environment which induces attachment, proliferation, growth, and differentiation of cells. A diverse range of biomaterials, including natural and synthetic polymers, ceramics, metals, and composites, have been utilized for the fabrication of tissue scaffolds to mimic native tissues [8]. The designing and producing of tissue scaffolds possessing ideal properties like biocompatibility, biodegradability, and mechanical and surface characteristics is important for their effective usage in tissue engineering applications [9]. Tissue scaffolds with the ability to enhance cellular behaviors such as adhesion, proliferation, and migration are crucial for tissue engineering applications, both *in*

vitro and *in vivo*. Furthermore, to prevent a significant inflammatory response that could potentially lead to the deterioration of the healing process or lead to rejection upon transplantation, it is imperative for the tissue scaffold to seamlessly integrate with the host tissue without eliciting any immunological reactions [10]. Another crucial property of biomaterials used in the production of tissue scaffolds is bioactivity, which serves as a mechanism for guaranteeing the attachment, proliferation, migration, and differentiation of cells in the neighboring tissues through interaction with biomaterials.

In addition to biocompatibility, biodegradability, bioactivity, and mechanical and surface characteristics, timely and adequate vascularization is also essential for successful tissue formation and healing. In tissue engineering applications, vascularization strategies have been investigated to enhance the viability of engineered scaffolds and facilitate their integration and vascularization after implantation [11-13]. Considering vascularization studies essential in bone tissue engineering, skin tissue engineering, and cancer research, human umbilical vein endothelial cells (HUVECs) play a pivotal role. As they represent terminally differentiated cells, HUVECs retain the capability to proliferate and modify the properties of their niche, including altering the ECM [14]. Therefore, they are employed in numerous *in vitro* studies to define cell-cell interactions.

In tissue engineering, both *in vivo* animal models and *in vitro* cell culture models are employed in clinical and basic research to comprehend the biological mechanisms underlying natural tissue development. Although *in vivo* studies help understand tissue development and disease mechanisms and are useful in developing therapeutic approaches, human disease models cannot be fully replicated due to the use of animals. In addition, the use of *in vivo* models is quite limited due to ethical issues. *In vitro,* cell culture studies provide cost-effective experiments, accelerate experimental timelines, and offer broad applicability in scientific investigations compared to *in vivo* animal studies. Cell culture studies using eukaryotic cells are also frequently used to examine basic cell biology and tissue morphology, to establish *in vitro* two-dimensional (2D) models mimicking biological mechanisms involved in natural tissue development or disease processes, or to evaluate the toxicity of novel drugs or bioactive compounds. While *in vitro* 2D studies offer several advantages such as simplicity, cost-effective maintenance of cell cultures, and suitability for conducting functional tests, cell-cell and cell-extracellular matrix interactions are not

accurately represented in 2D cultures and they are limited in their ability to mimic the natural three dimensional (3D) structure of tissues [15]. Due to the numerous drawbacks associated with 2D cell culture studies, there has been extensive research into the development of 3D cell culture models, with the goal of more accurately mimicking the complex 3D *in vivo* environment [16]. 3D cell culture has demonstrated advancements in various research areas including morphology, cell number monitoring, proliferation, response to stimuli, differentiation, drug metabolism, and protein synthesis, and has versatile applications encompassing the investigation of various disease conditions, stem cell research, drug discovery, and tissue engineering.

In some 3D cell culture studies, cells are combined with hydrogels with a porous structure consisting of synthetic or natural polymers. Hydrogels, which are 3D polymer networks with high water retention capacity and chemically or physically cross-linked networks, are leading materials in creating tissue scaffolds for 3D cell culture and tissue engineering studies [17-19]. This is because they closely resemble the natural extracellular matrix in terms of their 3D and physicochemical properties. Their ability to retain water, degrade biologically, and mimic the ECM structure makes them suitable materials for tissue scaffolding. Synthetic or natural polymers can be used to prepare hydrogels. Natural hydrogels are preferred in tissue engineering compared to synthetic ones because they contain less cytotoxic and more ECM-like features [20]. ECM has a rich structure in terms of structural fibrous proteins such as collagen and keratin. Therefore, it would be appropriate to use these structural proteins in the tissue scaffolds. ECM is composed of many fibrous proteins among which collagen is the most abundant one. Likewise, keratin is another important structural fibrous protein found in epithelial cells. Thus, harboring such structural proteins in tissue scaffolds is beneficial. Although scaffolds supply advanced three-dimensional properties for tissue development, vascularization as a fundamental phase for tissue development is lacking in bare hydrogels. The oxygen and nutrient exchange between tissue and the external environment is imperative. It is challenging work to organize a vascular network *in vitro* systems. Natural polymers, chosen for their ECM-mimicking and highly biocompatible properties, were combined with biological molecules like growth factors and interfering RNAs in hydrogels to promote angiogenesis [21].

Numerous microRNAs (miRNAs) have been linked to the regulation of angiogenesis, either by promoting or inhibiting it. miRNAs are short oligonucleotides (~22 nucleotides) found to be very important in protein expression regulation within cells. Micro RNA 21 (miR-21) has been extensively studied since it has been expressed in almost every cell and performs key regulations in healthy and diseased conditions such as cancer, and cardiovascular diseases [22, 23]. mir21, also known as an oncomir, has been in a controversial position in literature due to its linkage to various pathological conditions from tumorigenesis to autoimmune diseases [24]. However, it requires further investigation because of its non-specificity as a biomarker in many diseases and its vital role in healthy cells. In recent times, extensive research has been conducted on the biological functions of miR-21 in the area of cardiovascular systems and diseases. It was shown in a study that the expression of miR-21 was high in vascular smooth cells and endothelial cells [25]. Yet, there are conflicting literature sources regarding the role of miR-21 in angiogenesis. For instance, it was stated in a study conducted by Sabatal *et al*. that over-expression of miR-21 decreased the angiogenesis in HUVECs [26], yet, in another study done by Jiang *et al.*, it was claimed that HUVECs migration capacity induced by VEGF was significantly developed by miR-21's over-expression [27].

Currently, micro RNAs have been used in molecular biology and biotechnology for their regulatory properties. The number of studies focusing on miRNA-loaded matrices/hydrogels has expanded in recent years in tissue engineering applications, 3D cell cultures, and organoid studies [28, 29]. With these developments, tissue engineering possesses a high potential to model drug studies, diseases, and tissue structures, to create therapeutic alternatives. Briefly, the subject of the thesis covers and combines miRNAs, and hydrogels under the term of angiogenesis by creating a genetically controlled environment with miRNAs loaded hydrogel matrices.

This thesis study aims to examine the angiogenic potentials of PEI:miR-21 expression vector complex loaded and unloaded Col/Ker/Alg (CKA) hydrogels as gene-activated tissue scaffolds. For this purpose, firstly keratin and collagen were isolated from waste human hair and bovine Achilles tendon, respectively. Isolated keratin and collagen were characterized using Fourier transform infrared spectroscopy (FTIR) and sodium dodecyl sulfate-polyacrylamide gel electrophoresis (SDS-PAGE). Col/Ker/Alg hydrogels with different

ratios were prepared and their chemical, microstructural properties, percent porosity*, in vitro* hydrolytic degradation behavior, water uptake properties, *in vitro* protein release behaviors, and biocompatibility were characterized to optimize the hydrogels for the preparation of PEI:miR-21 plasmid complex loaded hydrogels for subsequent investigations. Simultaneously, mir-21 expressing plasmid was transfected into HUVECs and their expressions in cells were checked with the reporter gene, green fluorescent protein (GFP). For subsequent transfection studies, the PEI:miR-21 plasmid complex was prepared and examined for its stability, particle size, and zeta potential. Another scope of this study is to observe the ability of PEI:miR-21 plasmid complex loaded and unloaded Col/Ker/Alg hydrogels to modulate *in vitro* angiogenesis on the HUVECs. To observe the effects of PEI:miR-21 plasmid complex loaded and unloaded hydrogels on HUVECs, fluorescent microscopy, confocal laser scanning microscopy, and RT-qPCR for gene expression analysis were conducted. For relative mRNA expression, miR-21, direct and indirect targets of miR-21 regulating angiogenesis such as VEGFA, PTEN, SPRY1, and SPRY2 [30] were examined.

2. LITERATURE

2.1. Regenerative Medicine

Regenerative medicine gathers its scopes around functional restoration, replacement, and repair of the cells, tissue, and organs damaged or impaired by age, trauma, disease, or various other factors [31]. The ability of regenerative medicine to alleviate problems affecting a wide variety of organ systems and contexts is supported through preclinical and clinical trial evidence up to the present day, in particular concerning the treatment for both acute illnesses and unforeseen injuries [32]. The fusion of regenerative medicine and transplant medicine holds great promise in the realm of repairing and designing de novo engineered whole organs for transplantation [33].

Progress in stem cell research, gene therapy, and tissue engineering has accelerated the advancement of technology in tissue and organ regeneration. Tissue engineering, one of the major areas of regenerative medicine, holds the potential to create effective biological replacements that can restore, maintain, or improve tissue function by integrating principles from both natural science and engineering [34]. Tissue engineering relies extensively on the use of advanced biomaterials, cellular components, cellular signaling pathways, and engineering principles to mimic the natural tissue and restore the injured tissue. Tissue engineering is an interdisciplinary field that bridges medicine with the disciplines of biology, chemistry, physics, material science, and engineering principles. In the past few decades, both experimental research and clinical practices have increasingly showcased the potential of stem cell therapy as a prime method in regenerative medicine and tissue engineering [35]. Stem cells hold great promise in regenerative medicine due to their capacity for self-renewal, proliferation, and differentiation into various cell types. Gene therapy represents another area of interest within regenerative medicine, offering a highly promising and appealing technology that entails the introduction of exogenous genes into cells for both biological and therapeutic applications [36]. In gene therapy, non-viral vectors emerge as potentially reliable and effective options for viral vectors.

2.1.1. Stem cell-based approaches in regenerative medicine

Due to their robust capacity for self-renewal and straightforward extraction process, stem cells are extensively used in regenerative medicine and tissue engineering [37, 38]. Stem cells, being primitive and undifferentiated, possess the ability to replicate themselves, undergo multidirectional differentiation, and exhibit homing potential, while also retaining the characteristics inherited from their parent cells [37, 39]. The available evidence in the literature indicates that stem cells possess the capacity to expedite the progression of tissue regeneration employing a diverse range of mechanisms [40]. Stem cell-based therapies have demonstrated their potential in modulating immune responses and facilitating regeneration in various organs, with over 5,000 clinical trials primarily focused on ensuring safety and efficacy [41].

Stem cells, categorized into totipotent, multipotent, and unipotent stem cells based on their differentiation potential, possess the ability to differentiate into a variety of cell types such as bone cells, nerve cells, cardiomyocytes, etc. Embryonic stem cells (ESCs), multipotent hematopoietic stem cells (HSC), mesenchymal stem cells (MSCs), and induced pluripotent stem cells (iPSCs) are the most widely used cells to promote tissue regeneration [42]. ESCs and iPSCs are pluripotent stem cells with the capability to generate all cell types found within the body's tissues. Although human ESCs remain an ethically controversial cell source, their ability to be expanded *in vitro* while maintaining a pluripotent state makes them potentially powerful tools for therapeutic applications in tissue regeneration. iPSCs also can be expanded *in vitro* and have the capability to differentiate into all derivatives of the three germ layers. A study conducted by Maffioletti *et al.* pointed out that artificial skeletal muscle tissue was created by using iPSCs acquired from muscular dystrophy patients when the cells were induced in hydrogel with a controlled environment [43].

MSCs are the most widely studied and used stem cells in regenerative medicine and tissue engineering applications. MSCs frequently employed in clinical trials for cellular therapies, demonstrate considerable potential for both self-renewal and differentiation into various lineages. As an example, a study conducted by Prochazka *et al.* showed that therapy with healthy MSCs derived from patients could decrease the rate of amputation resulting from chronic limb ischemia [44]. MSCs can be derived from different adult tissues, such as

adipose tissue, amniotic fluid, umbilical cord, and bone marrow [45]. According to the source, MSCs can be classified as adipose-derived MSCs, umbilical cord MSCs, bone marrow MSCs, etc. Adipose-derived MSCs have exhibited considerable potential in clinical applications and possess the capacity for future advancements, such as organoids and tissue elements [46].

A substantial part of pre-clinical research studies has demonstrated that stem cell therapies can delay the onset of disease in multiple organs, such as the kidney, lung, heart, and liver, through mechanisms involving immunomodulation [41, 47]. Employing stem cells in regenerative medicine not only allows to production of personalized tissues tailored to the patient's requirements but also diminishes the risk of immune rejection and limited adverse effects [48]. However, the differentiation of stem cell populations into the desired target graft sites remains an unresolved challenge [49]. Additionally, the therapeutic potential of stem cells is hindered by the limited ability of transplanted cells to survive and differentiate when compared to their differentiated counterparts [50].

2.1.2. Tissue engineering approaches in regenerative medicine

Tissue engineering is an interdisciplinary field that endeavors to restore, maintain, or improve tissue function by combining clinical medicine, material science, and life science [51]. Tissue engineering integrates cells, tissue scaffolds, biochemical, structural, and mechanical signals, and engineering technologies to regenerate tissues or restore damaged tissue [52].

Three essential elements of tissue engineering, known as the tissue engineering triad, are the relevant selection of cells, biomaterial used in tissue scaffold, and appropriate signal molecules such as nucleic acids, transcription factors, growth factors, and others (Figure 2.1). In tissue engineering, mature cell types or stem cells are employed in facilitating the restoration and rejuvenation of impaired tissues [53]. Tissue scaffolds, which mimic the extracellular matrix (ECM), have been used as a supporting structure for cellular attachment and facilitating the proliferation of cells in the repair of damaged tissues or organs. During tissue development or regeneration, tissue scaffolds aid in cell regeneration and gradually biodegrade either during or after healing, thus eliminating the need for later material removal

and mitigating the side effects caused by foreign materials remaining in the body [54]. Cellular fate and tissue development depend on biochemical and biophysical factors, like growth factors, ECM components, features of the material's surface, mechanical forces, and electrical stimuli [41].

Biochemical factors play an important role in guiding and regulating cell responses during tissue regeneration by mediating molecular signaling mechanisms and facilitating communication between cells and their surrounding microenvironment [55]. Understanding the impacts of biochemical and biophysical factors on cell fate in tissue engineering is crucial. Factors like proliferation, differentiation, adhesion, and migration determine the lineage that stem cells will follow, and these processes are influenced by the physical and chemical environment [56].

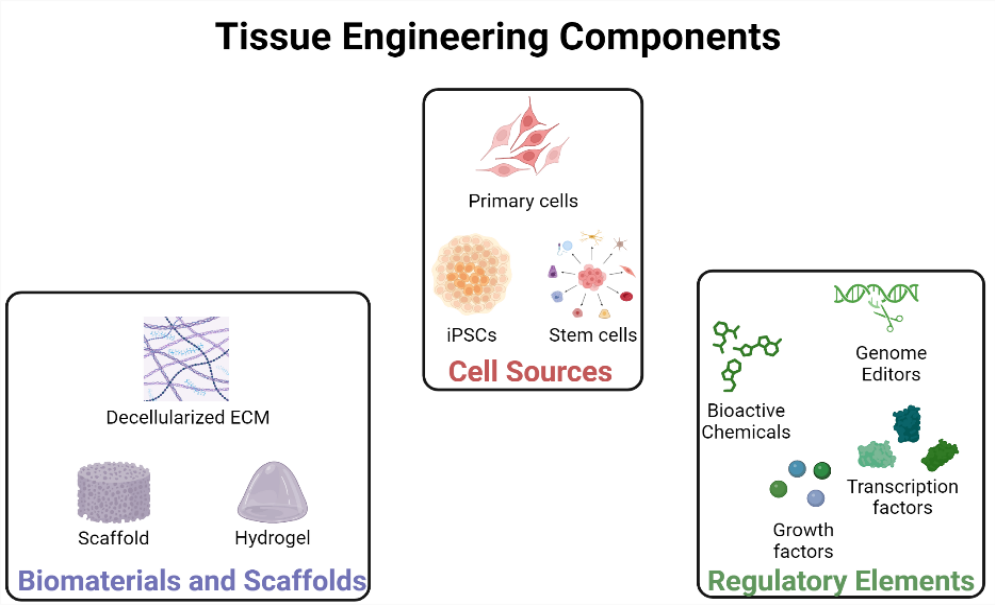

Figure 2. 1. Essential components of tissue engineering

Clinical examinations in the domain of tissue engineering have mainly focused on evaluating the safety and efficacy of tissue-engineered products for regenerative medicine. These investigations involve preclinical evaluations utilizing in vitro models and experimental animals to evaluate the compatibility of tissue-engineered products with biological systems. The conclusions derived from these investigations have revealed

promising results, as tissue-engineered constructs fabricated from hydrogels, biopolymers, tissue scaffolds, and encapsulated stem cells have displayed both compatibility with biological systems and the capability to foster tissue regeneration [23]. In the European Union, a total of 90 clinical trials have been conducted utilizing tissue-engineered products, with a specific focus on therapeutic areas such as musculoskeletal disorders, cardiovascular conditions, and disorders related to the skin and connective tissues [57]. In stem cell therapy, tissue engineering approaches have been employed to enhance the survival and reproductive potential of stem cells to surmount the aforementioned constraints in Section 2.2.1 [58].

In addition to the clinical applications, tissue engineering involves the development of 3D cell culture models that are based on scaffold-based or scaffold-free approaches, encompassing the investigation of various disease conditions, stem cell research, and drug discovery [59, 60]. The creation of 3D engineered tissue models involves mimicking native tissue and environment, including the utilization of ceramics and composites for tissue engineering of hard tissues like bone, the deployment of polymers for the engineering of soft tissues, the construction of polyester scaffolds from lactide and glycolide for pancreatic tissue, and utilizing bioreactors to provide the necessary conditions for cell culture and prevent cell necrosis [61].

2.2. Scaffold based tissue engineering strategies

In scaffold-based approaches, biomaterials have been used as a supporting structure for cellular attachment and facilitating the proliferation of cells in the repair of damaged tissues or organs [54]. The utilization of biomaterials as tissue scaffolds serves to enhance the process of tissue regeneration and establish an environment that fosters cellular attachment, proliferation, migration, and differentiation [62]. The fundamental idea of scaffolding is to mimic the ECM of the native tissue, ensuring that both mechanical structure and biological functions displayed by the tissue scaffolds closely resemble the functions performed by the ECM [9]. Scaffolds for tissue engineering must fulfill specific criteria tailored to their intended use. Some of these criteria are clearly defined, while others continue to evolve alongside advancements in the comprehension of developmental and regenerative cellular processes. An ideal scaffold should possess the ability to repair tissues [63]. Moreover, biomaterials used in the preparation of tissue scaffolds should possess a 3D

structure with appropriate chemical properties and mechanical functionality, while also being non-toxic and capable of natural degradation either during or after the healing process [9, 54].

In scaffold fabrication, both conventional techniques and additive manufacturing methods are utilized, each resulting in distinct features concerning the internal architecture of the scaffold, including pore size, structure, interconnectivity, and mechanical characteristics [9]. Advancements in tissue scaffold fabrication technologies have facilitated the development of multi-compartment constructs that mimic tissue heterogeneity, both for *in vivo* implantable tissue scaffolds and *in vitro* 3D models [64]. Conventional techniques include solvent casting and particulate leaching methods, freeze drying, thermally induced phase separation (TIPS), gas foaming, powder foaming process, sol-gel methods, and electrospinning techniques. Additive manufacturing methods or solid free form fabrication (SFF), used to develop direct forms of material using computer-aided design (CAD) models, contain stereolithography (SLA), fused deposition modeling (FDM), selective laser sintering (SLS), binder jetting technique, inkjet printing, laser-assisted printing and bio-printing [9]. Tissue engineering, which incorporates the use of 3D bio-printing, provides the potential to fabricate functional tissue components and complete organs, offering advantages over traditional methods [65].

2.2.1. Biomaterials used for tissue scaffold

Biomaterials used in tissue scaffold preparation can be composed of either natural or synthetic polymers and exhibit diverse characteristics contingent upon their application. Biomaterial selection for the production of scaffolds presents a significant challenge within the realm of tissue engineering. The examination of both natural and synthetic materials encompasses assessing characteristics such as biocompatibility, bioactivity, and biodegradation, alongside discussions regarding the impact of their physicochemical properties, including surface morphology, porosity, chemical composition, and mechanical strength, on interactions with cells and living systems [66].

Synthetic polymers are frequently utilized in the field of tissue engineering due to their versatility and customizable properties, allowing intentional modifications to fulfill specific

functionalities required for various tissues [67]. Commonly used synthetic polymers in the field of tissue engineering include polyethylene glycols (PEG), poly(ε-caprolactone) (PCL), poly(lactic acid) (PLA), poly(glycolic acid) (PGA), poly(lactide-co-glycolic acid) (PLGA) and more [68]. These polymers exhibit the advantageous characteristic of being capable of being tailored to show specific biodegradable and mechanical properties, on the other hand, they possess a low immunogenicity, rendering them highly suitable for the development of tissue scaffolds [69]. In addition to these, other types of synthetic polymers, such as dendritic polymers and hyper-branched polymers, possess the capability to interact with the mechanisms of cellular regeneration and take various roles in the regeneration of damaged tissues [70]. Synthetic polymers are capable of facilitating the delivery of genes and drugs, modulating surface chemistry, and promoting polymer cross-linking for wound healing [71]. Nevertheless, there exist restrictions in employing synthetic polymers, such as their relatively lower compatibility with biological systems and their diminished ability to degrade compared to natural polymers [72]. To overcome these limitations, various approaches have been investigated, such as employing crosslinking methods triggered by chemicals, temperatures, pH, or light sources, to enhance the properties of synthetic polymers. [73]. The progress of tissue engineering and regenerative medicine is enhanced by the advancements in synthetic polymers and their combinations with natural polymers.

Biomaterials can be derived from either natural sources or their by-products, and they assume a pivotal role within the realms of tissue regeneration and stem cell differentiation strategies [50, 51]. Natural polymers have been extensively studied and used in tissue engineering applications thanks to their beneficial characteristics, including biocompatibility, biodegradability, and low cytotoxicity when they are compared to synthetic polymers [74]. Natural polymers possess intrinsic biocompatibility when compared to synthetic polymers, and they produce non-cytotoxic degradation products [75]. They possess the capability to mimic the ECM and can be derived from diverse natural sources [67]. Additionally, natural polymers can contain cell-binding motifs, being able to influence cell behavior such as cell adhesion, spreading, and bioactive cues [20].

The most common natural polymers used in tissue engineering encompass chitosan, hyaluronic acid, gelatin, collagen, gellan gum, xanthan gum, guar gum, peptides, polysaccharides, alginate, carrageenan, fucoidan, etc. [76]. Similar to synthetic polymers,

natural polymers can be modified to improve their mechanical properties and achieve better characteristics tailored for specific tissue engineering applications [77].

2.2.2. Hydrogels

Among tissue engineering applications, hydrogels offer distinct advantages, such as their similarity to the ECM, shape adaptability, controlled delivery of components such as drugs, bioactive molecules, nucleic acids, and self-healing capabilities, rendering them highly promising for tissue repair and regeneration [78]. Hydrogels, characterized by their 3D polymer networks with high water retention capacity and chemically or physically cross-linked networks, are key materials utilized in the development of tissue scaffolds for 3D cell culture and tissue engineering studies [17, 19]. Hydrogels, polymers with a high affinity for water due to their hydrophilic nature, feature abundant polar functional groups like carboxyl, amide, amino, and hydroxyl moieties, which are interconnected through chemical bonds or attractive forces that occur within the molecule itself (intra-molecular) or between different molecules (inter-molecular) [79]. Hydrogels exhibit the remarkable ability to absorb significant amounts of water or biological fluids while maintaining their structural integrity, as they can swell without undergoing degradation or disintegration, making them highly suitable for a wide range of applications in various fields such as biomedical engineering, drug delivery, and tissue engineering [80]. Furthermore, hydrogels can be produced through various crosslinking methods, offering adjustable physicochemical properties, and closely mimicking the ECM of native tissues [20].

Hydrogels can be synthesized from both synthetic and natural polymers. Synthetic hydrogels are well-designed hydrogels having controllable degradation and functionalization to maintain various mechanical stiffnesses and physiochemistry [81]. However, synthetic hydrogel degradation products may have side products leading to increased local acidity thus locally killing the cells and increasing inflammation [82]. In recent years, natural hydrogels have been under the spotlight [83]. Natural hydrogels possess key properties such as biocompatibility, bioactivity, biodegradability, the ability to be tailored into injectable gels, and their similarity to the physiological environment [84]. However, natural hydrogels have some limitations, notably, they lack robust mechanical properties and are not easily controllable due to variations from batch to batch.

2.2.3. Collagen

Collagen (COL), one of the most important elements of the ECM, is a fibrous protein, abundant in tissues such as connective tissue, skin, tendon, cornea, and cartilage. COL can be obtained from various natural sources such as bovine, pig, fish, and jellyfish and is a biocompatible material for various tissue engineering applications [85]. COL is made up of amino acids which are dominantly glycine, hydroxyproline, and proline. COL has high mechanical stability and a very high propensity to allow cell attachment and proliferation owing to its functional groups [86]. There are more than 20 types of collagens which have three polypeptide chains, α-chains, bound to each other and ordered in the form of a triple helix (Figure 2.2.)**.** Collagen type I is the most common collagen protein among all types establishing 25-35 % of all proteins in humans [87]. While COL exhibits high stability in cell culture *in vitro*, it can be degraded in the body when implanted with the help of collagenases [88]. In this sense, collagen provides excellent biocompatibility and biodegradability when utilized as a biomaterial in tissue scaffolds. As an example, the utilization of collagen-based approaches includes predominantly as a covering substance for the enhancement of the internal surface of vascular grafts, as a mechanism for administering medicinal substances to release pro-endothelialization agents, and as physiologically significant vascular models in laboratory settings [88].

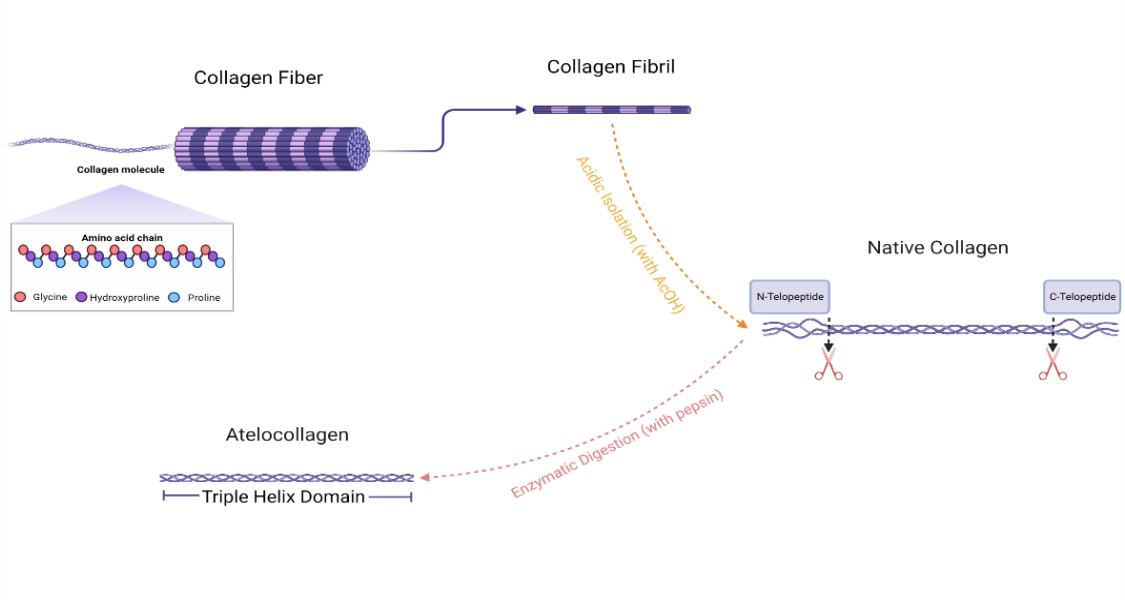

Figure 2. 2. Structure of collagen

2.2.4 Keratin

Keratin, a structural protein found in the hair, wool, horn, hoof, and nail tissues of mammals, consists of α-keratin structures with polypeptide chains arranged as α-helices and β-keratin structures with polypeptide chains arranged as β-sheets [89]. The molecular weight of α-keratin is approximately 40 kDa, while β-keratins typically fall within the range of 10 to 22 kDa [90]. α-Keratins cover 50-60% of all keratins in the body and create long filaments and are resistant to rupture [91]. Keratin can be categorized as either acidic or basic depending on their isoelectric points. Hair, horns, feathers, and nails constitute hard keratins classified as types Ia (acidic-hard) and IIa (basic-hard), while the epidermis in the skin has soft keratin classified as Ib (acidic-soft) and IIb (basic-soft) [92, 93].

In numerous recent studies on 3D tissue constructs, keratin (KER) has garnered significant attention due to its favorable traits of biocompatibility and biodegradability [94]. KER is a polypeptide polymer having alpha-keratin and beta-keratin conformations with high concentrations of glycine, serine, proline, and cysteine amino acids (Figure 2.3.). Spontaneous self-assembly of keratin is responsible for the reproducible architecture, dimensionality, and porosity of keratin-based materials [95]. Furthermore, keratin biomaterials sourced from wool and human hair have demonstrated the presence of cell-binding motifs, such as leucine-aspartic acid-valine and glutamic acid-aspartic acid-serine binding residues, which facilitate cellular attachment.

Keratin has emerged as a promising naturally derived biomaterial because of its biocompatibility, distinct chemical composition, biodegradability, and ability to facilitate cellular attachment [96]. In recent years, keratin obtained from human hair has attracted great attention as an alternative biomaterial due to its excellent biocompatibility and potential in human origin [97]. Keratin has been widely used in biomedicine ranging from wound healing to nerve regeneration [98]. Jelodari, S. et al. showed that the release of antimicrobial peptide LL-37 from keratin hydrogel provided better wound healing and resulted in higher fibroblast attachment, and proliferation which accelerated wound closure [99].

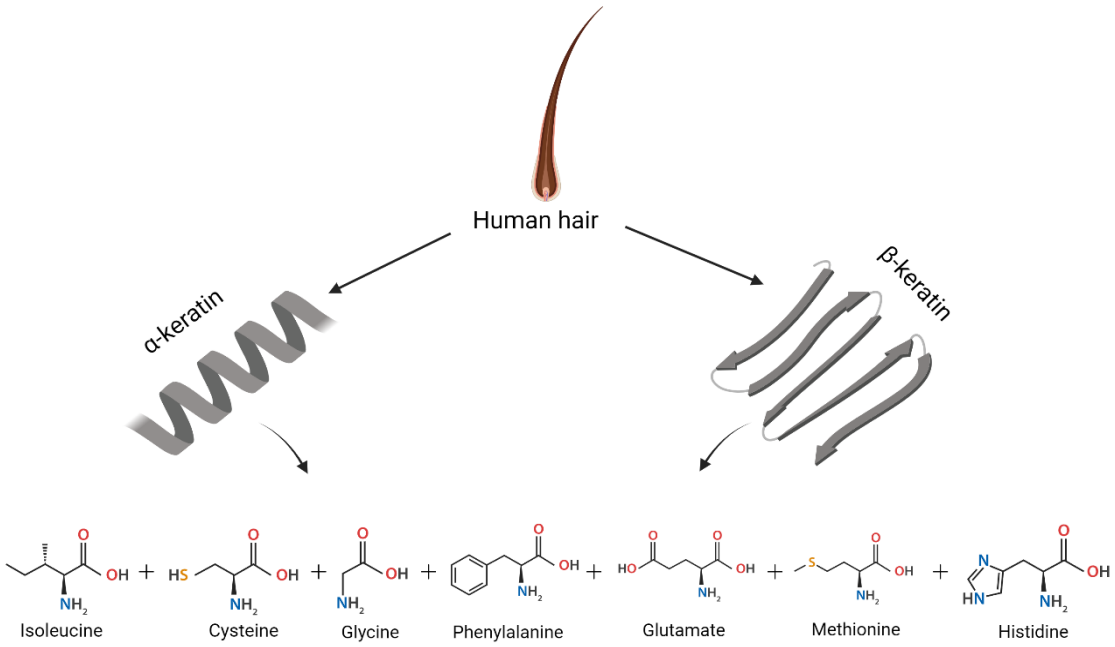

Figure 2. 3. Structure of keratin

2.2.5. Alginate

Alginate is a naturally occurring biocompatible polymer that can be isolated from brown seaweed. Alginate has a wide range of uses in various sectors including biomedical engineering, pharmaceuticals, food, and cosmetics [100]. The ratio of mannuronic acid and glucuronic acid determines the gelation behavior, viscosity, and mechanical properties of alginate [101]. In the literature, cross-links are generally created between polymer chains using divalent cations such as calcium or barium to produce alginate hydrogels. Since the gelation time is reversible and not in harsh conditions, alginate hydrogels are used as tissue scaffolds to assist in the formation of new tissue in tissue engineering applications [102]. In addition, alginate hydrogels provide advantages in applications that require the delivery of cells and sensitive bioactive compounds [103]. The mechanical properties of alginate hydrogels can be easily changed by changing the alginate concentration, polymer molecular weight, or cross-linking density [104]. This tunability in mechanical properties enables the creation of a wide range of hydrogels, from soft and flexible hydrogels that mimic soft tissues to more hydrogels that mimic hard tissues such as cartilage or bone. Additionally, the fact that alginate-based hydrogels retain high amounts of water in their three-dimensional

structures, creating a moist environment and therefore stimulating cell migration, proliferation, and tissue regeneration, causes these hydrogels to be frequently used in various tissue engineering applications, including wound healing [105].

2.2.6. Gene-activated matrices

A cutting-edge technology known as a gene-activated matrix (GAM) combines tissue engineering with gene therapy to provide more precise, controlled, and sustained release of therapeutic factors compared to traditional methods of direct growth factor delivery [106]. The GAM strategy involves encapsulating or coating gene poly-plexes onto scaffolds, condensing nucleic acids with cationic transfection reagents, and facilitating the release of genes from the matrix upon insertion into damaged tissue, leading to the expression of desired proteins [107]. A key benefit of GAM is its capacity to attain sustained and localized expression of transgenes within the cellular microenvironment. Nucleic acids such as DNA, RNA, and small interfering RNA are encapsulated in GAMs to protect their stability, prevent systemic dissemination, and reduce the immune response to the vector [107].

2.3. 2D and 3D cell culture models

In tissue engineering, both *in vivo* animal models and *in vitro* cell culture models have been conducted to understand the natural tissue development process. *In vitro* 2D and 3D cell culture studies provide cost-effective experiments, accelerate experimental timelines, and offer broad applicability in scientific investigations compared to *in vivo* animal studies. Although 2D models provide advantages like simplicity, cost-effective maintenance of cell cultures, and suitability for functional tests, they fail to accurately represent cell-to-cell and cell-to-ECM interactions and are restricted in their ability to replicate the 3D structure of natural tissues [15]. Moreover, 2D models prevent cells from acting as if they are in their natural environment, thus 2D cultures are not truly facilitating the cell-environment interactions [108].

3D cell culture models can mimic more accurately the complex 3D *in vivo* environment [16]. In this context, cells grown in an architecture similar to their natural niche can improve their differentiation through the physical, mechanical, and even transcriptional

levels [9]. Besides cellular colonization and providing physical and mechanical confinement, 3D models taking tissue architecture into account illustrated that an environment that mimics the stiffness, porosity, and fibrotic nature of the ECM can indeed force rapid differentiation and may provide a strong interaction when implanted [109]. Especially with the use of hydrogels in tissue engineering, their chemically and biologically dynamic nature can be utilized as a 3D environment to controllably release bioactive factors to maintain cells, degrade in time to replace de novo forming tissue, and allow cells to reach equilibrium in size and number in a well-defined architecture [110].

3D cell culture has demonstrated advancements in various research areas including morphology, cell number monitoring, proliferation, response to stimuli, differentiation, drug metabolism, and protein synthesis, and has versatile applications encompassing the investigation of various disease conditions, stem cell research, drug discovery, and tissue engineering [16].

2.4. Angiogenesis

Angiogenesis refers to the newly formed blood vessels from the existing vessels which is a process that can originate either via endothelial sprouting or non-sprouting microvascular growth. Endothelial sprouting starts under low blood oxygen and needs the degradation of the endothelial cell basement membrane (Figure 2.4.), whereas non-sprouting angiogenesis occurs when the already existing vessels split and form vascular lumen known as tissue pillars [111, 112].

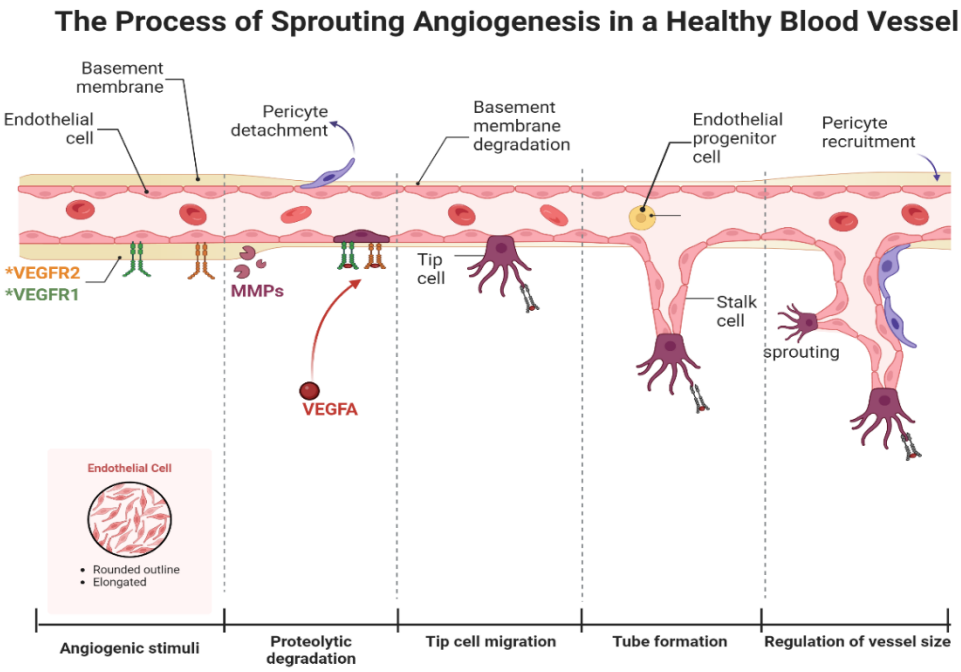

Figure 2. 4. Schematic representation of sprouting angiogenesis (modified from Łazarczyk, [113])

Oxygen and factors in the blood play a critical role in maintaining vascular networks [114]. Angiogenesis occurs during whole life in almost every tissue (healthy or not) because all tissues need capillaries that are essential for nutrient exchange and metabolite transport. The formation of new vascular networks sustains normal development, helps wound healing, and gives adaptive responses to vascular problems and ischemia [115].

Vascular endothelial growth factor (VEGF), fibroblast growth factor (FGF), tumor necrosis factor-alpha (TNF-α), transforming growth factor-beta (TGF-β), and the angiopoietins (Ang) are the main angiogenic growth factors and cytokines [116]. In addition, hypoxia-inducible factors (HIFs) play a very important role in the stimulation of angiogenesis when the environment lacks oxygen [117]. The sources of these growth factors are mainly endothelial cells, fibroblasts, platelets, and even cancer cells [118].

The promotion of vascularization and angiogenesis has gained importance in tissue scaffold fabrication because the quick formation of new vessels is needed for the engineered tissue once it is placed in a living system to maintain tissue repair/regeneration while

supplying nutrients and oxygen to the cells. The necessity for a functional vascular network becomes more pronounced as the complexity and size of the target tissue or organ increases [11]. In tissue engineering applications, vascularization strategies have been investigated to enhance the viability of engineered scaffolds and facilitate their integration and vascularization after implantation [11-13].

Considering vascularization studies essential in bone tissue engineering, skin tissue engineering, and cancer research, human umbilical vein endothelial cells (HUVECs) play a pivotal role. As they represent terminally differentiated cells, HUVECs retain the capability to proliferate and modify the properties of their niche, including altering the ECM [14]. Therefore, they are employed in numerous *in vitro* studies to define cell-cell interactions.

2.5. Interfering RNAs

Interfering RNAs (RNAi) are 20 – 30 nucleotide RNA molecules that lack coding capacity and have the capability to temporarily impede the expression of particular genes [119]. They perform their function by selectively targeting and degrading the messenger RNA (mRNA) molecules responsible for the production of specific proteins [120]. The types of interfering RNAs are small interfering RNA (siRNA), microRNA (miRNA), small hairpin RNA (shRNA), and others. The application of RNA-interfering technology has been extensively employed in medical research to address a wide range of hereditary and acquired diseases [121]. The employment of RNAi mechanisms has gained substantial popularity due to their capacity to induce targeted suppression of gene expression. The efficacy of interfering RNAs is influenced by factors such as the identification of target mRNA and the participation of pivotal proteins, namely Dicer and RNA-induced silencing complex (RISC) [122]. Recent progress in RNAi technologies has resulted in the development of therapeutically approved agents for various diseases by the United States Food and Drug Administration (FDA) [123].

miRNAs display post-transcriptional control over gene expression and play critical roles in numerous cellular processes and their altered levels can be linked to many diseases [124]. Several miRNAs such as miR-181, and miR-23 have been shown as potential cancer biomarkers for both diagnosis and prognosis [124]. On the other hand, an understanding of

miRNA biogenesis and regulatory mechanisms can provide insights in terms of their functions in healthy and diseased conditions [125].

miR-21, mostly known as an oncomir, has earned popularity by being one of the most controversial miRNAs. miR-21 has been widely studied in terms of its proliferative and inducing effects on angiogenesis. miR-21 has been also studied in the field of oncology and cardiovascular pathology [25]. Jianzhong *et al*. showed that miR-21 has the potential to induce angiogenesis by promoting the viability, migration, and tube-forming ability in endothelial cells by regulating matrix metalloproteinase-2 (MMP2) and matrix metalloproteinase-9 (MMP9) expressions [126]. The biological source of miR-21, its direct targets, and its role in angiogenesis are displayed in Figure 2.5. miR-21 directly targets and inhibits the mRNA expression of essential proteins that act as tumor suppressors, including PTEN (phosphatase and tensin homolog), Sprouty1 and Sprouty2, and PDCD4 (programmed cell death protein 4) [127]. By targeting PTEN, miR-21 induces angiogenesis and activates AKT and ERK1/2 signaling pathways, ultimately leading to the upregulation of hypoxia-inducible factor 1α (HIF1α) and vascular endothelial growth factor (VEGF) expression [128]. HIF1α is a key downstream target of miR-21 in the regulation of angiogenesis and the overexpression of HIF1α and HIF2α has been linked to increased VEGF expression [129].

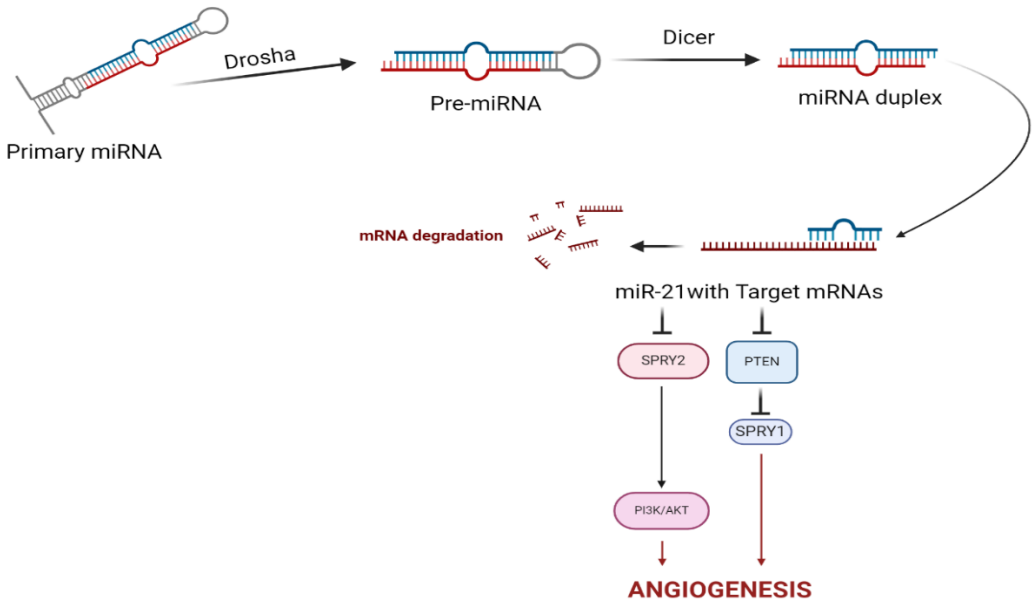

Figure 2. 5. Biosynthesis of miR-21 and its direct targets in angiogenesis

Nucleic acids, genome editors, and RNA interfering have become alternative therapies to renew damaged tissues. miRNAs, or synthetic miRNA inhibitors, plasmids can be introduced into many somatic cells such as HUVECs, and help to reprogram and regenerate tissues [130]. For instance, it was shown by Baek *et al*. that inhibition of miR-449a and miR-203 ameliorated chondrogenesis in animal osteoarthritis models [131]. Another example is that in a porcine model, miR-21-5p loaded silica nanoparticles were created to treat myocardial infarction, and delivered nanoparticles enhanced the local neo-vascularization [132].

3. MATERIALS AND METHODS

3.1. Materials

For Protein Isolation and Hydrogel Preparation Studies: Acetic acid (glacial), acrylamide, ammonium persulfate, bis-acrylamide, bromophenol blue, β-mercaptoethanol, bovine serum albumin, calcium chloride, Coomassie brilliant blue, bovine gelatin powder, bovine collagen type I solution, sodium acetate, sodium alginate, sodium bisulfite, sodium chloride, sodium dodecyl sulfate, sodium hydroxide, sodium sulfite, tetramethylethylenediamine (TEMED), tris-base (TRIS), tris(hydroxymethyl)aminomethane, urea were purchased from Sigma Aldrich, Germany. 14 kDa cellulose dialysis membrane was purchased from CliniSciences, France. 1-Ethyl-3-(3-dimethyl aminopropyl) carbodiimide and N-Hydroxysuccinimide were purchased from Ambeed, USA.

Pepsin from the porcine stomach was purchased from Genaxxon, Germany. Protein weight markers were purchased from GeneDireX, Inc., Taiwan, and Abcam Inc., UK. Keratin was extracted from waste human hair which was obtained from local barbershops. Collagen was isolated from bovine Achilles tendons, and they were kindly given by The Meat and Milk Institution. Micro BCA reagent was purchased from Thermo Scientific, USA.

or Cell Culture Studies: L929 CCL-1 mouse fibroblast cell line and Endothelial Cell Growth Kit-BBE were purchased from ATCC, USA. The human umbilical vein endothelial cell (HUVEC) line (CRL-1730) was purchased from ATCC, USA. Dulbecco's Modified Eagle Medium high glucose with L-glutamine, fetal bovine serum, and 1X trypsin-EDTA were purchased from Capricorn Scientific, Germany. Ham's F-12K Nutrient Mixture (Kaigh's modified) was purchased from Wisent, Canada. Endothelial cell growth kit – BBE was purchased from ATCC, USA. Opti-MEM Reduced Serum was purchased from Gibco, Thermo Fisher Scientific, USA. Tryphan blue was purchased from Biological Industries, Israel. Resazurin sodium salt was purchased from Sigma Aldrich, Germany.

For Transformation and Transfection Studies: Agar agar for microbiology, agarose for molecular biology, ethylenediamine tetraacetic acid, glucose, glycerol, kanamycin sulfate, magnesium chloride, magnesium sulfate, sodium acetate, Luria Broth, tryptone, yeast extract was purchased from Merck, Germany. Tri-track loading dye, DNA molecular weight marker, Rnase A, ethidium bromide, and acridine orange were purchased from Thermo Scientific, USA. Escherichia coli strain DH5alpha (p2B1862-1dhL-ara) was kindly given by the Başkent University. MIR21 Human MicroRNA Expression Plasmid (MI0000077) was obtained from OriGene Technologies (Rockville, MD). PEIpro transfection agent was purchased from PolyPlus, France.

For RNA Isolation, cDNA Synthesis, and qPCR Studies: A total RNA isolation kit was purchased from Genaxxon, Germany. Dnase I was purchased from Thermo Fisher Scientific, USA. cDNA synthesis kit was purchased from Applied Biological Materials, Canada. cDNA synthesis kit for miRNA and SYBR Green qPCR mix were purchased from Quanta Biosciences, USA. Primer pairs were purchased from Oligomer, Turkey.

3.2. Methods

3.2.1. Isolation of keratin from human hair

Keratin, one of the main protein components of the hydrogel groups, was isolated from waste human hair samples collected from local barbershops, without any distinction regarding age and gender group. Raw hair, not subjected to any chemical processing such as dyeing, was first washed in 70% (v/v) ethyl alcohol and distilled water, and dried in the oven (Nüve, Turkey) overnight at 40ºC. Cleaned and dried hair delipidated with a mixture of chloroform and methanol in the ratio of 2:1 (v/v) for 24 hours at room temperature. The hair was subsequently dried in the oven at 70 °C for 2 hours. To decolorize the dried hair, hair was incubated in a mixture of hydrogen peroxide and ammonia in the ratio of 2:1 (v/v) in the dark for 15 minutes with the application of 15s UV light activation. After the decolorization process, the hair was air-dried for 24 hours. For keratin isolation, dried hair was immersed in an extraction solution containing 8.0 M urea (CH_4N_2O), 0.10 M sodium bisulfite ($NaHSO_3$), 0.125 M sodium sulfide (Na_2S), and 0.10 M sodium dodecyl sulfate

(SDS) at 50°C for 6 hours. The resulting mixture was centrifuged at 10,000 rpm for 20 minutes at room temperature. The supernatant was dialyzed against deionized water in a 14 kDa cellulose dialysis membrane for 5 days on a magnetic stirrer (Daihan Scientific, S. Korea) with changes at regular intervals at room temperature. After dialysis, the obtained samples were lyophilized using a freeze dryer (Gyrozen, S. Korea) to obtain keratin in powder form.

3.2.2. Isolation of collagen from bovine Achilles tendon

Another fundamental component of the hydrogel group, collagen type I, was isolated from the bovine Achilles tendon. Bovine Achilles tendons were kindly given by the Meat and Milk Board. All materials were kept at -20°C until they were used for isolation. The isolation method of collagen type I from the bovine Achilles tendon was modified based on techniques described in two previous studies [133, 134]. Initially, individual tendon sections, isolated from adjacent tissues, were washed with ethyl alcohol, followed by three subsequent rinses with distilled water. Then, they were dissected into 1-cm^3-sized cubes. Tendons were immersed into 0.10 M sodium hydroxide (NaOH) solution in the ratio of 1:8 (w/v) for 6 hours to get rid of lipids and non-collagenous proteins and the solution was refreshed every 2 hours. At the end of the alkali treatment, tendon sections were taken out and washed 3 times with dH_2O. For the acid solubilized method, tendon sections were immersed in a beaker containing a 0.70 M acetic acid solution in a ratio of 1:17 (w/v) for tendon to solution, followed by homogenization using a hand blender. The collagen-acetic acid mixture was stirred on a magnetic stirrer for 16 hours at 4 °C.

For the enzymatic treatment, pepsin (10,000 N.F. U/mg) was added to the collagen-acetic acid mixture at a ratio of 1:50 (w/w) for pepsin to tendon. Pepsin digestion was carried out over 72 hours at 4 °C. To stop the enzymatic digestion, the pH of the solution was changed by adding 0.20 M sodium-acetate buffer solution. The resulting solution was centrifuged at 10,000 g for 30 minutes at 4°C to remove undigested parts of tendons. Hence, the solubilized collagen-containing supernatant was used in subsequent precipitation steps. The pH of the supernatant solution was raised to 7.0 with the addition of 0.050 M Tris(hydroxymethyl)aminomethane. Subsequently, sodium chloride (NaCl) was added to the solution, achieving a final concentration of 2.60 M, while vigorously stirring. White clouds

of collagen formed after an overnight incubation at 4 °C. The collected collagen clouds were subjected to centrifugation at 10,000 g for 1 hour and 30 minutes. Supernatants were discarded, and collagen pellets were dissolved in 0.5 M acetic acid. Later, the collagen solution was dialyzed against 0.10 M acetic acid using a 14 kDa cellulose dialysis membrane at 4 °C for 24 hours on a magnetic stirrer. This step was followed by dialysis against distilled water at room temperature for 48 hours. After dialysis, the resulting samples were lyophilized to obtain collagen in powder form. The extraction yield was calculated by the formula given in Equation 3.1.

$$Yield(\%) = \frac{Freezed\ dried\ collagen\ weight\ (g)}{Dry\ tendon\ weight\ (g)} x\ 100 \qquad (3.1)$$

3.2.3. Characterization of isolated keratin and collagen

The chemical characteristics of the lyophilized keratin and collagen were examined through Fourier transform infrared spectroscopy (FTIR, Agilent Varian 660-IR, USA) using KBr discs, within the range of 400-4000 cm^{-1}.

Additionally, lyophilized keratin and collagen were examined by Sodium Dodecyl Sulphate-Polyacrylamide Gel Electrophoresis (SDS-PAGE) to distinguish molecular mass distribution specific to human hair keratin and collagen. For the SDS-PAGE analysis, 4% stacking gel was prepared for both proteins, while 10% and 7.5 % separating gels were prepared for keratin and collagen, respectively. For SDS-PAGE analysis, the gel compositions are given in Table 3.1. with the order of ingredients.

Separating gel was poured into the bottom part of glass layers and topped with isopropyl alcohol to even the surface layer and to prevent oxidation. The gel was allowed to set for at least 30 minutes at room temperature. After polymerization of the resolving gel, isopropanol was discarded, and a 4% stacking gel solution was prepared and poured immediately on top of the separating gel. Well-forming combs were quickly and carefully placed on top without creating air bubbles and then sealed with paraffin film to minimize oxidation. The gel was left to set at room temperature for a minimum of 30 minutes. When the polymerization was complete, combs were lifted slowly to form wells without bubbles

and/or tears. Glass plates containing gels were soaked vertically into the tank filled with 1X running buffer (pH 8.3). Before sample loading, wells were also filled with running buffer.

Table 3. 1. SDS-PAGE setup for lyophilized keratin and collagen

7.5 % Separating Gel for Collagen	**10 mL**
30% Acrylamide solution	2.5 mL
1% Bisacrylamide solution	1.93 mL
1.5 M Tris, pH 8.7-8.8	2.70 mL
20% SDS	66.67 µL
Distilled Water (dH_2O)	2.83 mL
10% Separating Gel for Keratin	**10 mL**
30% Acrylamide/Bisacrylamide solution	3.33 mL
1.5 M Tris, pH 8.7-8.8	2.50 mL
10% SDS	100 µL
Distilled Water (dH_2O)	4.10 mL
10% Ammonium persulfate (APS)	100 µL
TEMED	10 µL
4% Stacking Gel for Both	**10 mL**
30% Acrylamide/Bisacrylamide solution	650 µL
0.5 M Tris, pH 6.7-6.8	1.25 mL
10% SDS	50 µL
Distilled Water (dH_2O)	3.10 mL
10% Ammonium persulfate (APS)	50 µL
TEMED	5 µL

Lyophilized keratin was dissolved in dH_2O, and collagen type I was dissolved in 0.1M acetic acid; both were diluted with dH_2O to a concentration of 50 µg/mL. Three volumes from samples (15 µL) and one volume from 4X Laemmli [135] loading buffer (5 µL) were taken and mixed well by pipetting. Then, 1 µL of 10 M NaOH solution was added to the mixture for neutralization. After mixing well, the sample solution was heated at 95°C for 5 minutes and then centrifuged at 12,000 rpm for 5 minutes. Keratin and collagen samples and

a pre-stained protein ladder in equal volumes (20 μL) were loaded onto the gel. Firstly, the gel was run at 60 V for stacking gel until loads reached on top of the second gel and then at 100 V for separating gel. The run-time (60 minutes for keratin, 90 minutes for collagen) was also longer than that for keratin since the molecular mass of collagen is much bigger than that of keratin.

When polyacrylamide gel electrophoresis had finished, glass plates were separated without damaging the gels. The stacking gel was cut off and the separating gel was removed without tearing/damaging for the fixing and staining procedure. The separating gel was then soaked in the fixing solution for 1 hour to fix the proteins. At the end of 1 hour, the fixing solution was removed and next, acrylamide gel was incubated in the staining solution containing Coomassie Brilliant Blue R-250 for 2 hours.

After the staining procedure, the gel was washed three times with dH_2O to clear the excess stain away. Later, the destaining solution was poured onto the gel in the plastic box and left overnight until the distinct purplish-blue bands were visible on the clear gel background. At this step, the gel was photographed and visualized with a gel imaging system (Syngene, UK). According to the protein molecular weight marker, human hair keratin-specific bands were determined.

3.2.4. Preparation of collagen/keratin/alginate (C/K/A) hydrogels

For the optimization studies, four hydrogel groups with different ratios were prepared by mixing different concentrations (w/v %) of collagen, keratin, and alginate stock solutions. Stock solutions of the components were mixed in a 1:1:1 volume ratio. The stock solutions of different concentrations (w/v %) were prepared at 45 °C with 150 rpm stirring on a stirrer. 0.50M acetic acid was used as a solvent for the preparation of collagen stock solution, while distilled water was used to prepare keratin and alginate stock solutions. The final concentrations of components in hydrogel groups are given in Table 3.2.

Table 3. 2. Final compositions of four different hydrogel group

Hydrogel Group	Collagen % (w/v)	Keratin% (w/v)	Alginate% (w/v)	Total% (w/v)
CKA1	1%	1%	1%	3%
CKA2	1%	2%	1%	4%
CKA3	2%	1%	1%	4%
CKA4	2%	2%	1%	5%

After gathering clear and homogeneous stock solutions, keratin solution was added to collagen solution at a ratio of 1:1 (v/v) under rapid stirring (around 250-300 rpm) on a stirrer, then alginate solution was poured onto the collagen/keratin mixture at a ratio of 1:1:1 (v/v/v). When the solution was mixed well, 50 µL of 10.0 M NaOH solution was added for each mL of 0.50 M acetic acid to neutralize the pre-gel solution. The solution was allowed to stir until all particles dissolved, and the solution became clear once again. The pre-gel mixture was then left to cool down at room temperature before being poured into the wells of a 48-well plate in equal volumes. Samples were chilled at 4°C for at least 30 minutes to attain the desired pre-gel consistency. After solid gel formation, 0.10 M calcium chloride ($CaCl_2$) in 70% (v/v) ethanol solution was dropped onto samples, allowed to crosslink for 30 mins at 4°C, and subsequently, samples were flipped for the bottom side to undergo crosslinking. For the next step, physically crosslinked hydrogels were immersed in absolute ethanol for 30 minutes to induce dehydration and bring the polymer chains closer together. This step was repeated with fresh absolute ethanol. Subsequently, the dehydrated hydrogels were washed with distilled water twice and air-dried for 20-30 minutes.

For a covalent crosslinking of hydrogels, hydrogel groups were immediately dipped into EDC/NHS solution in dH_2O with acetic acid (pH 5.5) and incubated at 4°C overnight. For the preparation of EDC/NHS crosslinking solution 1.150 g EDC and 0.276 g NHS per one gram of collagen were used. The crosslinked hydrogel samples were washed with distilled water before lyophilization. The main steps of hydrogel preparation are depicted in Figure 3.1.

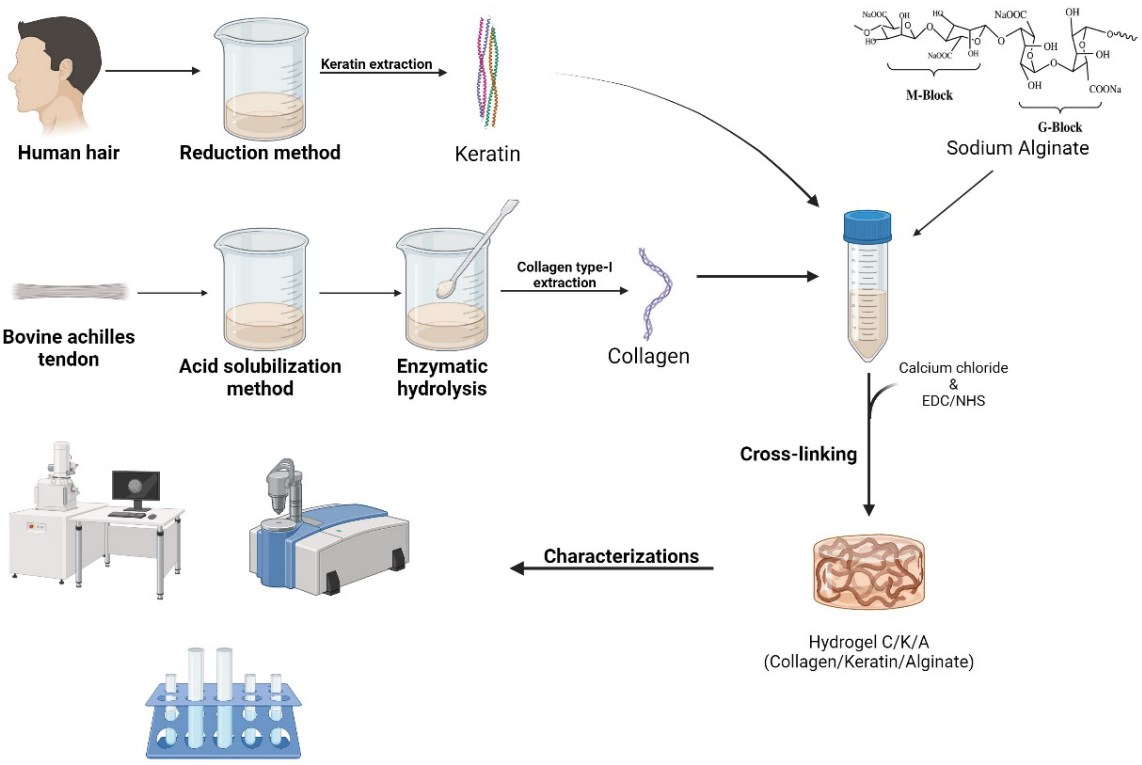

Figure 3. 1. Schematic representation of hydrogel preparation

3.2.5. Characterizations of collagen/keratin/alginate hydrogels

The chemical characteristics of the lyophilized hydrogel groups and powder mixture of collagen, keratin, and alginate powders were investigated with FTIR using potassium bromide (KBr) discs, within the range of 400-4000 cm^{-1}.

The microstructural properties of lyophilized hydrogel groups were examined through a scanning electron microscope (Hitachi SU5000 FE-SEM, Japan) with a voltage of 10 kV under vacuum condition. Before SEM observation, the lyophilized hydrogels were placed onto a carbon tape on stabs and they were coated with an ultrathin layer of gold using sputter coating (Leica, Germany).

In vitro hydrolytic degradation of lyophilized hydrogel groups was studied in 2 mL of serum-free cell culture medium (DMEM High Glucose with L-glutamine) containing 0.02% sodium azide (NaN_3, pH 7.40) (n=4). Firstly, the mass lyophilized hydrogels were measured

(m_0), and they were incubated in the incubation media at 120 rpm at 37°C for 21 days using an incubator shaker (Jeio Tech, IST-4075R, South Korea). At the end of the 1st, 2nd, 3rd, 7th, 10th day, 14th, and 21st day, hydrogel samples were carefully taken out from the media, washed with deionized water, and lyophilized. After lyophilization, the mass of dried hydrogels was measured (m_1). The weight loss percentage of the hydrogels was determined using the following formula [136]:

$$Weight\ loss\ \% = \frac{m0-m1}{m0}\ x\ 100 \tag{3.2}$$

where m_0 = initial dry weight, m_1 = dry weight at a given time.

The gravimetric method was used to determine the water uptake properties of hydrogel groups (n=4). Firstly, the mass lyophilized hydrogels were measured (m_0), and they were incubated in the 2 mL of serum-free cell culture medium containing 0.02% NaN_3 (pH 7.40) at 120 rpm at 37°C for 96 hours. At the predetermined time intervals (15 and 30 minutes, 1, 2, 4, 6, 12, 24, 48, 72, and 96 hours), hydrogels were removed from the incubation media, and they were weighed (m_1) after removing the excess liquid on their surface with a filter paper. The percent water uptake values of the hydrogels were determined using the following equation [136]:

$$Swelling\% = \frac{\mathrm{m1-m0}}{\mathrm{m0}} x\ 100 \tag{3.3}$$

where m_1 is the weight at the instance, and m_0 is the initial dry weight.

For the *in vitro* release of total protein content from hydrogels, lyophilized hydrogels were immersed into 2 mL of serum-free cell culture medium containing 0.02% NaN_3 (pH 7.40) at 120 rpm at 37°C for 15 days (n=4). 500 µL of aliquots from the release media were collected after the 1st, 2nd, 3rd, 10th, and 15th days and they were stored at 4°C until the protein quantification. 500 µL of fresh incubation medium was added after sample collection. The released protein amount from the hydrogels was quantified using Bicinchoninic acid assay (BCA). BCA assay is a colorimetric method and this assay depends on the formation of a complex between Cu^{2+} ions and proteins in an alkaline environment, which is then reduced

to Cu^{+} ions [137]. Briefly, equal volumes of aliquots from the release media and BCA working solution containing 25 parts of sodium carbonate monohydrate-sodium tartrate buffer solution (pH 11.25), 24 parts of Micro BCA reagent, and 1 part of 4% (w/v) copper sulfate pentahydrate solution were incubated at 37°C for 2 hours. After cooling to room temperature, the total amount of protein was determined by measuring the optical density (OD) at 562 nm with a microplate reader (BioTek Synergy Neo2 Hybrid Multimode Reader, Agilent, USA). The calibration curve (Appendix C) was constructed with different concentrations of bovine serum albumin (BSA) (1-0.125 µg/ml) prepared in a serum-free cell culture medium containing 0.02% NaN_3. Additionally, the incubation medium was used as the blank solution for control and samples, respectively.

The liquid displacement method was used to measure the percent porosity of the hydrogel groups (n=4). Briefly, the lyophilized hydrogels with known dry masses (m_0) and volumes (V) were placed inside a 5 mL syringe filled with cyclohexane, and a mild vacuum was created by pulling the injector up. By this action, air bubbles moving out were observed and hydrogel sunk inside the liquid. Immediately after, the hydrogels were taken out from cyclohexane followed by gentle removal of the surface cyclohexane. The percent porosity of the hydrogels was measured using the liquid saturating method and calculated by the formula below [138]:

$$Porosity\% = 100 \times \frac{m(saturated) - m(dry)}{V \times d} \quad (3.4)$$

here m(saturated) was the mass of hydrogel when it was completely sunk in liquid, and m(dry) was the dry weight of hydrogel. V was the volume of the hydrogel and d was the density of cyclohexane.

3.2.6 *In vitro* cell viability

L929 mouse fibroblast cell line (NCTC clone 929, derivative of *Strain L*) is the recommended strain to be used *in vitro* cytotoxicity studies, as in ISO 10993-5. All cell culture experiments were practiced with sterile equipment under biosafety cabinet class II (Metisafe, Turkey).

The cells were cultured in Dulbecco's Modified Eagle Medium (DMEM) - high glucose with L-glutamine containing 10% (v/v) fetal bovine serum (FBS) and 0.10 % (v/v) streptomycin/penicillin at 37°C under a humidified atmosphere of 5% CO_2 in an incubator (PHCbi Corp., Japan). The medium was changed after every three days. The cells grown to confluency were detached with Trypsin 0.25% - EDTA 0.02% in Hank's Balanced Salt Solution (HBSS) for sub-culturing.

For the sterilization process, hydrogels were incubated in a 70% (v/v) ethanol solution for 1 hour. Subsequently, each side of the hydrogel was exposed to UV light for an additional hour. Sterilized hydrogel groups were placed into the 24-well cell culture plates (n=4). They were washed with sterile phosphate-buffered saline (PBS) twice to remove residues. Cell culture medium was then added dropwise to wet the hydrogel surface. 100 µL of cell suspension with a density of 5.0×10^4 cells/mL was seeded on the sterilized hydrogels and incubated in a CO_2 incubator at 37°C for 1, 4, and 7 days in a 5% CO_2 atmosphere. Cell culture medium, the cells incubated without hydrogels (TCP) and hydrogels without seeding cells were used as control groups. At the end of each incubation period, changes in the cell viability of cells incubated with hydrogels were evaluated by Resazurin reduction assay [139]. Briefly, 0.50 mg/mL Resazurin salt solution was prepared in sterile PBS and filtered with a 0.2-micron membrane filter to make 10X Resazurin solution. This solution was diluted to 1X working solution with DMEM high glucose without phenol red. At the end of each incubation period, the cell culture medium was removed from TCP and the hydrogel groups, and 500 µL of working solution was added to each well. TCP and hydrogel groups were incubated with a working solution for 4 hours at 37°C in a 5% CO_2 atmosphere. At the end of the incubation, the Resazurin working solution was removed and transferred into a 96-well plate. The OD was recorded at 570 nm and 600 nm with a microplate reader (Agilent, USA). The molar extinction coefficients for the oxidized and reduced Resazurin are given in Table 3.3. and the following absorbance equation given in the Resazurin assay technical datasheet was used:

$$Reduction\ \% = \frac{(\varepsilon OX_{600nm} \times A570nm_{tx}) - (\varepsilon OX_{570nm} \times A600nm_{tx})}{(\varepsilon RED_{570nm} \times A600nm_{t0}) - (\varepsilon RED_{600nm} \times A570nm_{t0})} \quad (3.5)$$

where ε is the molar extinction coefficient for Resazurin, A is the absorbance at the given wavelength, t_0 is the first measurement, and t_x is the measurement at a given time x.

Table 3. 3. The molar extinction coefficients of oxidized and reduced Resazurin

Wavelength	Reduced Resazurin	Oxidized Resazurin
570 nm	155,677	80,586
600 nm	14,652	117,216

3.2.7. Transformation with miR-21 expression vector and plasmid isolation

Competent cells were needed to transform *Escherichia coli (E.coli)* with the mir21 expression plasmid to copy it in number and make cryo-preserved stocks. To start with, a single colony of *E.coli* DH5α strain was inoculated in 10 mL LB broth, and the LB broth containing 25 µg/mL kanamycin was picked as control. The single colony was then incubated overnight in a shaking incubator (Panasonic, Japan), at 200 rpm and 37°C.

When the culture's optical density at 600 nm (OD_{600}) reached between 0.3 – 0.5 (middle of the log phase), the bacteria culture was centrifuged at 7000 rpm, 4°C, for 10 minutes. The supernatant was discarded, and the cell pellet was re-suspended with 20 mL of ice-cold, sterile 50 mM calcium chloride solution. Cell suspensions were left on ice for 15 minutes, and then collected with centrifugation again. The supernatant was poured off and 5 mL of sterile, ice-cold 50 mM $CaCl_2$ with 15% (v/v) glycerol was added into each pellet and homogeneously mixed. The mixture was aliquoted in 50 µL volumes and stored at -86 °C ultra-freezer (Thermo Scientific, USA) for up to 1 year.

1-5 µL of plasmid DNA, corresponding to 10 pg - 100 ng, was mixed into the 20-50 µL of competent cells (DNA: competent cells, 1:10, v/v) in an Eppendorf tube. The mixture was mixed gently and allowed to sit on ice for 20-30 minutes. Later, each transformation tubes were heat-shocked by placing ½ of the tube's bottom into a 42 °C water bath for 45-50 seconds and putting it back into the ice for 2 minutes. Cells were grown in SOC medium (Super Optimal Broth) inside a shaking incubator (225 rpm) at 37°C, for 60 minutes. The

culture was centrifuged at 4500 rpm, at RT for 5 minutes. The pellet of cells was reconstituted with the 100 µL of supernatant. Finally, the whole suspension was plated onto a kanamycin+LB agar plate and incubated for 18-24 hours. The grown colonies on the selective agar media were the confirmation of the transformation because the vector contained the kanamycin resistance gene. The single colonies were picked separately by a sterile pipette tip and were grown in a shaker incubator at 200 rpm and 37°C, for 18-24 hours. To obtain maximum yield, an 18–20 hour incubation period was strictly followed. Subsequently, transformant culture was aliquoted in LB containing 15% (v/v) glycerol for storage at -86 °C in an ultra-freezer.

For plasmid isolation, inoculum from frozen transformant stock was suspended in 2 mL of fresh antibiotic-selective LB broth and incubated at 37°C, overnight. 2 mL of transformed *E.coli* culture was transferred into two micro-centrifuge tubes and centrifuged at 10,000 g for 30 seconds. Solutions for plasmid isolation are given in Appendix B. The supernatant was poured off, and the pellet was resuspended in 100 µL of cold solution I. Later, 200 µL of solution II was added and the mixture became clearer and thicker as the proteins and DNA were denaturated. Solution II was not vortexed to prevent contamination. The solution was incubated on ice for 5 minutes before 150 µL of cold solution III was added to each tube. After this step, a white precipitate was formed which contained bacterial proteins and genomic DNA. The pellet included proteins, cell fragments, salts, and particles after centrifugation was done. The supernatant contained plasmid DNA (pDNA) and was collected into a new tube by pipetting carefully. To digest single-stranded RNAs, 5 µL of 2 mg/mL RNAse A enzyme was added to the supernatant and incubated at 37°C for 5 minutes. After RNAse treatment, 2.5 volumes of absolute ethanol and 0.1 volumes of 3 M sodium acetate solution (pH 4.8) were mixed well with plasmid DNA solution by inverting. Later, it was incubated in a - 86°C freezer for 30 minutes to help the precipitation. To collect the precipitated plasmid DNA, tubes were centrifuged at 12,000 rpm for 30 minutes, at 4°C. The pellet was first air-dried for 30 mins on ice and then, it was resuspended in 50 µL of Tris-EDTA (TE) buffer and stored in a -20°C freezer until usage.

Isolated plasmid DNA was quantified at 260 nm by using a nanodrop spectrophotometer (Biotek, USA). In addition, the absorbance value ratios, A260/A280, and A230/A26 were checked to see if there was any contamination. The A260/A280 and

A230/A260 ratios were used to check any contamination. In addition to quantification, qualification analysis was performed using agarose gel electrophoresis. 10 ng of isolated pDNA was mixed with 6X DNA gel loading dye in a ratio of 1:5 (v/v), and also 1 kb DNA ladder with the same ratio was mixed and loaded into wells of 1% agarose gel containing 0.5 µg/mL ethidium bromide (EtBr). Then, the gel was run in 1X Tris-Acetate EDTA (TAE) buffer at 90 volts for 30 minutes. After electrophoresis, EtBr containing agarose gel was visualized with a UV-transilluminator under 254-302 nm (Syn-Gene, UK).

3.2.8. pDNA: PEI complex preparation

The transfection process happens when exogenous nucleic acids are synthetically introduced into eukaryotic cells employing nano-complexes such as lipoplexes, liposomes, and polyplexes. Polyethyleneimine (PEI) is a linear cationic polymer that assembles itself around negatively charged nucleic acids to a form called polyplex. This complex is then used to deliver foreign genetic material into the target cell. For this purpose, a synthetic cationic linear polymer called PEIpro® (PolyPlus, France) was purchased to utilize in transfection experiments. Before cell culture, PEI and DNA complexes were established and examined for their stability and particle properties. Complexes were formed according to the manufacturer's protocol.

Table 3. 4. Parameters to prepare PEI:pDNA Complexation for transfection

Amount of pDNA	1 µg pDNA
pDNA:PEI ratio (µg: µL)	1:1 (1 µg pDNA:1 µL PEIPro®)
% of total culture volume	10 %
Incubation time	20 minutes
Complex medium	Opti-MEM™

Briefly, 1 µg of miR-21 plasmid was mixed with 1 µL of PEIpro solution (1 mg/mL) in Opti-MEM. The mixture was vortexed for 20 seconds and then, it was incubated at room temperature for 20 minutes to form complexes. Incubation time remained the same (20

minutes) for all the experiments for good, reliable transfection efficiency and the reactions were set aseptically in polypropylene tubes as recommended by the manufacturer.

3.2.8.1. Particle characterization

The complex solution was diluted to a 1:10 ratio with distilled water (1 mL) and vortexed well. The particle size and zeta potential analysis of PEIpro/miR-21 plasmid complexes were conducted using a Zetasizer Nano ZSP analyzer (Malvern Panalytical, UK). The refractive index (RI) for PEI was chosen as 1.45 and the solvent was chosen as distilled water.

3.2.8.2 Complex loading onto hydrogels and their characterizations

On account of the results from hydrogel characterizations, the CKA1 (1:1:1) group was chosen for the rest of the study. In advance of hydrogel loading, CKA1 hydrogels were prepared and sterilized according to the instructions described in Section 3.2.6.

The same amount of naked plasmid and complexes were first measured with a NanoDrop spectrophotometer, then added dropwise onto hydrogels in 100 µL of volume per each for a 1.9 cm^2 sized hydrogel (fitting in a 24-well plate). Loaded hydrogel groups and empty hydrogel groups were immersed in sterile PBS (pH 7.4) to be incubated at 37°C for 1 week. Each day, samples from the release solution were collected and measured via NanoDrop. To compare and eliminate background signals from hydrogels, collected samples were stained with acridine orange. For this, an acridine orange calibration curve was drawn with known concentrations of naked plasmid serially 2-fold diluted in PBS solution. PBS as blank, empty hydrogel, empty PEI solution as controls, and daily samples were incubated in 10 µg/mL acridine orange solution at 4°C, overnight. Afterward, 100 µL of solutions were transferred into a black 96-well plate with solid flat bottoms for fluorescent signal measurement from acridine orange at 500/526 nm for double-stranded (ds) DNA detection.

Besides the release study, gel retardation assay was applied to samples. In terms of the assay's principle to detect protein/DNA complexes by their differences in the electrophoretic mobility, PEI/pDNA complexes and naked pDNA were compared on agarose gel

electrophoresis. 1% (w/v) agarose (molecular biology grade) was completely dissolved in 1X TAE buffer by heating in a microwave. After the agarose solution was cooled down to 50-60°C, ethidium bromide solution to a final concentration of 0.5 µg/mL was added into the agarose solution and swirled to mix. By that time, the electrophoresis tank was filled with 1X TAE buffer containing EtBr, as well. Next, the gel solution was poured on the tray with the well comb placed immediately and then it was allowed for polymerization for 30 minutes. During polymerization, half of the samples and naked pDNA were treated with 5 µL of DNase1 solution (in its buffer) at 37°C for 1 hour to observe the PEIPro's preservation of plasmid from endonuclease activities. Next, the comb was removed carefully without distorting shapes and the agarose gel was placed into the tank to soak the buffer and pre-runned as empty for 5 minutes for the buffer to run inside. Loading dye (6X): The sample, as well as the molecular weight ladder, were mixed well in a ratio of 1:5 (v/v) and loaded into wells slowly and carefully. The electrophoresis continued for 1.5 hours at 30 milliamperes (mA). At the end of the procedure, the pDNA and complex samples in the agarose gel were visualized under a UV-transilluminator.

3.2.9. Transfection of HUVECs

By the completion of PEIpro:pDNA complex characterizations and stability, HUVECs were started to be cultured for transfection experiments. The cells were cultured in Ham's F-12K (Kaighn's) Medium (F-12K) containing endothelial cell growth kit – BBE and 0.10 % (v/v) streptomycin/penicillin at 37°C under a humidified atmosphere of 5% CO_2 in an incubator (PHCbi Corp., Japan). The supplements of the endothelial cell growth kit were transferred into the basal medium as indicated in Table 3.5. The medium was changed after every two days. The cells grown to confluency were detached with Trypsin 0.25% - EDTA 0.02% in Hank's Balanced Salt Solution (HBSS) for sub-culturing. Subcultivation was done at the recommended ratio of 1:2.

Table 3. 5. Supplements in endothelial cell growth kit – BBE

Ingredient	Volume	Final Concentration
Bovine Brain Extract (BBE)	1.0 mL	0.2%
rhEGF	0.5 mL	5 ng/mL
L-glutamine	25.0 mL	10 mM
Heparin sulfate	0.5 mL	0.75 Units/mL
Hydrocortisone hemisuccinate	0.5 mL	1 µg/mL
Fetal Bovine Serum	10.0 mL	2%
Ascorbic acid	0.5 mL	50 µg/mL

3.2.9.1 HUVEC seeding onto hydrogels

Foremost, hydrogels were sterilized as described in section 3.2.6. Sterilized hydrogels were placed into the 12-well cell culture plates (n=4). They were washed with sterile phosphate-buffered saline (PBS) twice to remove residues. Opti-MEM reduced medium was then added dropwise to wet and swell the hydrogel. Meanwhile, the PEI:pDNA complexes were prepared according to optimized amounts given in 3.2.8. 200 µL of the complex was dropped onto each hydrogel group (day 1, day 2, day 3, day 4) and TCP-miR -21, except TCP only. They were incubated at RT while HUVECs were detached and suspended in Opti-MEM. 200 µL of cell suspension comprising 5.0×10^5 cells was transferred to all experiment groups. The level of reduced medium in wells was filled up to 1 mL after 1-2 hours and then incubated for 4 hours. At the end of the incubation period for transfection, Opti-MEM was changed into the complete F-12K medium. One set of hydrogels and controls was fixed for imaging (n=4), and another set was used for gene expression analysis (n=4).

3.2.10. Imaging of miR-21 transfected HUVECs

Cells at their predetermined time points (for hydrogels: 24, 48, 72, 96 hours; for controls: 48 hours) were fixed with 4% paraformaldehyde solution in sterile PBS for 30

minutes after their medium was aspirated. Following fixation, fixed cells were washed with sterile PBS three times and stored in 1X PBS at 4°C until the next steps.

To visualize the nuclei of cells, fixed cells were stained with DAPI. For this purpose, 1 mg/mL stock DAPI solution was diluted to a ratio of 1:1000 in PBS (1 μg/mL as final concentration) and incubated at dark and room temperature, for 15 minutes. 1 mL of DAPI working solution was transferred into the wells and incubated at dark, RT for 30 minutes. Samples were then washed 3 times with PBS for 3 minutes. Storage was held in 1X PBS at 4°C covered with aluminum foil.

Fixed and stained cells of TCP groups were examined and photographed under an inverted fluorescent microscope (Leica DMi8, Germany) for the following images:

1. For the cells: Bright field, 10X magnification.
2. For nuclei: With standard DAPI filter, excitation/emission at 358/461 nm, 10X magnification.
3. For reporter protein: With standard FITC filter, excitation/emission at 489/508 nm, 10X magnification.

Since hydrogels are 3-dimensional structures, confocal scanning laser microscopy (CSLM) was utilized to image HUVECs on the surface and inside the hydrogels. Cells were imaged with a confocal microscope (LSM980, Zeiss, Germany) under 40X, 25 μm slices, with standard DAPI and eGFP filters. Z-stacks of images were processed by using ImageJ 1.54h (Rasband, W. & NIH, USA).

3.2.11. mRNA expression levels miR-21 and angiogenic markers in HUVECs

3.2.11.1 RNA isolation

The isolation of total RNA from miR21 transfected HUVEC cells in various time points (24, 48, 72, and 96 hours), was performed using a total RNA isolation kit (Genaxxon, Germany). Instructions from the manufacturer's protocol were followed. To sum up, the cell medium was aspirated, and cells were washed with PBS, and then lysis buffer including 1% β-mercaptoethanol was added into the wells. At this stage, hydrogels were sliced into big

chunks with a sterile scalpel and taken away into a -86 ºC ultra-freezer. The remaining protocol was applied for TCP controls. The lysis buffer was incubated for 1 minute with gentle shaking. The lysis solution was centrifuged at 14,000 g for 120 seconds, and the supernatant was transferred into an RNase-free reaction tube and 70% ethanol was added to the transferred supernatant by mixing well. The solution was put into an RNA Purification Column and spun for 15 seconds at 14,000 g. Flow-through was discarded and a mini-column was placed into a new collection tube. The column was washed with wash buffer II, beforehand the DNase I treatment. Samples were treated with 1 unit of DNase in its reaction buffer for 15 minutes at RT. Later, wash buffer I was added and centrifuged at 14,000 g for 15 seconds, flow through was discarded and the collection tube was re-used. Next, wash buffer II was transferred into the mini-column and centrifuged for 15 seconds, at 14,000 g. This step was repeated before centrifugation at 14,000 g for 90 seconds. The liquid part was discarded and the mini-column was put into an RNase-free 1.5 mL Eppendorf tube. Finally, the collected total RNA was eluted with 30 µL elution buffer by spinning at 14,000 g for 60 seconds. The isolated RNA was kept at -86°C for the downstream applications. The yield of RNA samples was determined by measuring optical density using a NanoDrop spectrophotometer (Agilent, USA). For total RNA extraction from hydrogels, hydrogels were frozen in lysis buffer before they were thawed on ice, and after thawing they were vortexed vigorously for 60 seconds. The centrifugation step was done twice to remove the remaining hydrogel debris and the rest of the procedure was applied as the same.

3.2.11.2. cDNA synthesis

Isolated RNAs were converted to cDNAs by using OneScript® Plus cDNA Synthesis Kit to determine the expression of angiogenic gene markers (PTEN, SPRY1, SPRY2, VEGFA). For cDNA synthesis, the reaction mix was prepared according to Table 3.6 and incubated at 65°C for 5 mins to denaturation 2° structures. It was then chilled on ice for 1 minute. Next, synthesis was performed at 50°C, for 30 mins. The reaction was stopped by heating at 85°C for 5 minutes. cDNA samples were chilled on ice and stored at -20°C for a short term.

Table 3. 6. cDNA synthesis reaction conditions

Components	Component Volume
5X RT Buffer	9 µl
dNTP	2 µl
Primers (Random hexamer + OligodT)	2 µl
Total RNA (1 ng - 2 µg/rxn)	30 µl
OneScript® Plus RTase	2 µl
Total	45 µl

cDNA synthesis for miR-21 and small nucleolar RNA was performed differently with qScript® microRNA cDNA Synthesis Kit. miR-21 and snRNAs were polyadenylated with poly(A)-tailing reaction before cDNA synthesis because these RNAs are not normally polyadenylated. RNA isolates were thawed on ice and the poly(A)-tailing reaction conditions were as follows (Table 3.7.).

Table 3. 7. miR-21 Poly(A)tailing reaction conditions

Components	Component Volume
5X Poly(A) tailing Buffer	8 µl
Poly(A) Polymerase	4 µl
Total RNA (up to 1 µg/rxn)	30 µl
Total	42 µl

Components were mixed gently and briefly centrifuged for a few seconds. Poly(A)tailing reaction was incubated at 37°C for 1 hour, followed by heating at 70°C for 5 minutes. Samples were spun shortly and chilled on ice for 1 minute before cDNA synthesis. cDNA synthesis was applied after poly(A)tailing. The reaction took place with the given in Table 3.8.

Table 3. 8. miR-21 cDNA synthesis reaction conditions

Components	Component Volume
Poly(A)tailing rxn (from previous)	40 µl
microRNA cDNA Reaction Mix	36 µl
qScript Reverse Transcriptase	4 µl
Total	80 µl

Reaction solutions were gently mixed and then briefly spun to collect contents at the bottom of the tube. The cDNA synthesis reaction was first incubated for 20 minutes at 42°C, then heated at 85°C for 5 minutes. Samples were chilled on ice and stored at –20°C for real-time PCR reactions.

3.2.11.3. Real-time polymerase chain reaction (qPCR)

Primer pairs for phosphatase and tensin homolog (PTEN), sprouty homolog 1 (SPRY1), sprout homolog 2 (SPRY2), and vascular endothelial growth factor A (VEGFA), glyceraldehyde-3-phosphate dehydrogenase (GAPDH)s for human were designed by using the online tool Primer3web version 4.1.0 [140]. The primer pair for miR-21 was supplied by the manufacturer. Primer pairs for RT-qPCR belonging to the related genes are supplied in Table 3.9**.**

Table 3. 9. Primer sequences for the target genes

Gene	Primer Sequence (5'-3')	Tm (ºC)	Product Size (bp)	NCBI Accession Number
PTEN	F-CATCAGCTACCGCCAAGTCC R-CTGTCATGTCTGGGAGCCTG	60	117	NM_000314.8
SPRY1	F-TCCTGTTTGGCCTGTAACCG R-TCGTCGTCATTGGAGCAGTG	60	113	NM_001258038.2
SPRY2	F-TCAGAGCCATCCGAAACACC R-CGTGTTTGTGCTGAGTGGAG	60	102	NM_005842.4
VEGFA	F-CTGCTCTACCTCCACCATGC R-GGGTCTCGATTGGATGGCAG	60	130	NM_001171623.2
GAPDH	F-CCCACTCCTCCACCTTTGAC R-CCACCACCCTGTTGCTGTAG	60	108	NM_002046.7
miR-21	F- GCTAGCTTATCAGACTGATGTTGAAA R-GCATAGACCTGAATGGCGGTA	59	84	MIMAT0000076
U6	F-GCAAATTCGTGAAGCGTTCC R-GCATAGACCTGAATGGCGGTA	59	84	NR_002752.1
SNORD44	F- GCAAATGCTGACTGAACATGAA R-GCATAGACCTGAATGGCGGTA	59	84	NR_002750.2

For the RT-qPCR reaction, PerfeCTa® SYBR® Green FastMix® was used. According to the instructions from the supplier's manual, reaction conditions were as given in Table 3.10.

Table 3. 10. RT-qPCR reaction conditions

Components	Component Volume
PerfeCTa SYBR Green FastMix (2X)	25 µl
Forward primer (10 µM)	1 µl
Reverse primer (10 µM)	1 µl
cDNA Template	23 µl
Total	50 µl

Reaction tubes were vortexed very gently to mix contents and spun briefly to collect components at the bottom of the reaction tube. A 3-step cycling protocol was applied and given below:

1) Pre-incubation: 95°C for 2 minutes
2) PCR (40 cycles):
   a. Denaturation: 95°C for 5 seconds
   b. Annealing: 60°C for 15 seconds (miR-21 and its house-keeping genes)
      59ºC for 15 seconds (Target genes and house-keeping gene)
   c. Extension: 70°C for 15 seconds

Fold changes in expressions were calculated by using the $2^{-\Delta\Delta ct}$ method [31].

3.2.12. Statistical Analysis

Statistical analysis was done for the results of hydrogel characterization tests, *in vitro* cell proliferation tests, and real-time polymerase chain reactions. To compare the treatment samples and controls within a single parameter, a one-way ANOVA test was applied with Tukey's multiple comparison test for the post hoc pairwise comparisons via SPSS 28.0 statistical software (IBM SPSS Statistics, USA). Differences/variations were established as significant for $p \leq 0.05$.

4. RESULTS AND DISCUSSION

4.1. Characterization of isolated keratin and collagen

FT-IR spectra of isolated keratin and collagen are given in Figure 4.1. In the FT-IR spectrum of isolated keratin, the broad absorption band at 3378 cm^{-1} can be assigned to the Amide A structure. The absorption peaks at 1644 cm^{-1} and 1531 cm^{-1} are related to Amide I and Amide II structure, respectively. The broad absorption band of about 1290 cm^{-1} is attributed to the Amide III structure of keratin. Amide A absorption band is associated with N-N and N-H stretching vibrations, Amide I peaks correspond to C=O stretching, Amide II peaks represent N-H bending and C-N stretching vibrations, while Amide III peaks indicate C-N stretching, C=O bending and the C-C stretching vibrations [141]. The peaks at 1061 cm^{-1} and 1025 cm^{-1} could belong to the asymmetric and symmetric S–O stretching vibrations resulting from cysteine-S-sulfonated residues that occurred during the extraction process [142]. The peaks at 985 cm^{-1} and 584 cm^{-1} could be attributed to the C-S stretching vibration or disulfide (S-S) bond inherent to the native keratin structure, while the absorption band around 2812 cm^{-1} indicates the presence of S-H stretching vibration of the thiol group (-SH) [143, 144].

In the FT-IR spectrum of isolated collagen, the characteristic peaks associated with the collagen structure, namely Amide A-B and Amide I-II-III peaks were observed (Figure 4.1.a). Amide A absorption band in the 3500-3300 cm^{-1} region indicates N-H stretching of collagen chains, while the Amide B peak due to C-N stretching vibrations of collagen type I was observed at 3000-2800 cm^{-1}. The two peaks within the 1700-1500 cm^{-1} region are related to Amide I (due to N-H bending vibrations coupled to C=O stretching vibrations) and Amide II (due to C-N stretching vibrations coupled to N-H bending vibrations) [145]. The Amide III peak in the 1250-1020 cm^{-1} region corresponded to the C-N stretching and N-H and $–CH_2$ bending vibrations of collagen type I structure [134, 146].

In addition to the FT-IR spectrum of isolated collagen, Figure 4.1.b illustrates the FT-IR spectra of commercially obtained lyophilized Type I bovine collagen and commercial bovine gelatin powder, serving to compare their respective chemical structure. Commercial

bovine Type I collagen was used as the commercial equivalent for isolated collagen, while commercial bovine gelatin powder was selected to discern native collagen peaks. Amide B and amide III peaks were absent, and the amide A peak was broader for gelatin compared to the collagen.

The molecular weight and structural stability of the isolated keratin and collagen were investigated by the SDS-PAGE analysis (Figure 4.2.) According to the results of SDS-PAGE, two major bands were detected in two human hair keratin samples (K1 and K2), with molecular weights around 45 kDa and 63 kDa. As demonstrated in a previous study, two bands observed in SDS-PAGE of keratin samples at 39–45 kDa and 50–55 kDa are associated with the presence of type I (acidic) and type II (basic) keratins [147]. As depicted in Figure 4.2.a, both isolated keratin samples, K1 and K2, displayed identical SDS-PAGE consistent with the results of previous studies [148, 149].

As shown in Figure 4.2.b, SDS-PAGE analysis of different collagen isolates (C1-C5) from bovine Achilles' tendons revealed the presence of four characteristic bands known as gamma (γ), beta (β), alpha I (α1), and alpha II (α2) around 300 kDa, 245 kDa, 135 kDa, and 100 kDa, respectively. This result was compatible with the results of a previous study [134, 150].

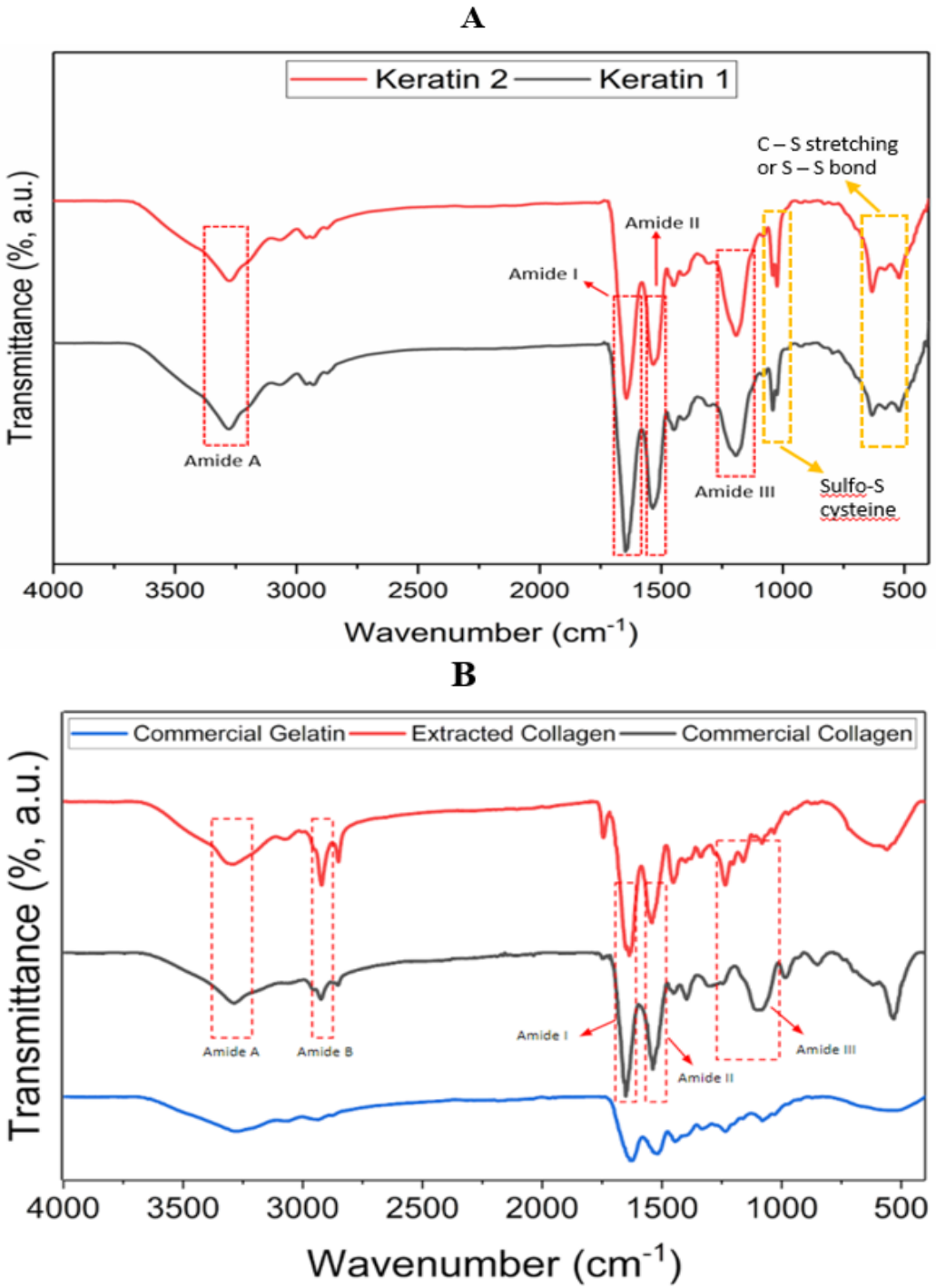

Figure 4. 1. FT-IR spectrum of isolated human hair keratin (A) and collagen isolated from bovine Achilles tendon, along with commercial collagen and gelatin (B)

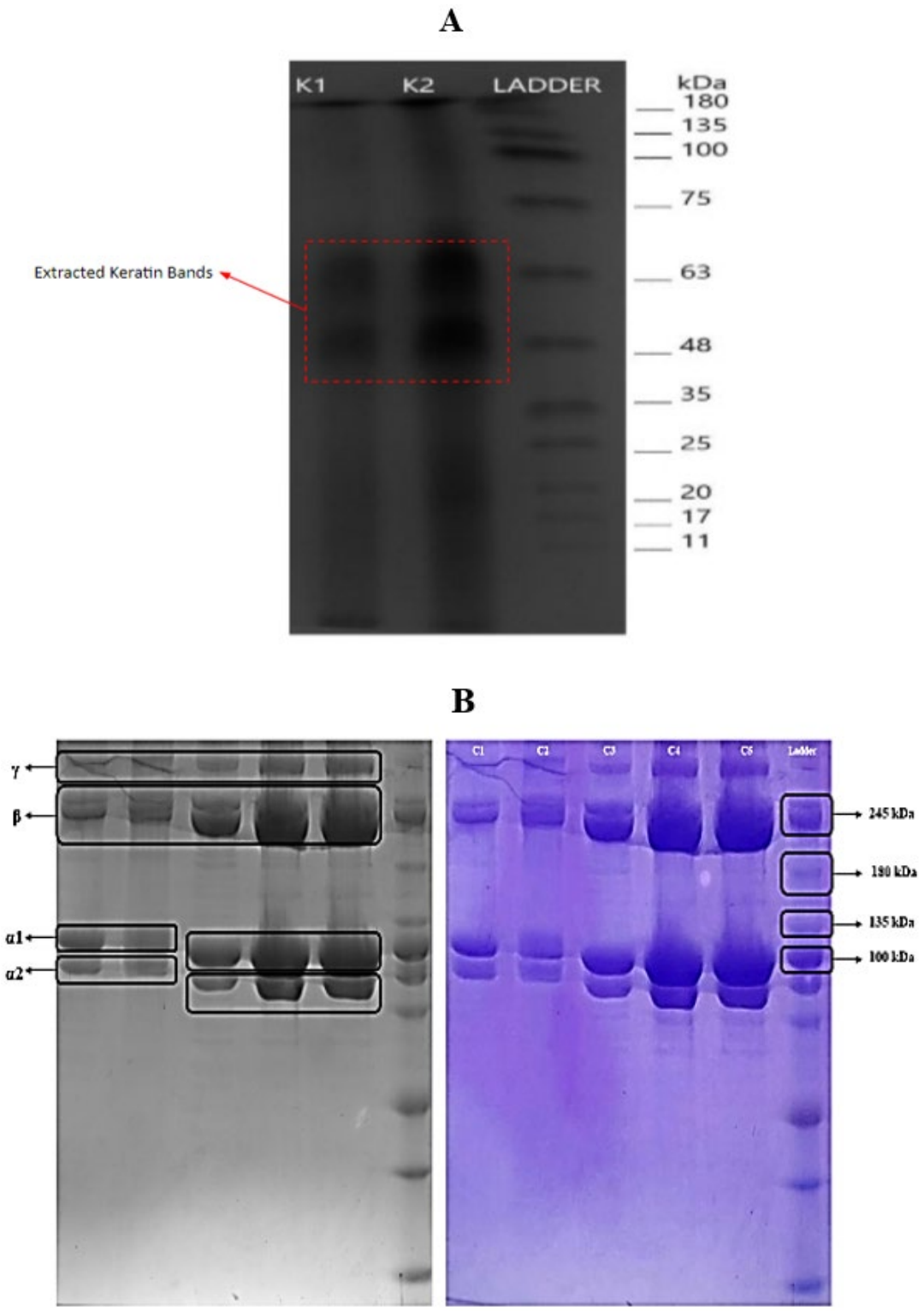

Figure 4. 2. SDS-PAGE results of extracted keratin (A) and collagen samples (B). Lane 1: keratin sample 1, K1; Lane 2: keratin sample 2, K2; and Lane 3: Standard protein marker (A). Lane 1 - 5: Different collagen extracts (C1-C5) and Lane 6: Standard protein marker (B)

4.2. Characterizations of collagen/keratin/alginate hydrogels

The physical, chemical, and biological characteristics of four different hydrogel groups with different ratios of collagen, keratin, and alginate were examined. Based on the optimization studies, the hydrogel group that exhibited the highest suitability was chosen for the preparation of PEI:miR-21 plasmid complex-loaded hydrogels for subsequent investigations.

4.2.1. Chemical characterization of hydrogels

FT-IR spectra of the hydrogel groups and the powder mixture of collagen, keratin, and alginate are given in Figure 4.3. Characteristic peaks and bands of collagen and keratin are described in Section 4.1. were observed in the FT-IR spectra of all hydrogel groups and the powder mixture. The stretching vibrations of O-H, the stretching vibration of C-H bonds, the asymmetric and symmetric stretching vibration of COO− groups, C-O-C stretching vibrations, and O-C-O- stretching vibrations of alginate were displaced at around 3300 cm^{-1}, 2800-2900 cm^{-1}, 1500 cm^{-1}, 1075 cm^{-1} and 1025 cm^{-1}, respectively [151]. However, these characteristic peaks associated with the alginate component were found to overlap with those related to keratin and collagen described in Section 4.1. When the FT-IR spectra of hydrogel groups and powder mixture were compared, it was noted that a certain peak disappeared at around 1200 cm^{-1} while a new peak appeared at around 800 cm^{-1}. In addition, the position of the amide I peak of keratin and collagen shifted, indicating that the hydroxyl group of alginate could interact with amino groups of keratin. This change might result from the cross-linking between functional groups of keratin, collagen, and alginate. In line with this observation, the CKA1 group showed more resemblance to the powder mix which might suggest more protein binding motifs such as GFOGER in protein's native proteins [152]. This is because of the fewer cross-linking points present in CKA1 compared to the other groups having higher protein content. CKA1 might have freely available functional groups that had not been cross-linked. Therefore, their IR spectra are visible in Figure 4.3.

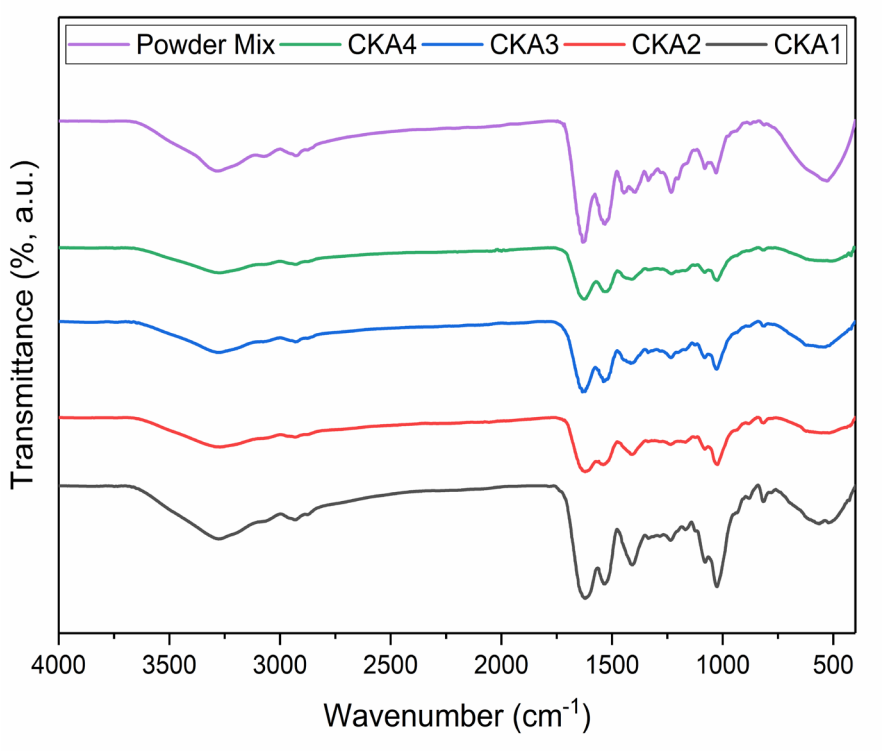

Figure 4. 3. FT-IR spectra of the hydrogel groups and the powder mixture of collagen, keratin, and alginate

4.2.2. Morphological characterization of hydrogels

The macroscopic images of hydrogels are given in Figure 4.4. The macroscopic images of hydrogels were captured at various stages: during the washing step before cross-linking (Figure 4.4.a), after cross-linking (Figure 4.4.b), and following the subsequent washing step (Figure 4.4.c). Upon the view of hydrogels, all groups exhibited a homogenous view in terms of ingredients mixture.

SEM images depicting the cross-section morphology of different hydrogel groups are given in Figure 4.5. All the hydrogel groups had porous three-dimensional structures with varying pore sizes. The CKA1 (consisting of consisting of 1% w/v of each component) group exhibited larger macropores (>400 µm) and superior interconnectivity when compared to the other groups. The cross-linking density likely contributed to the larger and more uniform pores observed in CKA1, as it accelerates sublimation during lyophilization since it causes the sublimation to occur faster during lyophilization [153].

In group CKA1, the distribution of the pores and their sizes appeared to be more uniform, as seen in Figure 4.5.a_1 and Figure 4.5.a_2. This difference might be due to the expected result of the increasing concentration of collagen, and keratin between groups. For instance, groups CKA2 and CKA4 had smaller pores and flake-like structures, potentially indicating an excess of uncrosslinked keratin (Figure 4.5.b_1, b_2 a, d_1, and d_2). Non-crosslinked excess keratin and collagen residues were observed on the SEM images of CKA2, CKA3, and CKA4 groups. When compared to the groups CKA2 and CKA4, group CKA3 with higher collagen concentration compared to other groups showed a more homogenous porous structure and larger pores (Figure 4.5.c_1, c_2). This might suggest that spontaneous cross-linking between collagen fibers might have been more effective than the self-assembly of keratin. Moreover, the ratio of collagen/keratin/alginate might have a role in pore formation, as evidenced by the observation that during hydrogel preparation, CKA1 (with a 1:1:1 ratio) exhibited the most homogenous and clearest mixture, and formed a pre-gel solution most rapidly at 4 °C. Chemical conditions, degree of cross-linking, size, and hardness could play a role in determining the pore size and distribution [148].

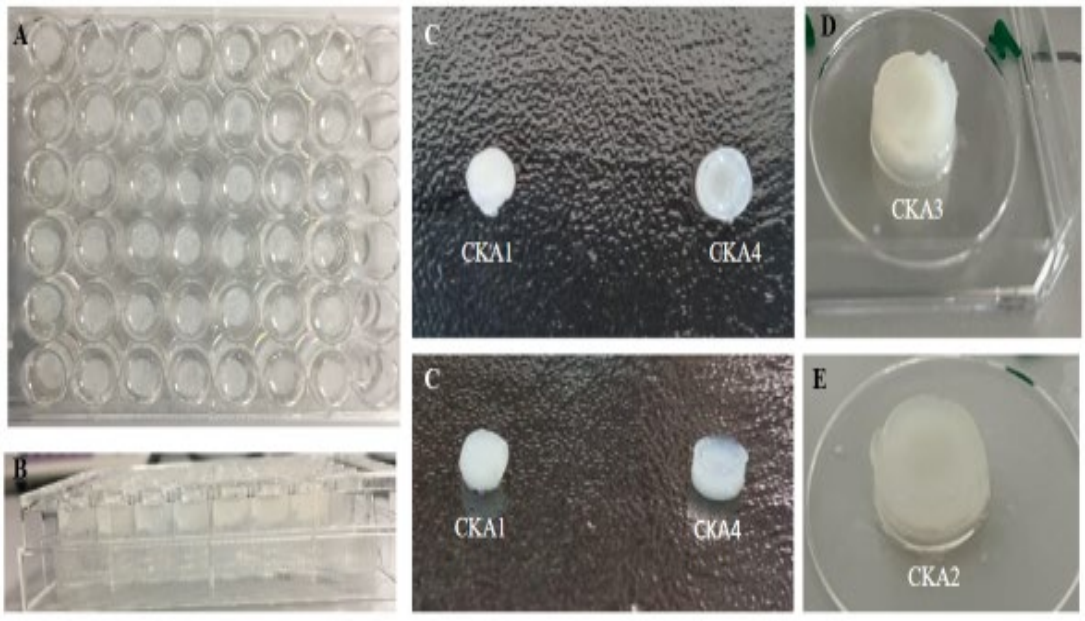

Figure 4. 4. The macroscopic images of hydrogels captured at various stages: during the washing step before cross-linking (A), after cross-linking (B) and following the subsequent washing step (C)

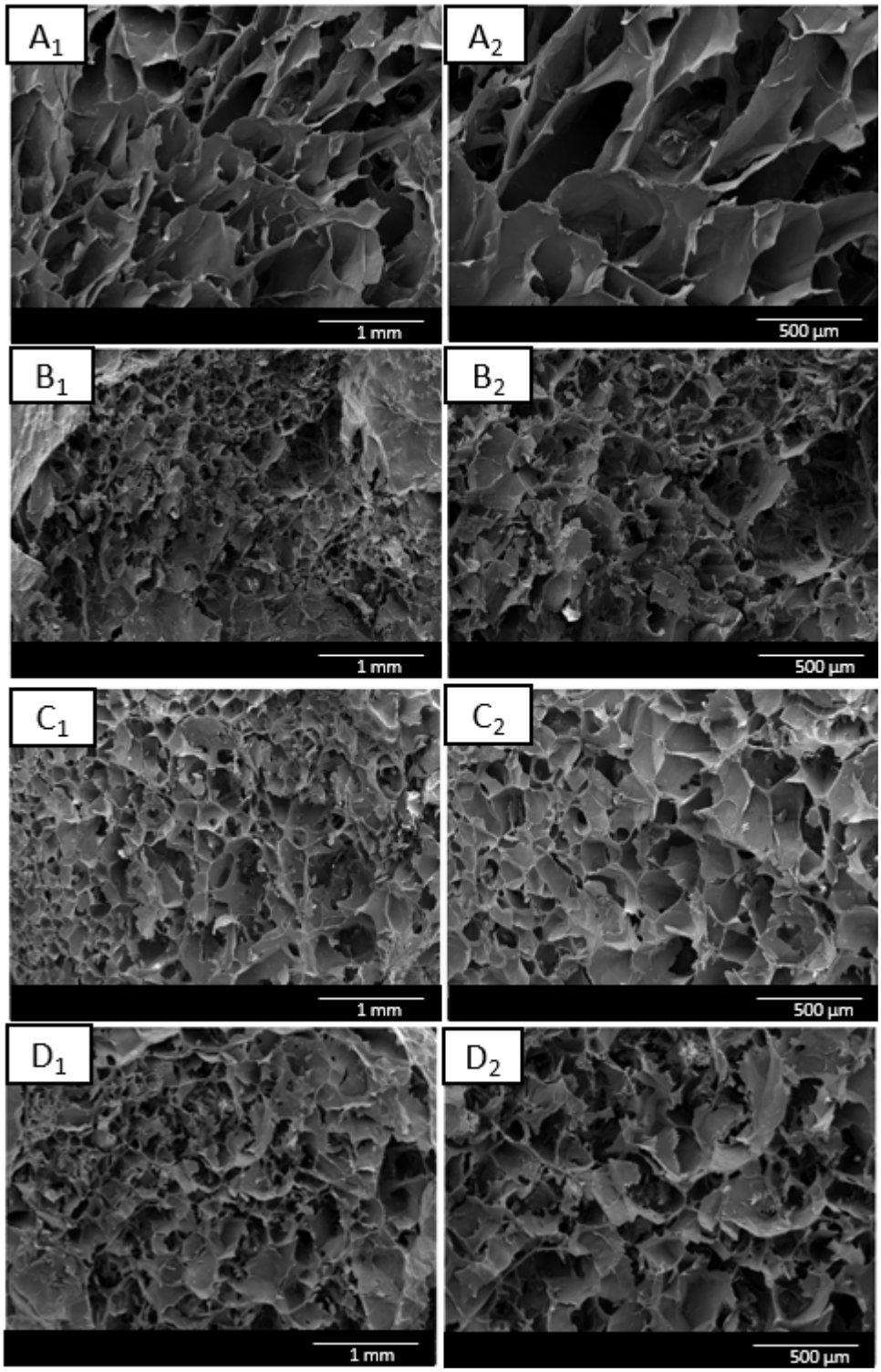

Figure 4. 5. SEM images of the cross-sections of different hydrogel groups: CKA1 (A_1 and A_2), CKA2 (B_1 and B_2), CKA3 (C_1 and C_2), CKA4 (D_1 and D_2) groups under 100x (A_1, B_1, C_1 and D_1) and 200x (A_2, B_2, C_2 and D_2) magnifications

4.2.3. Percent porosity of hydrogels

For biomaterials, porosity and pore size are fundamental properties that affect the biomaterial properties such as mechanical characteristics and drug encapsulation, and are important for cellular behaviors such as cell migration and angiogenesis, especially those with sizes larger than 300 μm [154]. Hydrogel preparation methods, the polymer properties [155], including type, molecular weight, and parameters related to crosslinking, such as degree of crosslinking, concentration, and type of crosslinker [156] could influence the porosity of the hydrogels [157].

According to the results of the liquid displacement method, the CKA1 group had the significantly highest percent porosity (80.89%) compared to other groups (Figure 4.6.). This result was found to be in accordance with the SEM results given in Section 4.2.2. Additionally, there is no significant difference between the percent porosity values of CKA2, CKA3 and CKA4 groups. As the amount of collagen used in the hydrogel preparation increased, the percent porosity decreased. In a previous study conducted by Riedel *et al.*, collagen hydrogels with varying concentrations were prepared by using electron-induced cross-linking to mimic ECM structure [158]. It was seen in the study that the pore sizes of hydrogels tended to decrease with the increasing collagen concentration and the dose of electron beam (cross-linker). The decline in percent porosity of the CKA2, CKA3, and CKA4 groups compared to the CKA1 group may be attributed to increased crosslinking capabilities of collagen as its concentration increases. The enhanced crosslinking capacity of the protein-based components is attributable to a significant rise in the abundance of free functional groups accompanying the increase in collagen content [159]. This implies that hydrogels with collagen content, such as CKA3 and CKA, could exhibit greater stiffness and potentially result in a slower release of encapsulated biological molecules compared to CKA1 and CKA2. Such controlled release kinetics may not be appropriate for wound healing applications, where prompt neo-tissue formation is essential. Therefore, CKA1 and CKA2 groups were found more suitable for the preparation of PEI:miR-21 plasmid complex-loaded hydrogels for subsequent investigations.

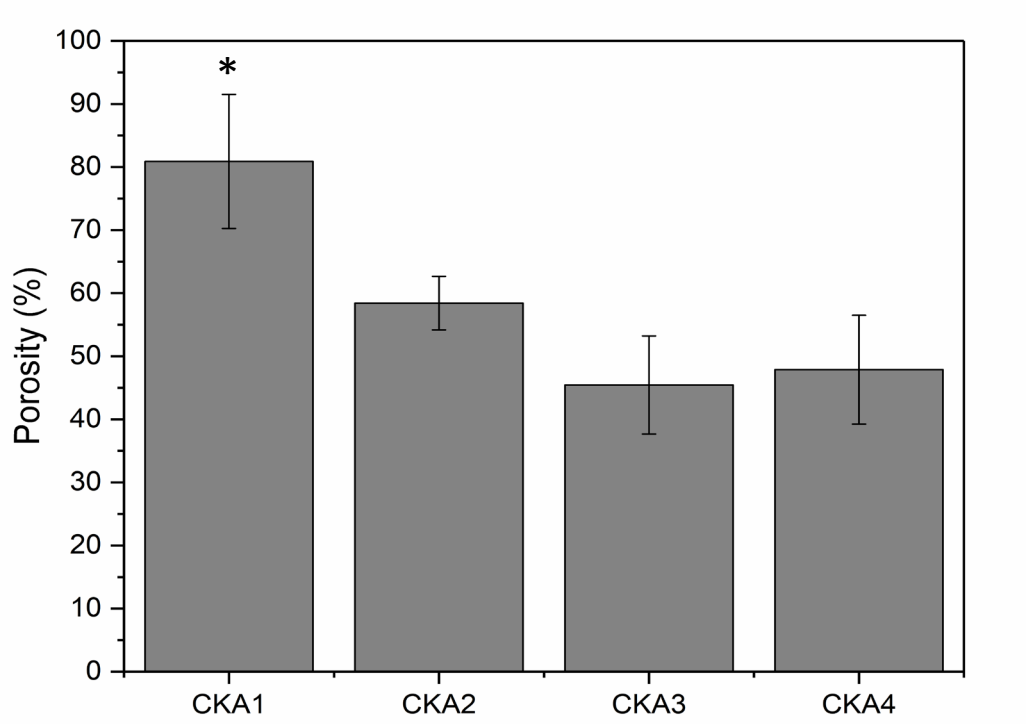

Figure 4. 6. Percent porosities of CKA1, CKA2, CKA3, and CKA4 hydrogel groups. Data are given as mean ± S.D ($p<0.5$)

4.2.4. *In vitro* hydrolytic degradation of hydrogels

Hydrogels should sustain their structural properties for the expected duration depending on the purpose of the study, while also being biodegradable. To assess this, hydrogel groups were immersed in a cell culture medium (pH 7.4) containing sodium azide (NaN_3) and incubated at 37 °C for 21 days (3 weeks). The percentage weight loss of hydrogels was calculated by the formula given in Equation 3.2. and the percent weight loss profiles of hydrogel groups are given in Figure 4.7.

According to the results depicted in Figure 4.7., CKA1 showed the lowest weight loss percentage among all groups. On the other hand, a significant increase in the amount of percent weight loss was observed after day 14. At the end of three weeks, the percentage weight loss ranged from least to most as follows: CKA1, followed by CKA4, with CKA2 and CKA3 exhibiting equivalent levels of percent weight loss. As displayed in Figure 4.7., the total amounts of percent weight loss of the CKA1, CKA2, CKA3, and CKA4 groups

were 15.19%, 41.43%, 42.38%, and 29.94%, respectively. Therefore, two groups (CKA1 and CKA4) were identified as more suitable for the further steps of the study compared to the other groups. It was observed that when the protein concentration increased.

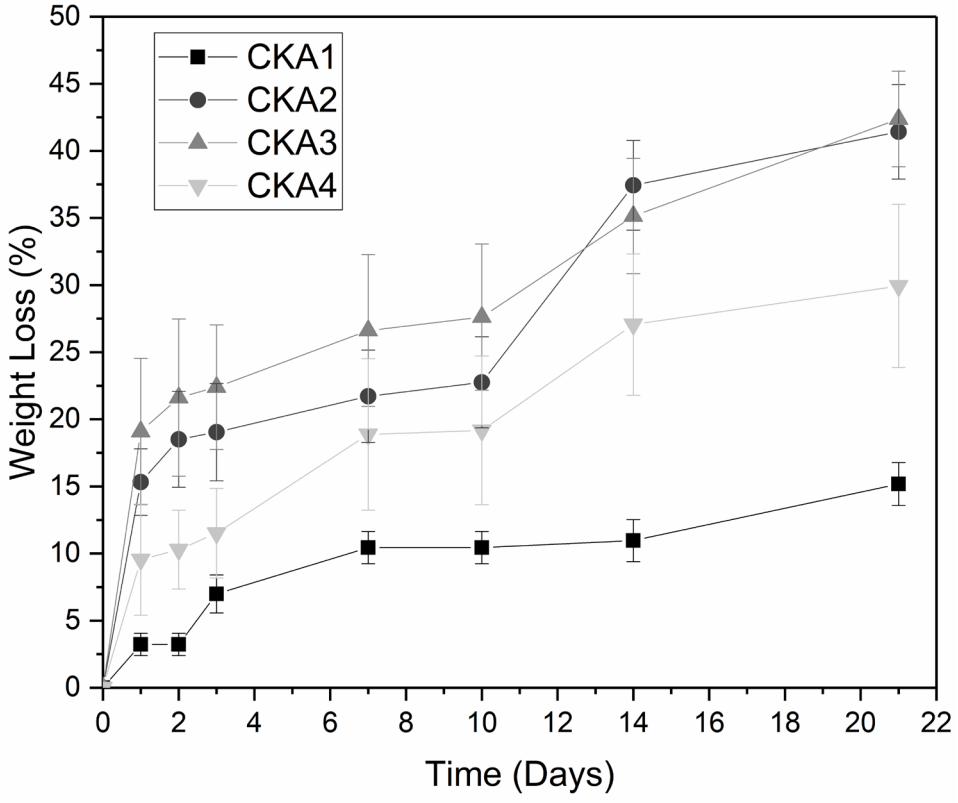

Figure 4.7. Percent weight loss profiles of hydrogel groups in serum-free cell culture medium containing 0.02% NaN_3 (pH 7.40) at 37°C for 21 days. CKA1 demonstrated significantly lowest weight loss compared to other groups in all time points ($p<0.01$). CKA2 and CKA3 showed significantly highest weight loss at the end of the analysis ($p<0.01$). Data are shown as mean ± S.D.

An increase in the keratin and collagen concentration alone, as in the CKA2 and CKA3, resulted in higher weight loss. However, increasing both values together, as in the case of CKA4, resulted in lesser weight loss than CKA2 and CKA3. Here, it could be pointed out that EDC/NHS zero distance cross linker could effectively crosslink free functional groups of -COOH and $-NH_2$. However, increasing the concentration may lead to non-crosslinked functional group presence, and this might lead to faster degradation. Also, lower concentrations of all components in CKA1 could bring about higher water uptake due to

higher inter-chain distance at cross-linked points compared to CKA4. Altogether, higher protein concentration in the hydrogel led to rapid degradation while preventing pore formation.

SEM images depicting the surface morphologies of different hydrogel groups after 21 days of incubation are given in Figure 4.8. These results were in accordance with the results of percentage weight loss. CKA1 surface morphology revealed higher porosity and, on the opposite, CKA4 showed lower porosity on the hydrogel surface. The formation of multiple new pores on the surface of hydrogel groups indicates the *in vitro* degradation potential of hydrogel groups.

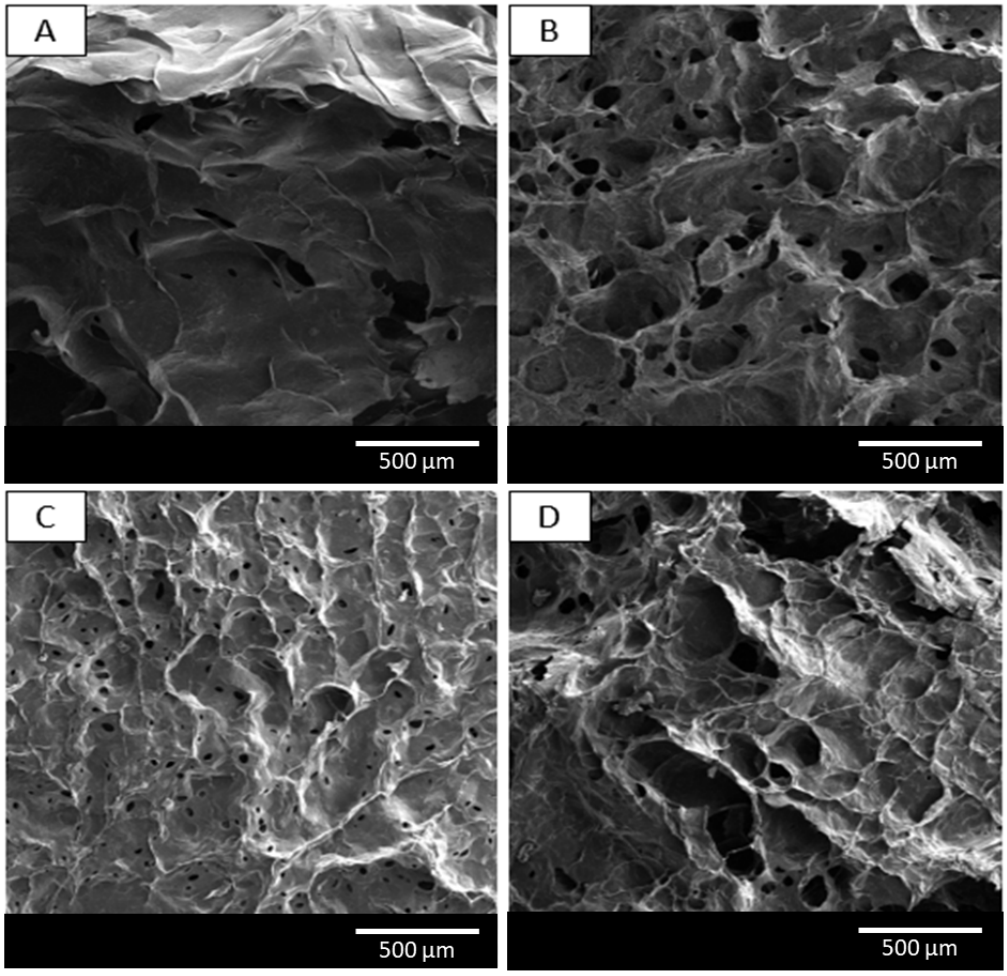

Figure 4. 8. SEM images of the surface morphologies of different hydrogel groups under 100X magnification after 21 days: CKA1(A), CKA2(B), CKA3(C), CKA4(D)

4.2.5. Water Uptake Properties of Hydrogel Groups

Hydrogels possess a remarkable ability to retain water well beyond their actual volume due to their extensively porous structure and the presence of hydrophilic functional groups. Percent swelling rates of each hydrogel group are given in Figure 4.9. The CKA1 group showed the highest swelling ratio compared to the other groups during the 96th hour (4th day), while the lowest swelling ratio was obtained in the CKA4 group. This result was in accordance with SEM results given in Section 4.2.2. and percent porosity results are given in Section 4.2.3. With the increase in percent porosity, the swelling ratios of hydrogels also increased. The increase in porosity directly correlates with a decreased number of crosslinks formed within the structure [160]. Because of the lower collagen content in CKA1 compared to CKA4, there is an increased potential for water molecules to be adsorbed between the polymer chains of the hydrogels and around active and free functional groups such as -OH of alginate and -NH_2 of collagen [161]. Consequently, higher water uptake capacity was observed in the CKA1 group.

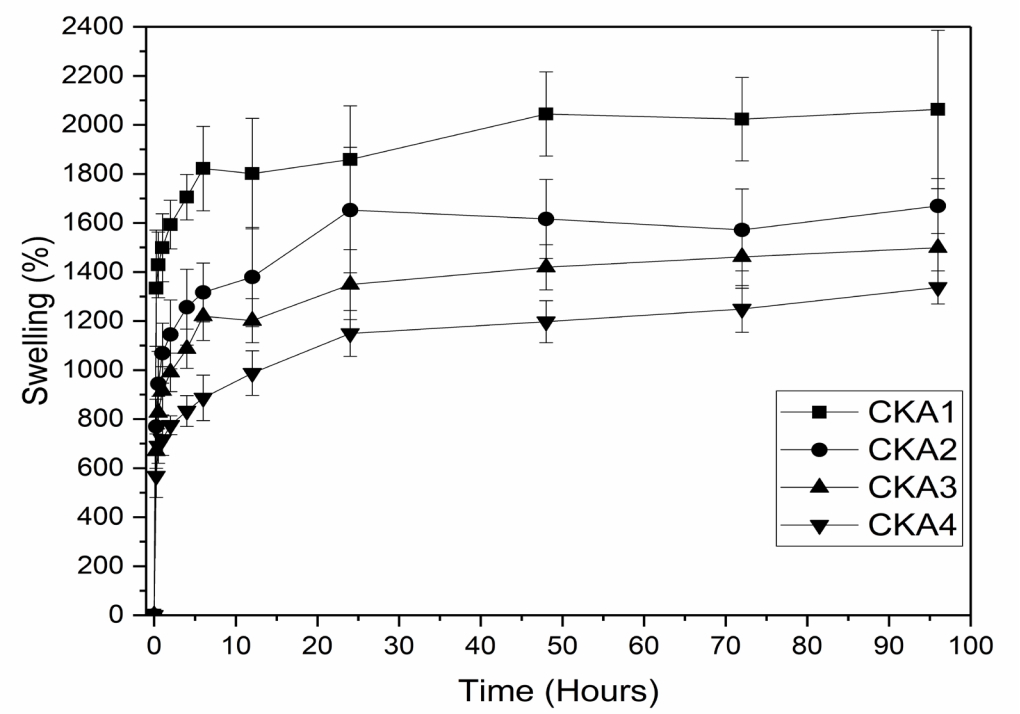

Figure 4. 9. The percent swelling ratios of CKA1, CKA2, CKA3, and CKA4 hydrogel. Data are shown as mean ± S.D.

4.2.6. *In vitro* Release of Protein from Hydrogels

In vitro protein release study from hydrogel groups was conducted for 14 days and total amounts of released keratin and collagen proteins from hydrogel groups were depicted in Figure 4.10. For the calculation of amounts of protein released from hydrogels, a calibration curve was constructed with a determined concentration of standard solutions (Appendix A). During the initial three days, burst releases were observed across all groups, followed by a slower release profile, ultimately reaching a plateau. The amount of protein released from CKA4 was found to be significantly higher than that of other groups at the end of 15 days. In addition, CKA1, CKA2, and CKA3 resulted in similar amounts of cumulative protein released although CKA2 and CKA3 weight loss values were highest and CKA1 showed the lowest weight loss. For these findings, it can be said that higher protein components present in CKA4 led to higher protein release in parallel to its rate of degradation. Moreover, it can also be pointed out that EDC/NHS crosslinking was not as effective in CKA4 as in CKA2 and CKA3 [162].

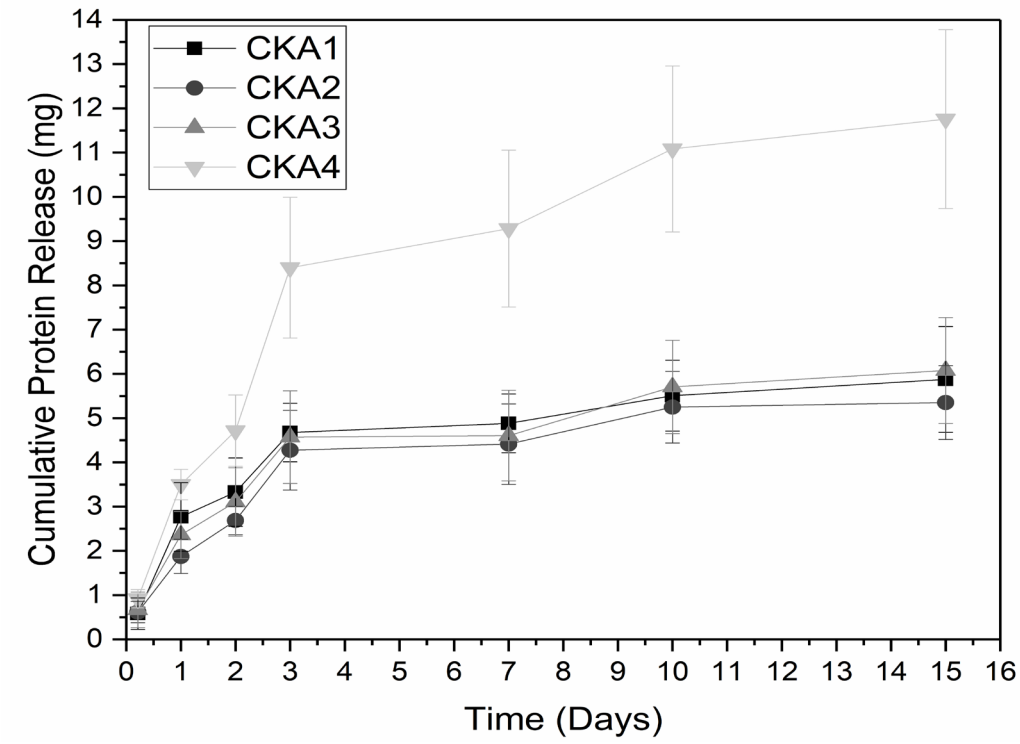

Figure 4. 10. *In vitro* cumulative protein release measured by BCA assay from hydrogels. Data are shown as mean ± S.D.

4.2.7. *In vitro* cell viability

Changes in the viability of L929 cells of all experimental groups were evaluated during 7 days by resazurin reduction assay. Resazurin is a dye indicator that undergoes a color change in reaction to the chemical reduction of the growth medium, which occurs because of cell metabolism. In other words, viable cells can reduce the dye, and the percent reduction in dye shows the change in cell proliferation.

Cell viability differences between the control group (TCP) and L929 cells incubated with hydrogel groups are given in Figure 4.11. a and b. The results showed that hydrogel groups did not inhibit the growth of the L929 cells. In addition, L929 cells demonstrated growth on the hydrogels; it was determined that cell proliferation increased over time at varying rates in all groups through the resazurin assay. The increase in cell proliferation of the CKA1 and CKA3 groups was found significantly higher, especially on the 4^{th} day, than the CKA2 and CKA4 groups. These two hydrogel groups might exert growth inhibition due to their higher keratin content, as discussed in the literature [163].

L929 cell-seeded hydrogel groups were also examined with SEM. L929 cells attached and invaded the hydrogel surface entirely while they were changing their morphology from round to characteristic fibroblastic morphology (Figure 4.12). Moreover, CKA1 and CKA3 demonstrated a larger cell attachment layer in parallel with the cell viability results. This result suggests that the surface of the designed hydrogels is suitable for cellular attachment and cell proliferation in 3D culture conditions.

Formation of cell layers observed with L929 over the incubation periods on the hydrogels (Figure 4. 12.) as well as continuously increasing resazurin reduction percentages could be a result of increasing cellular proliferation followed by the attachment of cells on the hydrogel. Collectively, none of the groups caused cytotoxic effects on L929 cells and, overall, CKA1 and CKA3 showed strong potential to encourage cellular attachment while CKA1 provided a more stable substrate for a longer period to improve ECM deposition capacity and growth of the invading cells as it demonstrated lower degradation rate with higher porosity.

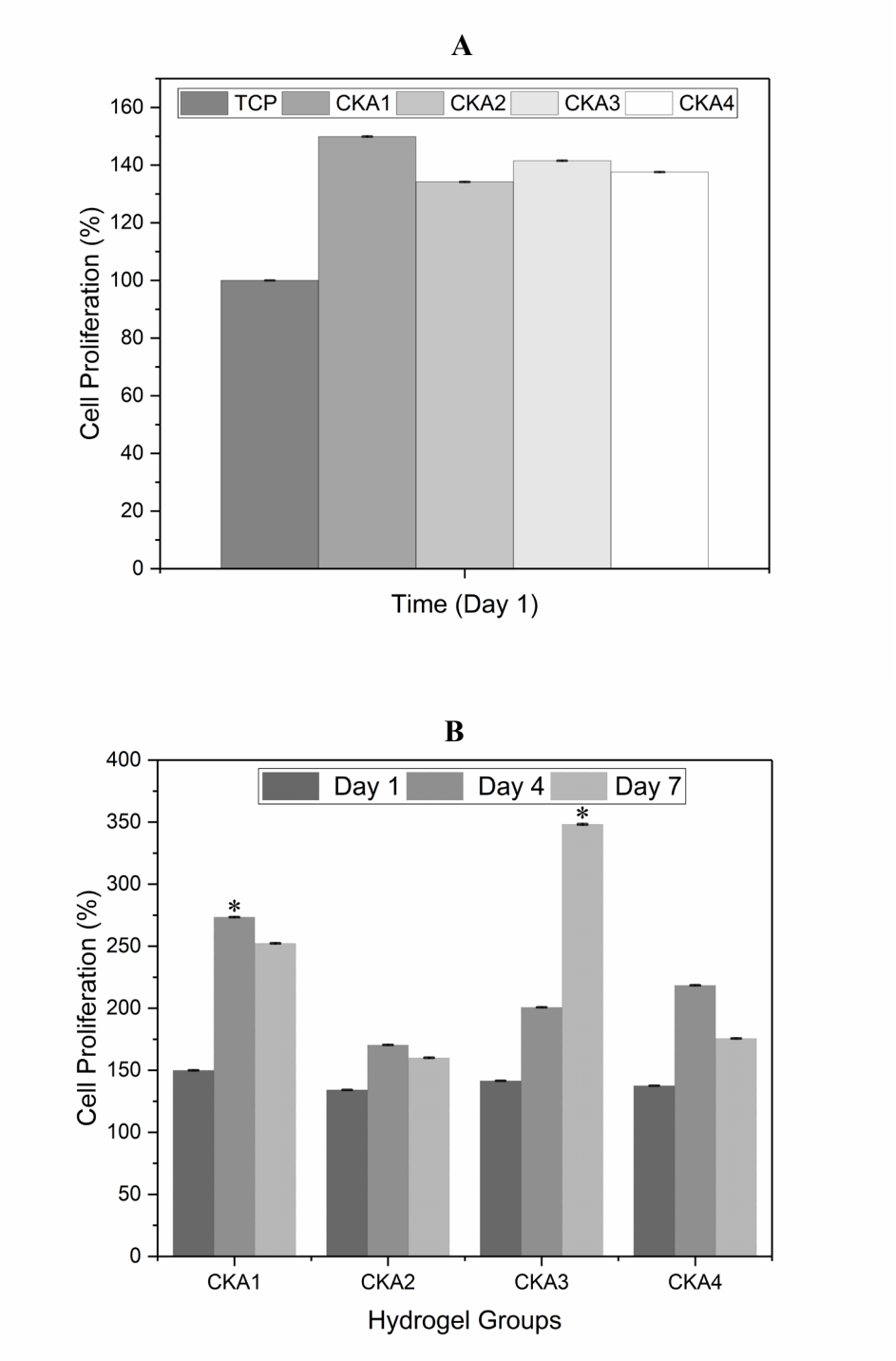

Figure 4. 11. Relative cell viability of L929 cells after incubation with hydrogel groups for 7 days compared to the control group (TCP). Relative viability of L929 cells on hydrogel groups and TCP on day 1 (A) and change in relative viability of L929 cells on hydrogel groups according to the days (B). Data are shown as mean ± S.D.

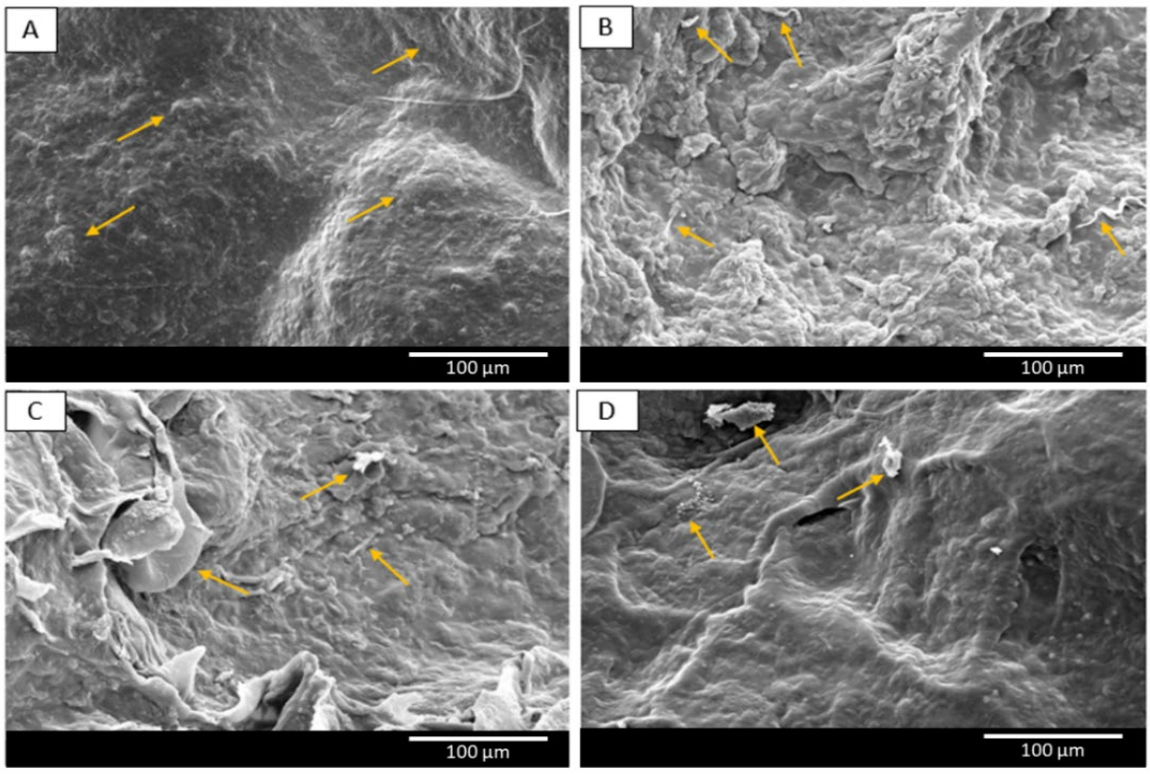

Figure 4. 12. SEM images of L929 cell-seeded hydrogels at the end of the 7th day incubation under 1000X magnification: (A) CKA1, (B) CKA2, (C) CKA3, (D) CKA4.

4.3. PEI: Plasmid complex characterizations

Size distribution and zeta potential results of the 1:1 ratio of PEI:pDNA complex were given in Figure 4.13.a and b. The complex had 38.7 mV zeta potential and a size of 140.8 nm. Its polydispersity index was 0.282. For ratios of 1:2, 1:3, and empty PEI there is no diagram to give any results due to too high a polydispersity index and high heterogenicity.

Polyethyleneimine (PEI) is a synthetic, water-soluble, linear or branched polymer. It is widely used in gene delivery systems due to the ability to build a complex with DNA and support the release of endosomal through the “proton sponge effect” [164] and also facilitating the intracellular transport into the nucleus [165].

Gel retardation assay results of complex release samples from hydrogels on day 1, day 4, and day 7 are given in Figure 4.14. a, b_1 & b_2, c as follows. Confirmation and stability of PEI: plasmid complexes were analyzed from day 1, day 4, and day 7. As seen in Figure 4.14,

miR-21 expression plasmid made a strong complex with PEI at a 1:1 ratio, and its stability had been preserved for 7 days. DNase and EtBr were not able to interact with complexes, whereas DNase I degraded the naked plasmid Figure 4.14.a, and b [166].

PCMV-MIR mammalian expression vector was carrying precursor sequence of hsa-miR-21 to be expressed in mammalian cells. Transient transfection took place in this study without doing any persistent selection with G418. The expression of GFP and the over-expression of miR-21 were dependent on the cell and the efficiency of the transfection.

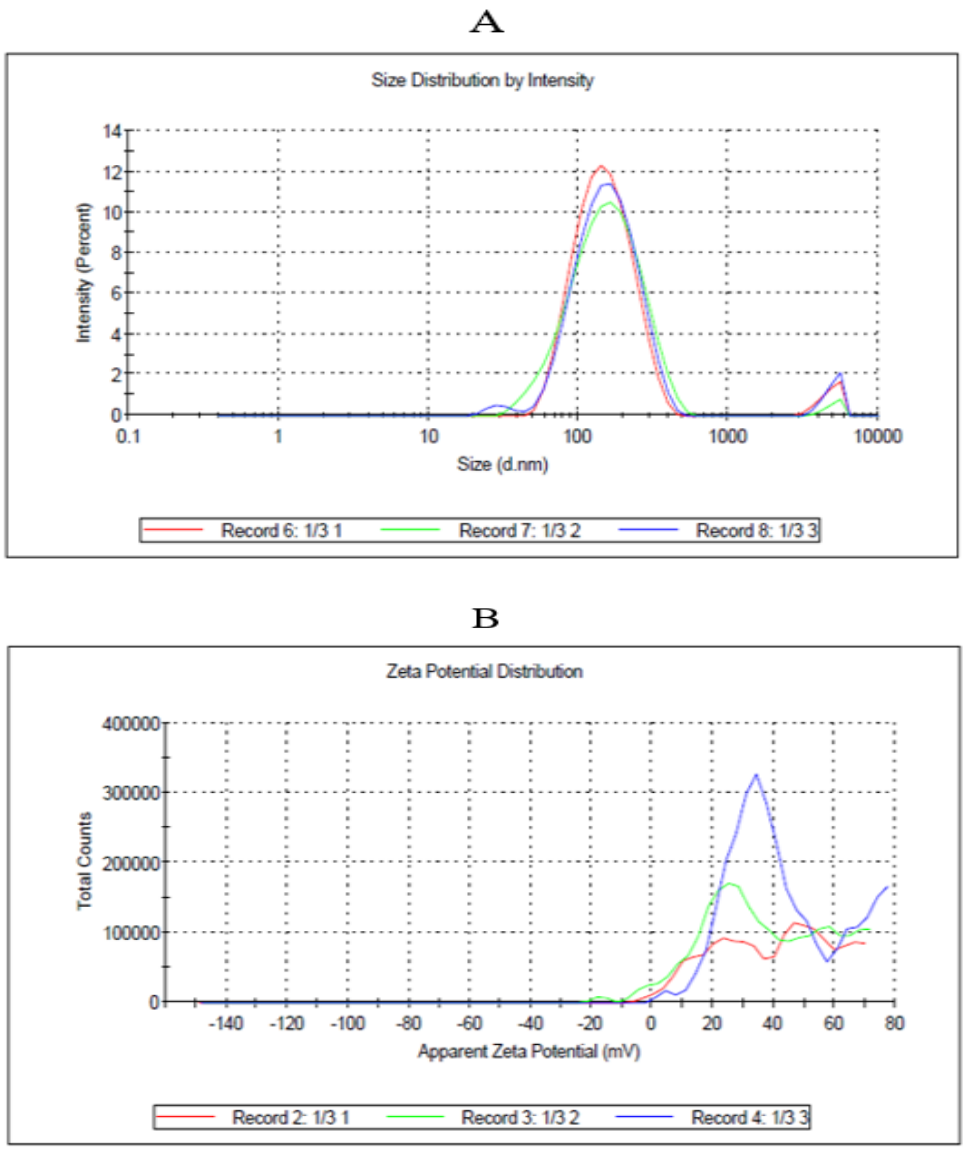

Figure 4. 13. Size distribution (A) and zeta potential (B) analysis of PEI:pDNA in a 1:1 ratio

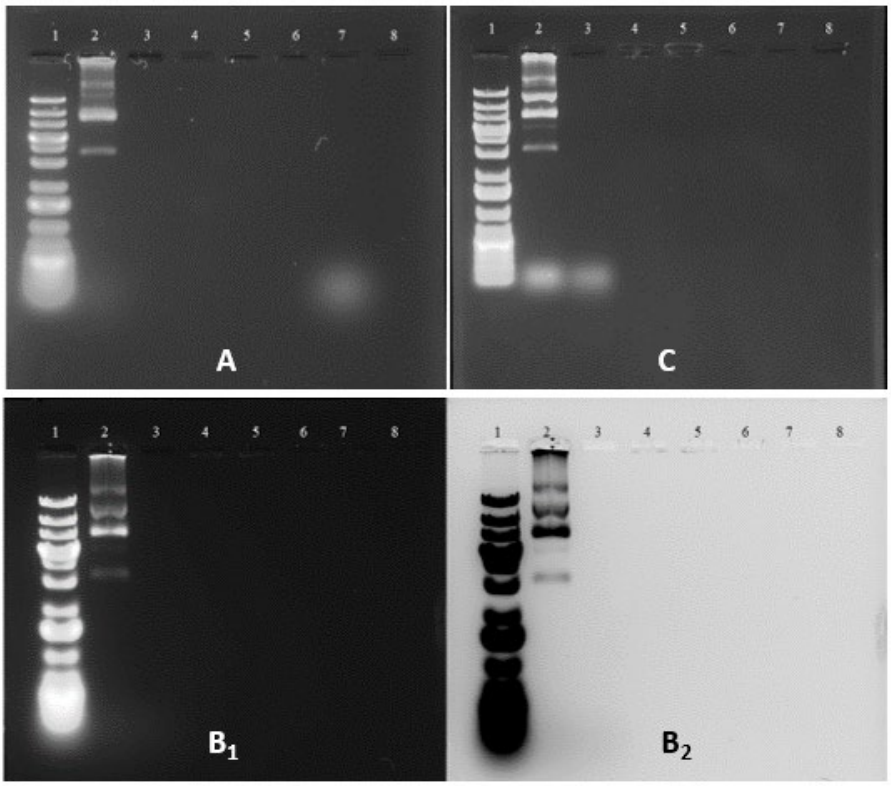

Figure 4. 14. Gel retardation results of 1:1 PEI:pDNA complexes on day 1 (A), day 4 (B_1 & B_2), and day 7 (C). Lane 1: 100 bp DNA ladder, Lane 2: Naked plasmid, Lane 3: Digested Naked plasmid (B_1 & B_2 & C); day 1 sample (A), Lane 4: Day 1 (A), day 4 (B_1 & B_2), day 7 (C) samples, Lane 5: Samples with same order, Lane 6: Dnase I treated samples, Lane 7: Digested naked plasmid (A), empty PEI (B_1 & B_2 & C), Lane 8: Empty PEI (A).

4.4. Transfection of HUVECs

4.4.1 Fluorescent Microscopy

HUVECs were transfected with miR-21 expression vector carrying GFP as the reporter. In Figure 4.15., successful transfection of HUVECs was observed on the tissue culture plate at 48 hours post-transfection. Cells seeded on TCP were used as a control group to confirm transfection and to analyze efficiency. Cells were fixed and stained with DAPI to visualize nuclei, and the GFP fluorescence, which was inserted into the vector as the reporter gene, by using a fluorescent microscope DMi8 (Leica, Germany). In Figure 4.16., it was

confirmed that the GFP fluorescence signal was obtained from the transfected cells only by looking at the cells stained with DAPI but lacking green fluorescence.

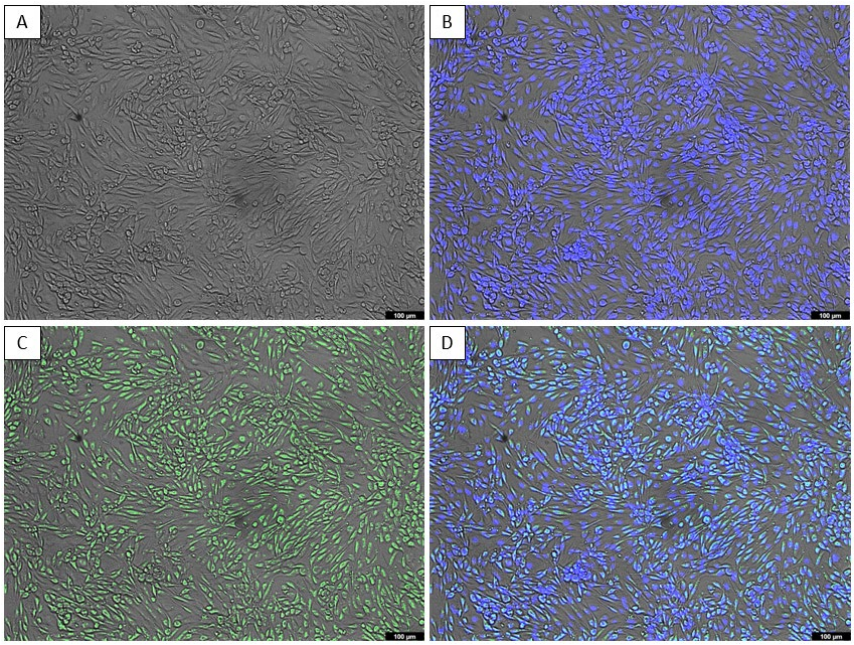

Figure 4. 15. Fluorescent microscopy images of HUVECs on TCP, 48 hours after transfection under 10X magnification. Bright field (BF) (A), DAPI (B), GFP (C), Overlay of BF, GFP, and DAPI (D)

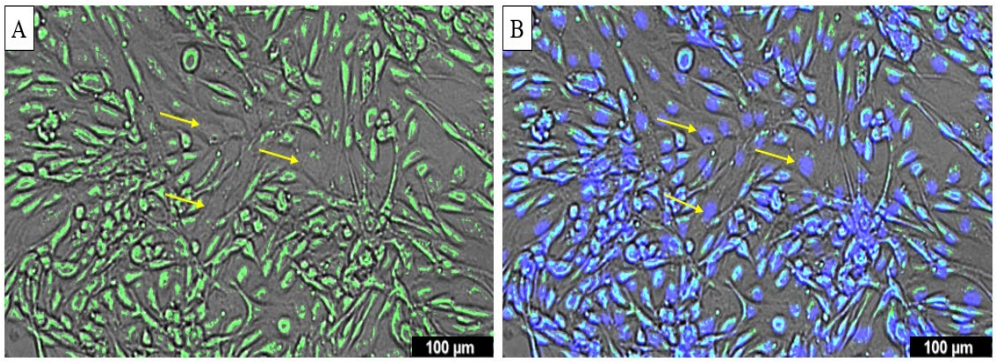

Figure 4. 16. Fluorescent microscopy images of transfected and untransfected HUVECs on TCP, 48 hours after transfection under 10X magnification. Overlay of bright field and GFP (A), Overlay of BF, GFP, and DAPI (B)

4.4.2. Confocal scanning laser microscopy (CSLM)

Confocal images of hydrogels on days 1, 2, 3, and 4 are given in Figure 4.17. a**,** b, c, d, respectively. The images are overlay of DAPI and GFP fluorescence from HUVECs. There was not any significant change in the fluorescence intensity among the day 1, 2, 3, and 4 groups. The crosstalk between fluorescent molecules might mask the actual results. However, there was a significant difference in GFP signal between groups, when it was compared according to the GFP, solely (Figure 4.18.). The fluorescence signal was significantly higher for the hydrogel on day 4 than for the hydrogels on day 1 and day 2.

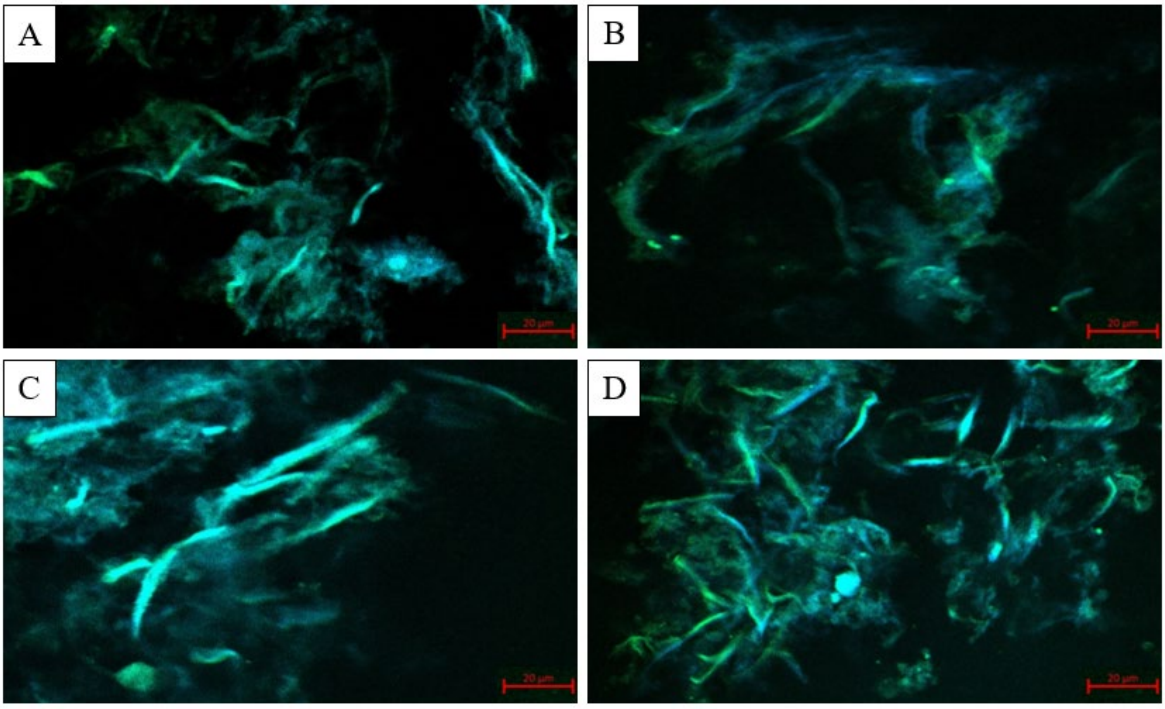

Figure 4. 17. CLSM images (GFP and DAPI) of the hydrogels on day 1 (A), day 2 (B), day 3 (C), day 4 (D)

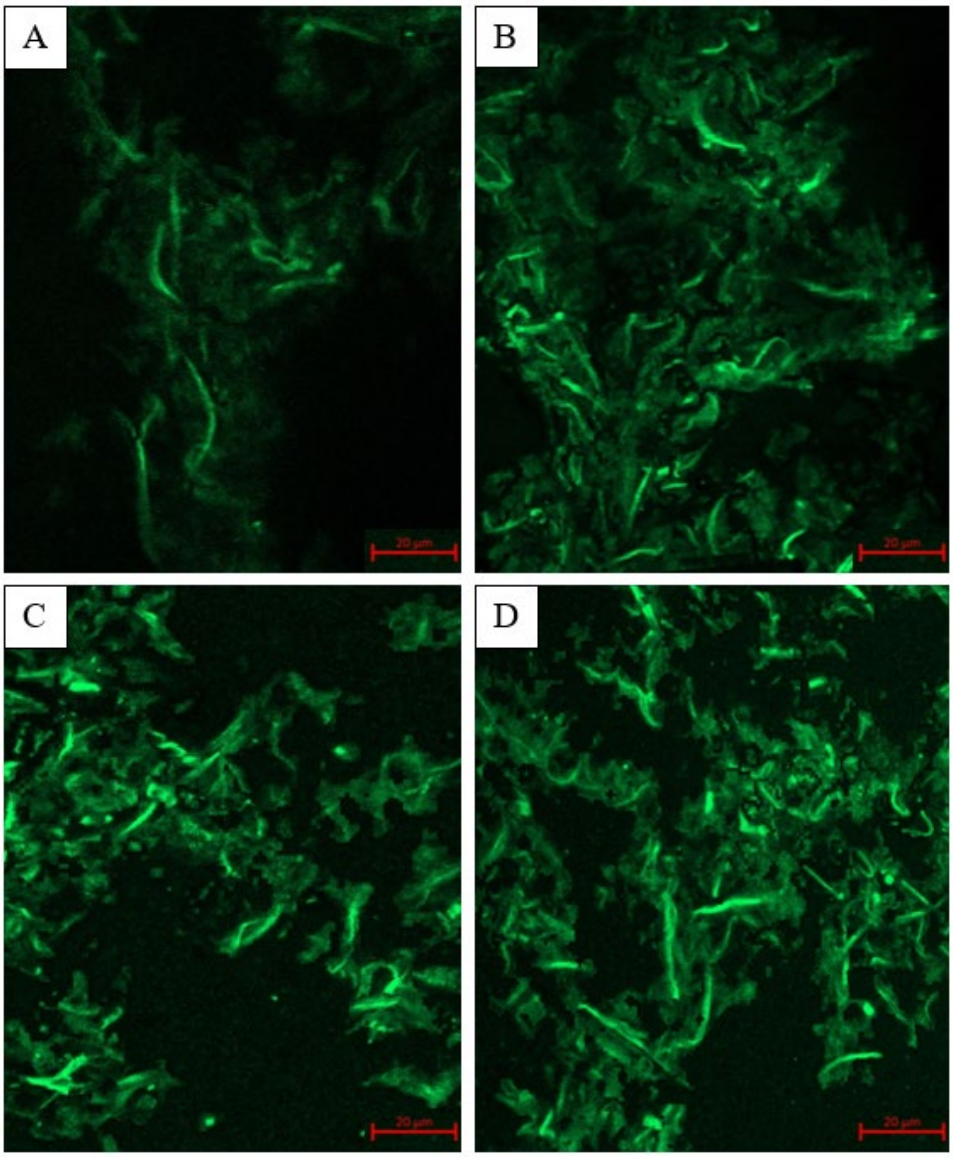

Figure 4. 18. CLSM images (GFP only) of the hydrogels on day 1 (A), day 2 (B), day 3 (C), day 4 (D)

4.5. Relative expression levels of miR-21, *VEGFA, PTEN, SPRY1* and *SPRY2*

Differences in the fold-changes of experimental groups for miR-21, *VEGFA, PTEN, SPRY1,* and *SPRY2* were displayed in Figure 4.19. and Figure 4.20. To conduct a link between miR-21 and its effects on HUVECs, known direct targets of miR-21 which take place in angiogenesis were chosen. When miR-21 directly targets and inhibits *PTEN, VEGF* secretion is increased and the proliferation rate of HUVECs is higher [167]. From the expression levels, *PTEN* expression was lower in transfected groups, while *VEGF* and miR-

21 expression increased. Some targets of miR-21 are cell cycle regulators, and proteins of cellular apoptosis [127].

miR-21 hampers the mRNA expression of pivotal tumor suppressor proteins like PTEN (phosphatase and tensin homolog) [168], Sprouty1 and Sprouty2 [169]. miR-21 was found to enhance the expression of hypoxia-inducible factor 1α (HIF1α) and vascular endothelial growth factor (VEGF) [128]. The relative expression level outcomes calculated from qPCR data were compatible with the previous studies. According to gene expression data given, expression of *VEGFA* increased in PEI:miR-21 expression plasmid-loaded hydrogel groups. It might be referred that when miR-21 targeted PTEN, its downregulation triggered AKT and ERK1/2 signaling, therefore expression of *VEGFA* increased [128]. Likewise, it was observed that over-expression of miR-21 decreased the expression of its direct targets *PTEN*, *SPRY1*, and *SPRY2* compared to control groups.

By evaluation of results, there was a significant change between the control group (untreated HUVECs) and both transfected groups of cells on TCP and hydrogels (miR-21 transfected HUVECs). There was no significant difference between hydrogel groups on different days. By the significant increase in *SPRY1, SPRY2,* and *PTEN* genes in the empty PEI group, it was possible to refer that empty agents might exert stress on HUVECs. There is more endosomal escape potential when the ratio of PEI and plasmid increases because of its higher resistance to pH changes [170]. Related to this, excessive free PEI can accumulate on the cell surface and eventually be taken up by the cell via endocytosis [171]. Free PEI can affect the surface charge of the PEI/plasmid particles. Therefore, this exerts more inclination toward the cell membrane, which is negatively charged, and can disrupt it [172].

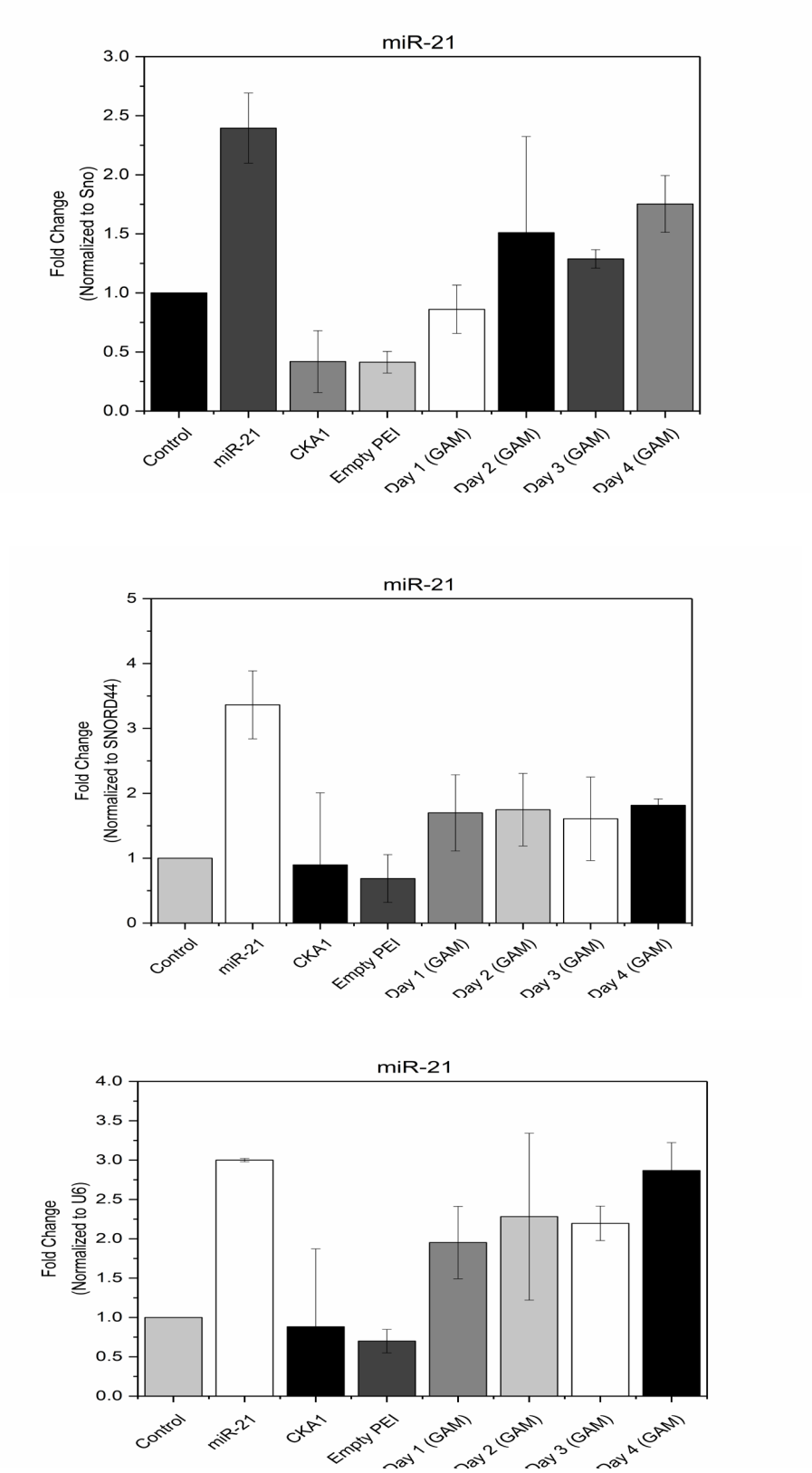

Figure 4. 19. Relative expressions of miR-21 (normalized to housekeeping genes) on HUVECs of control and treated groups. Data are shown as mean ± S.D.

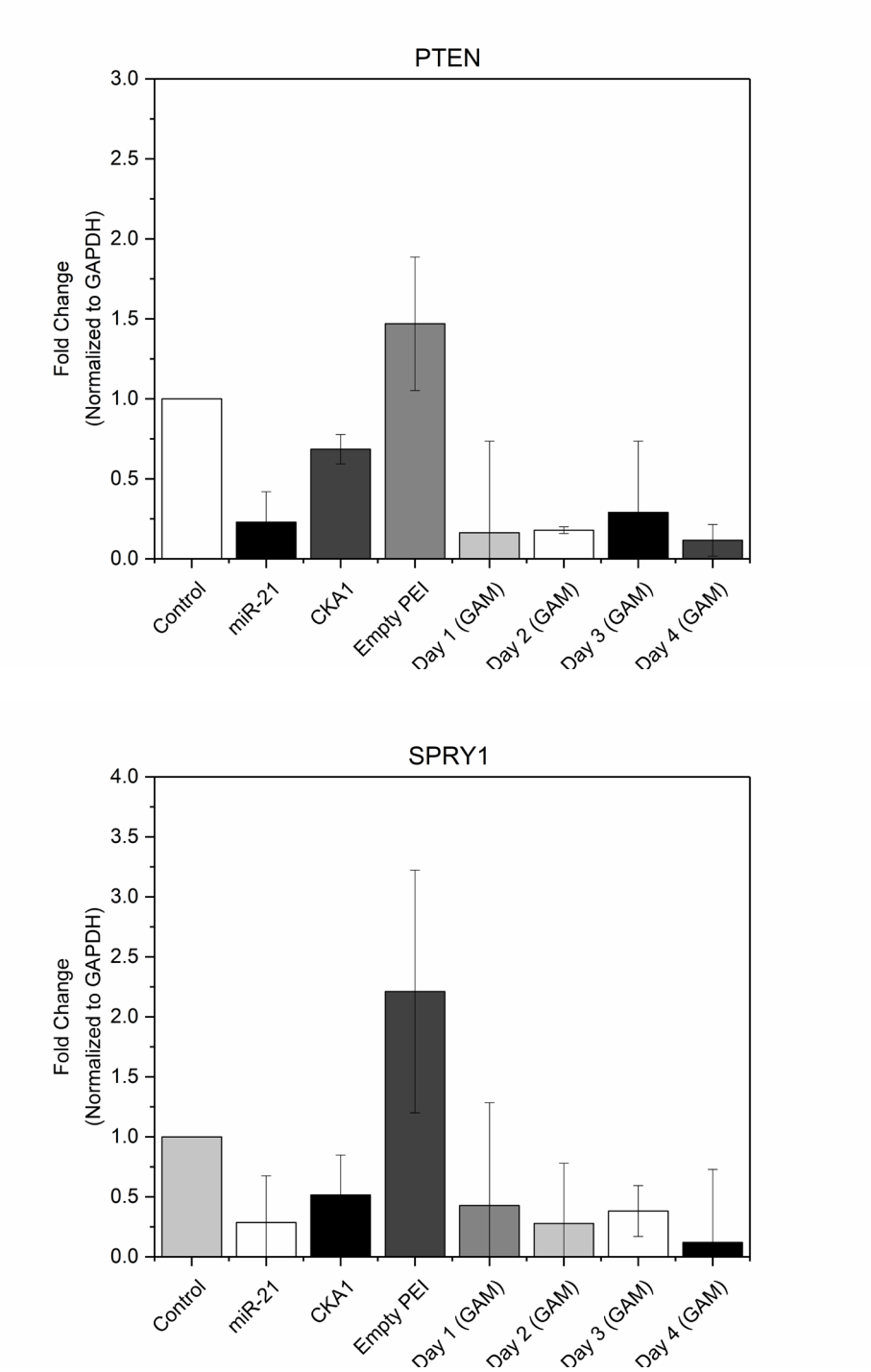

Figure 4. 20. Relative expressions of *VEGFA*, *PTEN*, *SPRY1*, *SPRY2* (normalized to *GAPDH*) on HUVECs of control and treated groups. Data are shown as mean ± S.D.

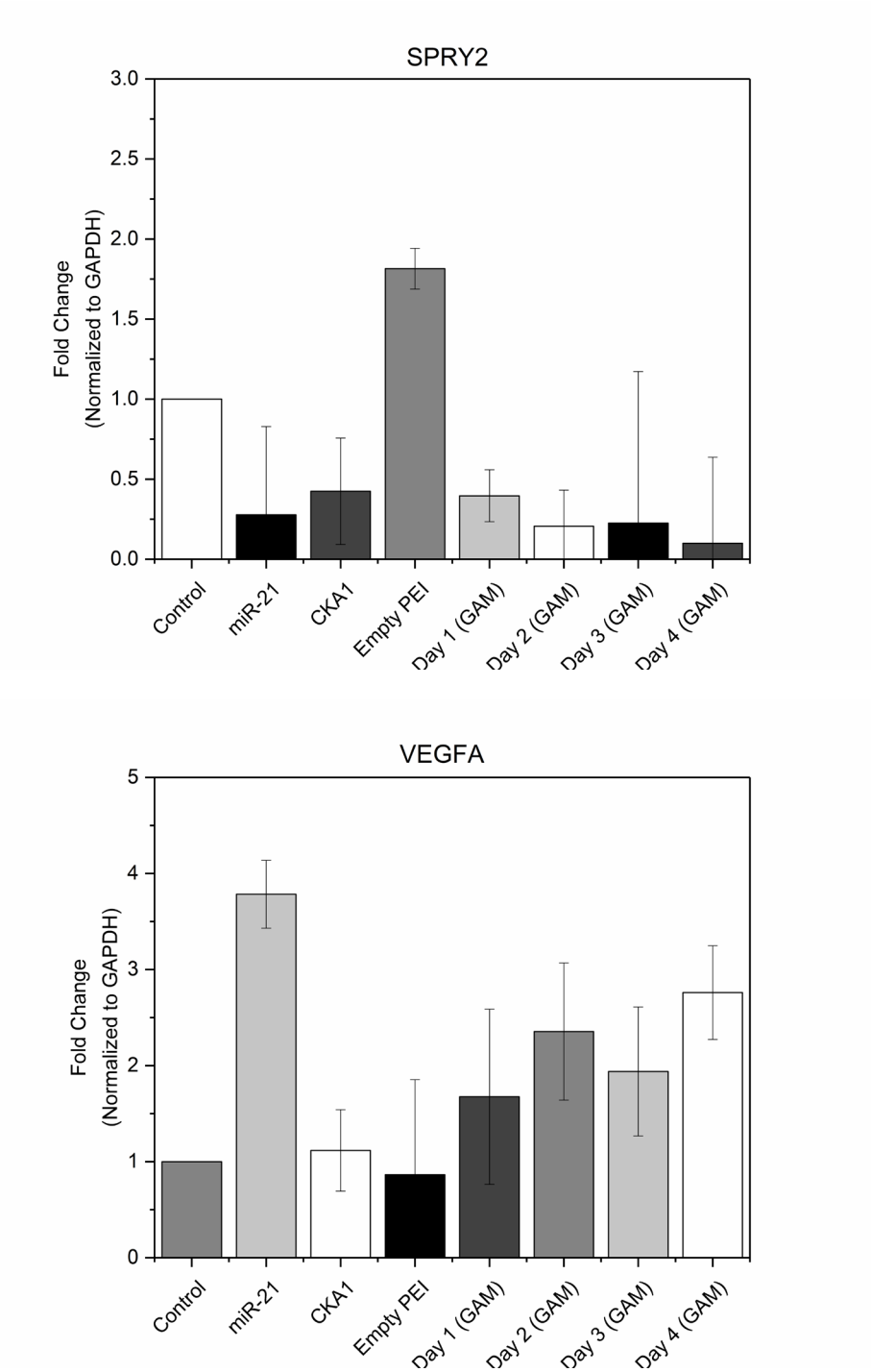

Figure 4. 21. (continued) Relative expressions of *VEGFA*, *PTEN*, *SPRY1*, *SPRY2* (normalized to *GAPDH*) on HUVECs of control and treated groups. Data are shown as mean ± S.D.

5. CONCLUSION

Advances in the pharmaceutical field have improved greatly in the past decades, however, there have been still limitations in treatments for autoimmune diseases, chronic diseases such as cardiovascular diseases, diabetes, cancers, tissue/organ failures, and organ transplantations. The challenges in these arise from their patient-specific variations, necessitating individualized solutions tailored to each patient's data. Regenerative medicine aims to repair or replace damaged tissues, organs, and systems through the utilization of scaffold-based technology, regulatory RNA treatments such as miRNA, genome editing tools, nanotechnology, stem cell therapies, organoids, bio-printers, organoids, as well as organ-on-a-chip models [173]. At this stage, regenerative medicine has been employing tissue engineering to solve these challenges, supporting biobanks, defining the underlying causes and biological mechanisms of diseases, and assessing the feasibility, and compatibility of existing applications. Furthermore, molecular biology tools like CRISPR and miRNAs enable the generation of tissue and disease models for further studies. For example, in a study conducted by Acun and Zorlutuna, an *in vitro* three-dimensional vascular tissue model was developed using CRISPR editing of HIF-1α in induced pluripotent stem cell (iPSC) derived endothelial cells (iESC), facilitating the investigation of aging and dysfunction [174]. In another example, Hu *et al*. examined the role of miR-21 on angiogenesis during spinal cord injuries in both HUVECs and *in vivo* rat models [126]. They found that miR-21 mimics ameliorated angiogenic capacity in spinal cord injury by enhancing cell migration, survival, and endothelial tube formation.

Tissue engineering relies on both *in vivo* animal models and *in vitro* cell culture to understand tissue development. While *in vivo* studies aid in comprehending disease mechanisms and therapy development, ethical constraints and human model limitations exist. *In vitro* studies offer cost-effective and versatile experiments, but traditional 2D models lack accuracy in mimicking tissue interactions. Consequently, extensive research into 3D cell culture aims to better replicate the complex in vivo environment, showcasing advancements in various research areas from morphology to drug discovery, broadening applications in disease study and tissue engineering.

In some 3D cell culture studies, cells are combined with hydrogels made of synthetic or natural polymers, forming porous structures. Natural hydrogels, preferred over synthetic ones for their ECM-like properties and lower cytotoxicity, often utilize structural proteins like collagen and keratin found abundantly in the ECM [175]. While hydrogel scaffolds provide crucial 3D properties for tissue development, they lack vascularization, a vital aspect of tissue growth. To address this, natural polymers are combined with biological molecules such as growth factors, transcription factors, and regulatory RNAs to induce the formation of angiogenesis within the hydrogels [176].

Several microRNAs (miRNAs) play crucial roles in regulating angiogenesis, with miR-21 being extensively studied due to its ubiquitous expression and involvement in various diseases like cancer and cardiovascular disorders. Despite its association with pathological conditions, miR-21's exact role in angiogenesis remains controversial as mentioned in the literature [26, 177]. Furthermore, the combination of collagen, keratin and alginate hydrogel loaded with miR-21 has not been studied in the literature. Therefore, in this study, the roles of miR-21, C/K/A, and both together have been examined for the angiogenic potential of HUVECs. The integration of miRNA-loaded matrices/hydrogels in tissue engineering offers significant potential for modeling diseases, studying drug responses, and developing vascular models and therapeutic interventions, forming the core focus of the thesis.

The thesis aims to assess the angiogenic potential of PEI:miR-21 complex-loaded and unloaded Col/Ker/Alg (CKA) hydrogels as gene-activated tissue scaffolds. For this purpose, firstly keratin and collagen were isolated from waste human hair samples and bovine Achilles tendon, respectively. Collagen and keratin were extracted from biological wastes which is a contribution to recycling. Re-use of disposed biological materials prevents pollution of natural sources and decreases the emission of greenhouse gases. For both isolated proteins, all the characteristic peaks of keratin and collagen were observed by Fourier transform infrared spectroscopy (FTIR). Two major bands were observed in human hair keratin samples at approximately 45 kDa and 63 kDa, while collagen samples exhibited four bands at around 300 kDa, 245 kDa, 135 kDa, and 100 kDa according to SDS-PAGE results.

Col/Ker/Alg hydrogels with different ratios were prepared and their chemical, microstructural properties, percent porosity, in vitro hydrolytic degradation behavior, water uptake properties, *in vitro* protein release behaviors, and biocompatibility were characterized to optimize the hydrogels for the preparation of PEI:miR-21 plasmid complex loaded hydrogels for subsequent investigations. The hydrogel group consisting of 1% collagen/ 1% keratin/ 1% alginate showed the highest rate of swelling and percent of porosity (80.89%), lowest degradation rate (only 15.19% at the end of 21 days), and better biocompatibility. According to previous studies, hydrogels have been examined for 21 days for their angiogenic bioactivity and formation of tubular structure [178, 179]. In accordance with the information, hydrolytic degradation study has extended to 21 days. Despite being made up of natural polymers, hydrogels exhibited remarkable durability over extended periods (21 days) with minimal weight loss. By adjusting the cross-linking type and degree, the physical and chemical properties of hydrogels can be tailored to suit specific tissue requirements. Thanks to their highly porous structure, hydrogels facilitated cell migration and could effectively accommodate transfection particles.

It was also examined on HUVECs that miR-21 has the potential to promote angiogenesis. PEI:miR-21 loaded hydrogels showed increased expressions of *VEGFA* and miR-21 compared to the control groups. By the CSLM images, transfection of HUVECs seeded increased by the following days, so hydrogel also showed gene activated matrix property as intended.

Further study must be done to monitor its long - term effects on cells to see their potential as a vascular tissue model. With detailed study of hydrogels under different parameters such as attuning pore sizes, degree of cross-linking, duration of transfection and incubation time with hydrogels, their long-term effects may be evaluated to use in skin tissue engineering applications such as wound healing with loading of different miRNAs as well as different molecules.

REFERENCES

[1] R. Webb, A. Mylona, and A. D'Souza, "Regenerative medicine," in *Medical Innovation*, ed: CRC Press, 2023, pp. 133-145.

[2] R. Gorodetsky, "Promises and Limitations in the Application of Cell Therapy for Tissue Regeneration," in *Stem Cell-Based Tissue Repair*, ed: The Royal Society of Chemistry, 2010, pp. 1-21.

[3] A. Grath and G. Dai, "Direct cell reprogramming for tissue engineering and regenerative medicine," *Journal of biological engineering,* vol. 13, pp. 1-15, 2019.

[4] L. De Bartolo and A. Piscioneri, "New Advanced Biomaterials for Tissue and Organ Regeneration/Repair," *Cells Tissues Organs,* vol. 204, pp. 123-124, 2017.

[5] E. K. Gähwiler, S. E. Motta, M. Martin, B. Nugraha, S. P. Hoerstrup, and M. Y. Emmert, "Human iPSCs and genome editing technologies for precision cardiovascular tissue engineering," *Frontiers in Cell and Developmental Biology,* vol. 9, p. 639699, 2021.

[6] W. Hong, M. Huang, Y. Wei, and X. Wei, "A new and promising application of gene editing: CRISPR-controlled smart materials for tissue engineering, bioelectronics, and diagnostics," *Science China. Life sciences,* vol. 62, pp. 1547-1549, 2019.

[7] M. Fathi-Achachelouei, H. Knopf-Marques, C. E. Ribeiro da Silva, J. Barthès, E. Bat, A. Tezcaner*, et al.*, "Use of nanoparticles in tissue engineering and regenerative medicine," *Frontiers in bioengineering and biotechnology,* vol. 7, p. 113, 2019.

[8] E. J. Lee, F. K. Kasper, and A. G. Mikos, "Biomaterials for tissue engineering," *Annals of biomedical engineering,* vol. 42, pp. 323-337, 2014.

[9] L. Suamte, A. Tirkey, J. Barman, and P. J. Babu, "Various manufacturing methods and ideal properties of scaffolds for tissue engineering applications," *Smart Materials in Manufacturing,* vol. 1, p. 100011, 2023.

[10] D. W. Hutmacher, "Scaffolds in tissue engineering bone and cartilage," *Biomaterials,* vol. 21, pp. 2529-2543, 2000.

[11] D. S. Masson-Meyers and L. Tayebi, "Vascularization strategies in tissue engineering approaches for soft tissue repair," *Journal of tissue engineering and regenerative medicine,* vol. 15, pp. 747-762, 2021.

[12] C. D. Devillard and C. A. Marquette, "Vascular tissue engineering: challenges and requirements for an ideal large scale blood vessel," *Frontiers in Bioengineering and Biotechnology,* vol. 9, p. 721843, 2021.

[13] H. Liu, H. Chen, Q. Han, S. Bin, Y. Liu, A. Zhang*, et al.*, "Recent advancement in vascularized tissue-engineered bone based on materials design and modification," *Materials Today Bio,* p. 100858, 2023.

[14] I. Kocherova, A. Bryja, P. Mozdziak, A. Angelova Volponi, M. Dyszkiewicz-Konwińska, H. Piotrowska-Kempisty*, et al.*, "Human umbilical vein endothelial cells (HUVECs) co-culture with osteogenic cells: from molecular communication to engineering prevascularised bone grafts," *Journal of clinical medicine,* vol. 8, p. 1602, 2019.

[15] M. Kapałczyńska, T. Kolenda, W. Przybyła, M. Zajączkowska, A. Teresiak, V. Filas*, et al.*, "2D and 3D cell cultures–a comparison of different types of cancer cell cultures," *Archives of Medical Science,* vol. 14, pp. 910-919, 2018.

[16] C. Jensen and Y. Teng, "Is it time to start transitioning from 2D to 3D cell culture?," *Frontiers in molecular biosciences,* vol. 7, p. 33, 2020.

[17] F. Xu, C. Dawson, M. Lamb, E. Mueller, E. Stefanek, M. Akbari*, et al.*, "Hydrogels for tissue engineering: Addressing key design needs toward clinical translation," *Frontiers in Bioengineering and Biotechnology,* vol. 10, p. 849831, 2022.

[18] M. W. Tibbitt and K. S. Anseth, "Hydrogels as extracellular matrix mimics for 3D cell culture," *Biotechnology and bioengineering,* vol. 103, pp. 655-663, 2009.

[19] S. Chaudhary and E. Chakraborty, "Hydrogel based tissue engineering and its future applications in personalized disease modeling and regenerative therapy," *Beni-Suef University Journal of Basic and Applied Sciences,* vol. 11, pp. 1-15, 2022.

[20] M. Gomez-Florit, A. Pardo, R. M. Domingues, A. L. Graça, P. S. Babo, R. L. Reis*, et al.*, "Natural-based hydrogels for tissue engineering applications," *Molecules,* vol. 25, p. 5858, 2020.

[21] Y. Wang, R. K. Kankala, C. Ou, A. Chen, and Z. Yang, "Advances in hydrogel-based vascularized tissues for tissue repair and drug screening," *Bioactive materials,* vol. 9, pp. 198-220, 2022.

[22] R. Kumarswamy, I. Volkmann, and T. Thum, "Regulation and function of miRNA-21 in health and disease," *RNA biology,* vol. 8, pp. 706-713, 2011.

[23] A. E. Jenike and M. K. Halushka, "miR-21: a non-specific biomarker of all maladies," *Biomarker research,* vol. 9, pp. 1-7, 2021.

[24] M. Hashemi, M. S. A. Mirdamadi, Y. Talebi, N. Khaniabad, G. Banaei, P. Daneii*, et al.*, "Pre-clinical and clinical importance of miR-21 in human cancers: Tumorigenesis, therapy response, delivery approaches and targeting agents," *Pharmacological Research,* vol. 187, p. 106568, 2023.

[25] M. Luo, X. Tan, L. Mu, Y. Luo, R. Li, X. Deng*, et al.*, "MiRNA-21 mediates the antiangiogenic activity of metformin through targeting PTEN and SMAD7 expression and PI3K/AKT pathway," *Scientific reports,* vol. 7, p. 43427, 2017.

[26] C. Sabatel, L. Malvaux, N. Bovy, C. Deroanne, V. Lambert, M.-L. A. Gonzalez*, et al.*, "MicroRNA-21 exhibits antiangiogenic function by targeting RhoB expression in endothelial cells," *PloS one,* vol. 6, p. e16979, 2011.

[27] F.-S. Jiang, S.-S. Tian, J.-J. Lu, X.-H. Ding, C.-D. Qian, B. Ding*, et al.*, "Cardamonin regulates miR-21 expression and suppresses angiogenesis induced by vascular endothelial growth factor," *BioMed research international,* vol. 2015, 2015.

[28] J. Wang, Y. Cui, H. Liu, S. Li, S. Sun, H. Xu*, et al.*, "MicroRNA-loaded biomaterials for osteogenesis," *Frontiers in Bioengineering and Biotechnology,* vol. 10, p. 952670, 2022.

[29] N. Carballo-Pedrares, I. Fuentes-Boquete, S. Díaz-Prado, and A. Rey-Rico, "Hydrogel-based localized nonviral gene delivery in regenerative medicine approaches—An overview," *Pharmaceutics,* vol. 12, p. 752, 2020.

[30] Y. Cheng and C. Zhang, "MicroRNA-21 in cardiovascular disease," *Journal of cardiovascular translational research,* vol. 3, pp. 251-255, 2010.

[31] X. Rao, X. Huang, Z. Zhou, and X. Lin, "An improvement of the 2ˆ (–delta delta CT) method for quantitative real-time polymerase chain reaction data analysis," *Biostatistics, bioinformatics and biomathematics,* vol. 3, p. 71, 2013.

[32] A. Jaklenec, A. Stamp, E. Deweerd, A. Sherwin, and R. Langer, "Progress in the tissue engineering and stem cell industry “are we there yet?”," *Tissue Engineering Part B: Reviews,* vol. 18, pp. 155-166, 2012.

[33] A. Petrosyan, F. Montali, A. Peloso, A. Citro, L. N. Byers, C. La Pointe*, et al.*, "Regenerative medicine technologies applied to transplant medicine. An update," *Frontiers in Bioengineering and Biotechnology,* vol. 10, p. 1015628, 2022.

[34] J. P. Vacanti and R. Langer, "Tissue engineering: the design and fabrication of living replacement devices for surgical reconstruction and transplantation," *The lancet,* vol. 354, pp. S32-S34, 1999.

[35] C. J. Esdaille, K. S. Washington, and C. T. Laurencin, "Regenerative engineering: A review of recent advances and future directions," *Regenerative Medicine,* vol. 16, pp. 495-512, 2021.

[36] H. Hosseinkhani, A. J. Domb, G. Sharifzadeh, and V. Nahum, "Gene therapy for regenerative medicine," *Pharmaceutics,* vol. 15, p. 856, 2023.

[37] Y. Jin, S. Li, Q. Yu, T. Chen, and D. Liu, "Application of stem cells in regeneration medicine," *MedComm,* vol. 4, p. e291, 2023.

[38] I. D. Klabukov, O. Krasilnikova, D. Baranovskii, S. Ivanov, P. Shegay, and A. Kaprin, "Comment on: Regenerative medicine, organ bioengineering and transplantation," *British Journal of Surgery,* vol. 108, pp. e386-e386, 2021.

[39] S. M. Alatyyat, H. M. Alasmari, O. A. Aleid, M. S. Abdel-Maksoud, and N. Elsherbiny, "Umbilical cord stem cells: Background, processing and applications," *Tissue and Cell,* vol. 65, p. 101351, 2020.

[40] Z. Tong, A. Solanki, A. Hamilos, O. Levy, K. Wen, X. Yin*, et al.*, "Application of biomaterials to advance induced pluripotent stem cell research and therapy," *The EMBO journal,* vol. 34, pp. 987-1008, 2015.

[41] A. Petrosyan, P. N. Martins, K. Solez, B. E. Uygun, V. S. Gorantla, and G. Orlando, "Regenerative medicine applications: An overview of clinical trials," *Frontiers in Bioengineering and Biotechnology,* vol. 10, p. 942750, 2022.

[42] W. Zakrzewski, M. Dobrzyński, M. Szymonowicz, and Z. Rybak, "Stem cells: past, present, and future," *Stem cell research & therapy,* vol. 10, pp. 1-22, 2019.

[43] S. M. Maffioletti, S. Sarcar, A. B. Henderson, I. Mannhardt, L. Pinton, L. A. Moyle*, et al.*, "Three-dimensional human iPSC-derived artificial skeletal muscles model muscular dystrophies and enable multilineage tissue engineering," *Cell Reports,* vol. 23, pp. 899-908, 2018.

[44] V. Procházka, J. Gumulec, F. Jalůvka, D. Šalounová, T. Jonszta, D. Czerný*, et al.*, "Cell therapy, a new standard in management of chronic critical limb ischemia and foot ulcer," *Cell transplantation,* vol. 19, pp. 1413-1424, 2010.

[45] B. Sawitzki, P. N. Harden, P. Reinke, A. Moreau, J. A. Hutchinson, D. S. Game*, et al.*, "Regulatory cell therapy in kidney transplantation (The ONE Study): a harmonised design and analysis of seven non-randomised, single-arm, phase 1/2A trials," *The Lancet,* vol. 395, pp. 1627-1639, 2020.

[46] R. Cancedda, J. M. Murphy, and M. Van Griensven, "Insights in tissue engineering and regenerative medicine 2021: Novel developments, current challenges, and future perspectives," vol. 10, ed: Frontiers Media SA, 2023, p. 1125027.

[47] S. Sedrakyan, S. Da Sacco, A. Milanesi, L. Shiri, A. Petrosyan, R. Varimezova*, et al.*, "Injection of amniotic fluid stem cells delays progression of renal fibrosis," *Journal of the American Society of Nephrology: JASN,* vol. 23, p. 661, 2012.

[48] S. A Patel, C. C King, P. K Lim, U. Habiba, M. Dave, R. Porecha*, et al.*, "Personalizing stem cell research and therapy: the arduous road ahead or missed opportunity?," *Current Pharmacogenomics and Personalized Medicine (Formerly Current Pharmacogenomics),* vol. 8, pp. 25-36, 2010.

[49] N. Chaicharoenaudomrung, P. Kunhorm, and P. Noisa, "Three-dimensional cell culture systems as an in vitro platform for cancer and stem cell modeling," *World journal of stem cells,* vol. 11, p. 1065, 2019.

[50] D. M. Hoang, P. T. Pham, T. Q. Bach, A. T. Ngo, Q. T. Nguyen, T. T. Phan*, et al.*, "Stem cell-based therapy for human diseases," *Signal transduction and targeted therapy,* vol. 7, p. 272, 2022.

[51] D. Park, S. J. Lee, D. K. Choi, and J.-W. Park, "Therapeutic Agent-Loaded Fibrous Scaffolds for Biomedical Applications," *Pharmaceutics,* vol. 15, p. 1522, 2023.

[52] F. Han, J. Wang, L. Ding, Y. Hu, W. Li, Z. Yuan*, et al.*, "Tissue engineering and regenerative medicine: achievements, future, and sustainability in Asia," *Frontiers in bioengineering and biotechnology,* vol. 8, p. 83, 2020.

[53] S. H. Shoushrah, A. Alzagameem, J. Bergrath, E. Tobiasch, and M. Schulze, "Lignin and Its Composites for Tissue Engineering," 2023.

[54] A. Eltom, G. Zhong, and A. Muhammad, "Scaffold techniques and designs in tissue engineering functions and purposes: a review," *Advances in materials science and engineering,* vol. 2019, 2019.

[55] S. M. Van Belleghem, B. Mahadik, K. L. Snodderly, and J. P. Fisher, "Overview of tissue engineering concepts and applications," in *Biomaterials Science*, ed: Elsevier, 2020, pp. 1289-1316.

[56] F. Xing, L. Li, C. Zhou, C. Long, L. Wu, H. Lei*, et al.*, "Regulation and directing stem cell fate by tissue engineering functional microenvironments: scaffold physical and chemical cues," *Stem cells international,* vol. 2019, 2019.

[57] K. Joyce, Z. Buljovcic, G. Rosic, M. Kaszkin-Bettag, and A. Pandit, "Issues with tissues: Trends in tissue-engineered products in clinical trials in the European Union," *Tissue Engineering Part B: Reviews,* vol. 29, pp. 78-88, 2023.

[58] S. G. Kwon, Y. W. Kwon, T. W. Lee, G. T. Park, and J. H. Kim, "Recent advances in stem cell therapeutics and tissue engineering strategies," *Biomaterials Research,* vol. 22, pp. 1-8, 2018.

[59] W. H. Abuwatfa, W. G. Pitt, and G. A. Husseini, "Scaffold-based 3D cell culture models in cancer research," *Journal of Biomedical Science,* vol. 31, p. 7, 2024.

[60] C.-M. Moysidou, C. Barberio, and R. M. Owens, "Advances in engineering human tissue models," *Frontiers in bioengineering and biotechnology,* vol. 8, p. 620962, 2021.

[61] S. Caddeo, M. Boffito, and S. Sartori, "Tissue engineering approaches in the design of healthy and pathological in vitro tissue models," *Frontiers in bioengineering and biotechnology,* vol. 5, p. 40, 2017.

[62] I. Hornyák, A. Jedlovszky-Hajdú, and S. Kehr, "Biomaterial applications in soft tissue engineering and replacement," *Frontiers in Bioengineering and Biotechnology,* vol. 11, p. 1227021, 2023.

[63] L. Roseti, V. Parisi, M. Petretta, C. Cavallo, G. Desando, I. Bartolotti*, et al.*, "Scaffolds for bone tissue engineering: state of the art and new perspectives," *Materials Science and Engineering: C,* vol. 78, pp. 1246-1262, 2017.

[64] A. Sanchez-Rubio, V. Jayawarna, E. Maxwell, M. J. Dalby, and M. Salmeron-Sanchez, "Keeping It Organized: Multicompartment Constructs to Mimic Tissue Heterogeneity," *Advanced Healthcare Materials,* p. 2202110, 2023.

[65] G. Saini, N. Segaran, J. L. Mayer, A. Saini, H. Albadawi, and R. Oklu, "Applications of 3D bioprinting in tissue engineering and regenerative medicine," *Journal of clinical medicine,* vol. 10, p. 4966, 2021.

[66] M. Yonesi, M. Garcia-Nieto, G. V. Guinea, F. Panetsos, J. Perez-Rigueiro, and D. Gonzalez-Nieto, "Silk fibroin: An ancient material for repairing the injured nervous system," *Pharmaceutics,* vol. 13, p. 429, 2021.

[67] S. H. Moon, H. J. Hwang, H. R. Jeon, S. J. Park, I. S. Bae, and Y. J. Yang, "Photocrosslinkable natural polymers in tissue engineering," *Frontiers in Bioengineering and Biotechnology,* vol. 11, p. 1127757, 2023.

[68] X. Tang, S. K. Thankappan, P. Lee, S. E. Fard, M. D. Harmon, K. Tran*, et al.*, "Polymeric biomaterials in tissue engineering and regenerative medicine," *Natural and synthetic biomedical polymers,* pp. 351-371, 2014.

[69] E. Hartley, H. Moon, and A. Neves, "Biodegradable synthetic polymers for tissue engineering: a mini-review," *Reinvention: an International Journal of Undergraduate Research,* vol. 15, 2022.

[70] R. Kannan, G. Wei, and P. X. Ma, "Synthetic polymeric biomaterials for tissue engineering," in *Tissue Engineering Using Ceramics and Polymers*, ed: Elsevier, 2022, pp. 41-74.

[71] M. Arkas, M. Vardavoulias, G. Kythreoti, and D. Giannakoudakis, "Dendritic Polymers Applications in Tissue Engineering," 2022.

[72] J. Delaey, L. Parmentier, L. Pyl, J. Brancart, P. Adriaensens, A. Dobos*, et al.*, "Solid-State Crosslinkable, Shape-Memory Polyesters Serving Tissue Engineering," *Macromolecular Rapid Communications,* p. 2200955, 2023.

[73] E. M. Trifanova, M. A. Khvorostina, A. O. Mariyanats, A. V. Sochilina, M. E. Nikolaeva, E. V. Khaydukov*, et al.*, "Natural and Synthetic Polymer Scaffolds Comprising Upconversion Nanoparticles as a Bioimaging Platform for Tissue Engineering," *Molecules,* vol. 27, p. 6547, 2022.

[74] M. S. B. Reddy, D. Ponnamma, R. Choudhary, and K. K. Sadasivuni, "A comparative review of natural and synthetic biopolymer composite scaffolds," *Polymers,* vol. 13, p. 1105, 2021.

[75] R. Reddy and N. Reddy, "Biomimetic approaches for tissue engineering," *Journal of Biomaterials Science, Polymer Edition,* vol. 29, pp. 1667-1685, 2018.

[76] S. Pina, R. L. Reis, and J. M. Oliveira, "Natural polymeric biomaterials for tissue engineering," in *Tissue Engineering Using Ceramics and Polymers*, ed: Elsevier, 2022, pp. 75-110.

[77] S. Pramanik, S. Kharche, N. More, D. Ranglani, G. Singh, and G. Kapusetti, "Natural Biopolymers for Bone Tissue Engineering: A Brief Review," *Engineered Regeneration,* vol. 4, pp. 193-204, 2023.

[78] X. Li, M. Xu, Z. Geng, and Y. Liu, "Functional hydrogels for the repair and regeneration of tissue defects," *Frontiers in Bioengineering and Biotechnology,* vol. 11, p. 1190171, 2023.

[79] S. Mantha, S. Pillai, P. Khayambashi, A. Upadhyay, Y. Zhang, O. Tao*, et al.*, "Smart hydrogels in tissue engineering and regenerative medicine," *Materials,* vol. 12, p. 3323, 2019.

[80] A. Khademhosseini and R. Langer, "A decade of progress in tissue engineering," *Nature protocols,* vol. 11, pp. 1775-1781, 2016.

[81] T. P. Kraehenbuehl, P. Zammaretti, A. J. Van der Vlies, R. G. Schoenmakers, M. P. Lutolf, M. E. Jaconi*, et al.*, "Three-dimensional extracellular matrix-directed cardioprogenitor differentiation: systematic modulation of a synthetic cell-responsive PEG-hydrogel," *Biomaterials,* vol. 29, pp. 2757-2766, 2008.

[82] A. E. Pazarçeviren, A. Tezcaner, and Z. Evis, "Multifunctional natural polymer-based metallic implant surface modifications," *Biointerphases,* vol. 16, 2021.

[83] P. Bédard, S. Gauvin, K. Ferland, C. Caneparo, È. Pellerin, S. Chabaud*, et al.*, "Innovative human three-dimensional tissue-engineered models as an alternative to animal testing," *Bioengineering,* vol. 7, p. 115, 2020.

[84] M. C. Catoira, L. Fusaro, D. Di Francesco, M. Ramella, and F. Boccafoschi, "Overview of natural hydrogels for regenerative medicine applications," *Journal of Materials Science: Materials in Medicine,* vol. 30, pp. 1-10, 2019.

[85] D. Coppola, M. Oliviero, G. A. Vitale, C. Lauritano, I. D'Ambra, S. Iannace*, et al.*, "Marine collagen from alternative and sustainable sources: Extraction, processing and applications," *Marine drugs,* vol. 18, p. 214, 2020.

[86] I. Kutschka, I. Y. Chen, T. Kofidis, T. Arai, G. Von Degenfeld, A. Y. Sheikh*, et al.*, "Collagen matrices enhance survival of transplanted cardiomyoblasts and contribute to functional improvement of ischemic rat hearts," *Circulation,* vol. 114, pp. I-167-I-173, 2006.

[87] C. Stani, L. Vaccari, E. Mitri, and G. Birarda, "FTIR investigation of the secondary structure of type I collagen: New insight into the amide III band," *Spectrochimica Acta Part A: Molecular and Biomolecular Spectroscopy,* vol. 229, p. 118006, 2020.

[88] F. Copes, N. Pien, S. Van Vlierberghe, F. Boccafoschi, and D. Mantovani, "Collagen-based tissue engineering strategies for vascular medicine," *Frontiers in bioengineering and biotechnology,* vol. 7, p. 166, 2019.

[89] S. Feroz, N. Muhammad, J. Ratnayake, and G. Dias, "Keratin-Based materials for biomedical applications," *Bioactive materials,* vol. 5, pp. 496-509, 2020.

[90] C. R. Chilakamarry, S. Mahmood, S. N. B. M. Saffe, M. A. B. Arifin, A. Gupta, M. Y. Sikkandar*, et al.*, "Extraction and application of keratin from natural resources: a review," *3 Biotech,* vol. 11, pp. 1-12, 2021.

[91] F. Costa, R. Silva, and A. Boccaccini, "Fibrous protein-based biomaterials (silk, keratin, elastin, and resilin proteins) for tissue regeneration and repair," *Peptides and proteins as biomaterials for tissue regeneration and repair,* pp. 175-204, 2018.

[92] H. H. Bragulla and D. G. Homberger, "Structure and functions of keratin proteins in simple, stratified, keratinized and cornified epithelia," *Journal of anatomy,* vol. 214, pp. 516-559, 2009.

[93] J. Yu, D.-w. Yu, D. M. Checkla, I. M. Freedberg, and A. P. Bertolino, "Human hair keratins," *Journal of investigative dermatology,* vol. 101, pp. S56-S59, 1993.

[94] B. Srinivasan, R. Kumar, K. Shanmugam, U. T. Sivagnam, N. P. Reddy, and P. K. Sehgal, "Porous keratin scaffold–promising biomaterial for tissue engineering and drug delivery," *Journal of Biomedical Materials Research Part B: Applied Biomaterials: An Official Journal of The Society for Biomaterials, The Japanese Society for Biomaterials, and The Australian Society for Biomaterials and the Korean Society for Biomaterials,* vol. 92, pp. 5-12, 2010.

[95] J. G. Rouse and M. E. Van Dyke, "A review of keratin-based biomaterials for biomedical applications," *Materials,* vol. 3, pp. 999-1014, 2010.

[96] M. Rajabi, A. Ali, M. McConnell, and J. Cabral, "Keratinous materials: Structures and functions in biomedical applications," *Materials Science and Engineering: C,* vol. 110, p. 110612, 2020.

[97] S. Sadeghi, J. Nourmohammadi, A. Ghaee, and N. Soleimani, "Carboxymethyl cellulose-human hair keratin hydrogel with controlled clindamycin release as antibacterial wound dressing," *International journal of biological macromolecules,* vol. 147, pp. 1239-1247, 2020.

[98] A. Patrucco, L. Visai, L. Fassina, G. Magenes, and C. Tonin, "Keratin-based matrices from wool fibers and human hair," in *Materials for Biomedical Engineering*, ed: Elsevier, 2019, pp. 375-403.

[99] S. Jelodari, H. Daemi, P. Mohammadi, J. Verdi, M. J Al-Awady, J. Ai*, et al.*, "Assessment of the Efficacy of an LL-37-Encapsulated Keratin Hydrogel for the Treatment of Full-Thickness Wounds," *ACS Applied Bio Materials,* 2023.

[100] I. Mamaloudis, K. Perivoliotis, C. Zlatanos, I. Baloyiannis, M. Spyridakis, E. Kouvata*, et al.*, "The role of alginate dressings in wound healing and quality of life after pilonidal sinus resection: A randomised controlled trial," *International Wound Journal,* vol. 19, pp. 1528-1538, 2022.

[101] K. Y. Lee and D. J. Mooney, "Alginate: properties and biomedical applications," *Progress in polymer science,* vol. 37, pp. 106-126, 2012.

[102] M. G. Barbosa, V. F. Carvalho, and A. O. Paggiaro, "Hydrogel enriched with sodium alginate and vitamins A and E for diabetic foot ulcer: a randomized controlled trial," *Wounds: a Compendium of Clinical Research and Practice,* vol. 34, pp. 229-235, 2022.

[103] S. Reakasame and A. R. Boccaccini, "Oxidized alginate-based hydrogels for tissue engineering applications: a review," *Biomacromolecules,* vol. 19, pp. 3-21, 2018.

[104] X. Huang, X. Zhang, X. Wang, C. Wang, and B. Tang, "Microenvironment of alginate-based microcapsules for cell culture and tissue engineering," *Journal of bioscience and bioengineering,* vol. 114, pp. 1-8, 2012.

[105] D. R. Sahoo and T. Biswal, "Alginate and its application to tissue engineering," *SN Applied Sciences,* vol. 3, p. 30, 2021.

[106] X. Yan, Y.-R. Chen, Y.-F. Song, M. Yang, J. Ye, G. Zhou*, et al.*, "Scaffold-based gene therapeutics for osteochondral tissue engineering," *Frontiers in Pharmacology,* vol. 10, p. 1534, 2020.

[107] Y. Esmaeili, E. Bidram, A. Bigham, M. Atari, R. N. Azadani, M. Tavakoli*, et al.*, "Exploring the evolution of tissue engineering strategies over the past decade: From cell-based strategies to gene-activated matrix," *Alexandria Engineering Journal,* vol. 81, pp. 137-169, 2023.

[108] Y. Fang and R. M. Eglen, "Three-dimensional cell cultures in drug discovery and development," *Slas discovery: Advancing Life Sciences R&D,* vol. 22, pp. 456-472, 2017.

[109] Y. S. Zhang and A. Khademhosseini, "Advances in engineering hydrogels," *Science,* vol. 356, p. eaaf3627, 2017.

[110] C. Owen-Woods and A. Kusumbe, "Fundamentals of bone vasculature: Specialization, interactions and functions," in *Seminars in Cell & Developmental Biology*, 2022, pp. 36-47.

[111] C. G. Kallenberg, "Biology and immunopathogenesis of vasculitis," in *Rheumatology*, ed: Elsevier, 2015, pp. 1280-1289.

[112] D. Ribatti and F. Pezzella, "Sprouting and nonsprouting angiogenesis in tumors," in *Tumor Vascularization*, ed: Elsevier, 2020, pp. 1-13.

[113] M. Łazarczyk, M. E. Mickael, D. Skiba, E. Kurzejamska, M. Ławiński, J. O. Horbańczuk*, et al.*, "The journey of cancer cells to the brain: challenges and opportunities," *International Journal of Molecular Sciences,* vol. 24, p. 3854, 2023.

[114] T. H. Adair and J.-P. Montani, "Angiogenesis," 2011.

[115] D. Stepanova, H. M. Byrne, P. K. Maini, and T. Alarcón, "Computational modeling of angiogenesis: The importance of cell rearrangements during vascular growth," *WIREs Mechanisms of Disease,* p. e1634, 2023.

[116] X. Jiang, J. Wang, X. Deng, F. Xiong, S. Zhang, Z. Gong*, et al.*, "The role of microenvironment in tumor angiogenesis," *Journal of Experimental & Clinical Cancer Research,* vol. 39, pp. 1-19, 2020.

[117] T. Hashimoto and F. Shibasaki, "Hypoxia-inducible factor as an angiogenic master switch," *Frontiers in pediatrics,* vol. 3, p. 33, 2015.

[118] R. P. Basilio-de-Oliveira and V. L. N. Pannain, "Prognostic angiogenic markers (endoglin, VEGF, CD31) and tumor cell proliferation (Ki67) for gastrointestinal stromal tumors," *World journal of gastroenterology: WJG,* vol. 21, p. 6924, 2015.

[119] R. W. Carthew and E. J. Sontheimer, "Origins and mechanisms of miRNAs and siRNAs," *Cell,* vol. 136, pp. 642-655, 2009.

[120] M. Patrick and S. D. Ray, "Small interfering RNA “siRNA”," 2023.

[121] D. P. Anobile and E. Z. Poirier, "RNA interference, an emerging component of antiviral immunity in mammals," *Biochemical Society Transactions,* vol. 51, pp. 137-146, 2023.

[122] R. C. Wilson and J. A. Doudna, "Molecular mechanisms of RNA interference," *Annual review of biophysics,* vol. 42, pp. 217-239, 2013.

[123] A. M. Arenas, A. Andrades, J. R. Patiño-Mercau, J. Sanjuan-Hidalgo, M. Cuadros, D. J. García*, et al.*, "Opportunities of miRNAs in cancer therapeutics," in *MicroRNA in Human Malignancies*, ed: Elsevier, 2022, pp. 153-164.

[124] A. Chakrabortty, D. J. Patton, B. F. Smith, and P. Agarwal, "miRNAs: Potential as Biomarkers and Therapeutic Targets for Cancer," 2023.

[125] B. Guo, J. Liu, and D. W. Binzel, "MicroRNAs: Biology and Role in RNA Nanotechnology," in *RNA Nanotechnology and Therapeutics*, ed: CRC Press, 2022, pp. 507-516.

[126] J. Hu, S. Ni, Y. Cao, T. Zhang, T. Wu, X. Yin*, et al.*, "The angiogenic effect of microRNA-21 targeting TIMP3 through the regulation of MMP2 and MMP9," *PloS one,* vol. 11, p. e0149537, 2016.

[127] L. Becker Buscaglia and Y. Li, "Apoptosis and the target genes of miR-21," *Chin J Cancer,* vol. 30, pp. 371-80, 2011.

[128] L.-Z. Liu, C. Li, Q. Chen, Y. Jing, R. Carpenter, Y. Jiang*, et al.*, "MiR-21 induced angiogenesis through AKT and ERK activation and HIF-1α expression," *PloS one,* vol. 6, p. e19139, 2011.

[129] B. C. Melnik, "MiR-21: an environmental driver of malignant melanoma?," *Journal of translational medicine,* vol. 13, pp. 1-16, 2015.

[130] B. Bakhshandeh, N. Ranjbar, A. Abbasi, E. Amiri, A. Abedi, M. R. Mehrabi*, et al.*, "Recent progress in the manipulation of biochemical and biophysical cues for

engineering functional tissues," *Bioengineering & Translational Medicine,* vol. 8, p. e10383, 2023.

[131] D. Baek, K.-M. Lee, K. W. Park, J. W. Suh, S. M. Choi, K. H. Park*, et al.*, "Inhibition of miR-449a promotes cartilage regeneration and prevents progression of osteoarthritis in in vivo rat models," *Molecular Therapy-Nucleic Acids,* vol. 13, pp. 322-333, 2018.

[132] Y. Li, X. Chen, R. Jin, L. Chen, M. Dang, H. Cao*, et al.*, "Injectable hydrogel with MSNs/microRNA-21-5p delivery enables both immunomodification and enhanced angiogenesis for myocardial infarction therapy in pigs," *Science advances,* vol. 7, p. eabd6740, 2021.

[133] X. G. Ran and L. Y. Wang, "Use of ultrasonic and pepsin treatment in tandem for collagen extraction from meat industry by-products," *Journal of the Science of Food and Agriculture,* vol. 94, pp. 585-590, 2014.

[134] H. Ju, X. Liu, G. Zhang, D. Liu, and Y. Yang, "Comparison of the structural characteristics of native collagen fibrils derived from bovine tendons using two different methods: modified acid-solubilized and pepsin-aided extraction," *Materials,* vol. 13, p. 358, 2020.

[135] U. K. Laemmli, "Cleavage of structural proteins during the assembly of the head of bacteriophage T4," *nature,* vol. 227, pp. 680-685, 1970.

[136] J. Ye, G. Yang, J. Zhang, Z. Xiao, L. He, H. Zhang*, et al.*, "Preparation and characterization of gelatin-polysaccharide composite hydrogels for tissue engineering," *PeerJ,* vol. 9, p. e11022, 2021.

[137] B. Otieno, C. Krause, and J. Rusling, "Bioconjugation of antibodies and enzyme labels onto magnetic beads," in *Methods in enzymology*. vol. 571, ed: Elsevier, 2016, pp. 135-150.

[138] P. S. Kumar, G. Praveen, M. Raj, K. Chennazhi, and R. Jayakumar, "Flexible, micro-porous chitosan–gelatin hydrogel/nanofibrin composite bandages for treating burn wounds," *Rsc Advances,* vol. 4, pp. 65081-65087, 2014.

[139] T. L. Riss, R. A. Moravec, A. L. Niles, S. Duellman, H. A. Benink, T. J. Worzella*, et al.*, "Cell viability assays," *Assay Guidance Manual [Internet],* 2016.

[140] T. Kõressaar, M. Lepamets, L. Kaplinski, K. Raime, R. Andreson, and M. Remm, "Primer3_masker: integrating masking of template sequence with primer design software," *Bioinformatics,* vol. 34, pp. 1937-1938, 2018.

[141] J. Ko, L. T. Nguyen, A. Surendran, B. Y. Tan, K. W. Ng, and W. L. Leong, "Human hair keratin for biocompatible flexible and transient electronic devices," *ACS applied materials & interfaces,* vol. 9, pp. 43004-43012, 2017.

[142] A. Mukherjee, Y. H. Kabutare, and P. Ghosh, "Dual crosslinked keratin-alginate fibers formed via ionic complexation of amide networks with improved toughness for assembling into braids," *Polymer Testing,* vol. 81, p. 106286, 2020.

[143] P. Ramadoss, R. Rangarajan, and K. Pavani, "Investigation of royal jelly as a promising substitute to fetal bovine serum in cell culture," *Annals of Biological Research,* vol. 6, pp. 60-64, 2015.

[144] P. Sihota, R. N. Yadav, V. Dhiman, S. K. Bhadada, V. Mehandia, and N. Kumar, "Investigation of diabetic patient's fingernail quality to monitor type 2 diabetes induced tissue damage," *Scientific reports,* vol. 9, p. 3193, 2019.

[145] E. M. YELKUVAN, Ö. ERDEMLİ, B. YILMAZ, and Ö. AKTÜRK, "Evaluation of photochemically cross-linked collagen/gold nanoparticle composites as potential skin tissue scaffolds," *Turkish Journal of Chemistry,* vol. 47, pp. 101-115, 2023.

[146] K. H. Sizeland, K. A. Hofman, I. C. Hallett, D. E. Martin, J. Potgieter, N. M. Kirby*, et al.*, "Nanostructure of electrospun collagen: Do electrospun collagen fibers form native structures?," *Materialia,* vol. 3, pp. 90-96, 2018.

[147] P. Hartrianti, L. Ling, L. M. M. Goh, K. S. A. Ow, R. M. Samsonraj, W. T. Sow*, et al.*, "Modulating mesenchymal stem cell behavior using human hair keratin-coated surfaces," *Stem Cells International,* vol. 2015, 2015.

[148] S. Wang, F. Taraballi, L. P. Tan, and K. W. Ng, "Human keratin hydrogels support fibroblast attachment and proliferation in vitro," *Cell and Tissue Research,* vol. 347, pp. 795-802, 2012.

[149] L. Langbein, M. A. Rogers, H. Winter, S. Praetzel, and J. Schweizer, "The catalog of human hair keratins: II. Expression of the six type II members in the hair follicle and the combined catalog of human type I and II keratins," *Journal of Biological Chemistry,* vol. 276, pp. 35123-35132, 2001.

[150] Y.-C. Huang, T.-W. Wang, J.-S. Sun, and F.-H. Lin, "Epidermal morphogenesis in an in-vitro model using a fibroblasts-embedded collagen scaffold," *Journal of Biomedical Science,* vol. 12, pp. 855-867, 2005.

[151] Q.-Q. Wang, Y. Liu, C.-J. Zhang, C. Zhang, and P. Zhu, "Alginate/gelatin blended hydrogel fibers cross-linked by Ca2+ and oxidized starch: Preparation and properties," *Materials Science and Engineering: C,* vol. 99, pp. 1469-1476, 2019.

[152] C. G. Knight, L. F. Morton, A. R. Peachey, D. S. Tuckwell, R. W. Farndale, and M. J. Barnes, "The Collagen-binding A-domains of Integrins α1β1 and α2β1recognize the same specific amino acid sequence, GFOGER, in native (Triple-helical) collagens," *Journal of Biological Chemistry,* vol. 275, pp. 35-40, 2000.

[153] H. Cao, L. Duan, Y. Zhang, J. Cao, and K. Zhang, "Current hydrogel advances in physicochemical and biological response-driven biomedical application diversity," *Signal transduction and targeted therapy,* vol. 6, p. 426, 2021.

[154] M. Dadsetan, T. E. Hefferan, J. P. Szatkowski, P. K. Mishra, S. I. Macura, L. Lu*, et al.*, "Effect of hydrogel porosity on marrow stromal cell phenotypic expression," *Biomaterials,* vol. 29, pp. 2193-2202, 2008.

[155] S. S. Karim, S. Farrukh, A. Hussain, M. Younas, and T. Noor, "The influence of polymer concentration on the morphology and mechanical properties of asymmetric polyvinyl alcohol (PVA) membrane for O2/N2 separation," *Polymers and Polymer Composites,* vol. 30, p. 09673911221090053, 2022.

[156] H. Chavda and C. Patel, "Effect of crosslinker concentration on characteristics of superporous hydrogel," *International journal of pharmaceutical investigation,* vol. 1, p. 17, 2011.

[157] R. Foudazi, R. Zowada, I. Manas-Zloczower, and D. L. Feke, "Porous Hydrogels: Present Challenges and Future Opportunities," *Langmuir,* vol. 39, pp. 2092-2111, 2023.

[158] S. Riedel, P. Hietschold, C. Krömmelbein, T. Kunschmann, R. Konieczny, W. Knolle*, et al.*, "Design of biomimetic collagen matrices by reagent-free electron beam induced crosslinking: Structure-property relationships and cellular response," *Materials & Design,* vol. 168, p. 107606, 2019.

[159] L. Salvatore, E. Calò, V. Bonfrate, D. Pedone, N. Gallo, M. L. Natali*, et al.*, "Exploring the effects of the crosslink density on the physicochemical properties of collagen-based scaffolds," *Polymer Testing,* vol. 93, p. 106966, 2021.

[160] J. M. Patel, R. C. Jackson, G. L. Schneider, S. A. Ghodbane, and M. G. Dunn, "Carbodiimide cross-linking counteracts the detrimental effects of gamma irradiation on the physical properties of collagen-hyaluronan sponges," *Journal of Materials Science: Materials in Medicine,* vol. 29, pp. 1-8, 2018.

[161] R. Sharif, J. Hjortdal, H. Sejersen, G. Frank, and D. Karamichos, "Human in vitro model reveals the effects of collagen cross-linking on keratoconus pathogenesis," *Scientific reports,* vol. 7, p. 12517, 2017.

[162] L. Abune and Y. Wang, "Affinity hydrogels for protein delivery," *Trends in pharmacological sciences,* vol. 42, pp. 300-312, 2021.

[163] J. Sajeev and R. Love, "Effect of Keratin Preparations on Cementoblast OCCM-30 and Fibroblast L929 Cells," *Austin J Biotechnol Bioeng,* vol. 7, p. 1105, 2020.

[164] A. Akinc, M. Thomas, A. M. Klibanov, and R. Langer, "Exploring polyethylenimine-mediated DNA transfection and the proton sponge hypothesis," *The Journal of Gene Medicine: A cross-disciplinary journal for research on the science of gene transfer and its clinical applications,* vol. 7, pp. 657-663, 2005.

[165] F. Besenbacher, K. A. Howard, J. Kjems, and X. Liu, "Nanoparticles for nucleic acid delivery," ed: Google Patents, 2010.

[166] S. Poudel, P. R. Napit, K. P. Briski, and G. Mattheolabakis, "Oral delivery of nucleic acids with passive and active targeting to the intestinal tissue using polymer-based nanocarriers," *Pharmaceutics,* vol. 13, p. 1075, 2021.

[167] J. Ma, H. Sawai, N. Ochi, Y. Matsuo, D. Xu, A. Yasuda*, et al.*, "PTEN regulate angiogenesis through PI3K/Akt/VEGF signaling pathway in human pancreatic cancer cells," *Molecular and cellular biochemistry,* vol. 331, pp. 161-171, 2009.

[168] F. Meng, R. Henson, H. Wehbe–Janek, K. Ghoshal, S. T. Jacob, and T. Patel, "MicroRNA-21 regulates expression of the PTEN tumor suppressor gene in human hepatocellular cancer," *Gastroenterology,* vol. 133, pp. 647-658, 2007.

[169] D. Sayed, S. Rane, J. Lypowy, M. He, I.-Y. Chen, H. Vashistha*, et al.*, "MicroRNA-21 targets Sprouty2 and promotes cellular outgrowths," *Molecular biology of the cell,* vol. 19, pp. 3272-3282, 2008.

[170] W. Godbey, K. K. Wu, and A. G. Mikos, "Poly (ethylenimine) and its role in gene delivery," *Journal of controlled release,* vol. 60, pp. 149-160, 1999.

[171] T. Merdan, J. Kopeček, and T. Kissel, "Prospects for cationic polymers in gene and oligonucleotide therapy against cancer," *Advanced drug delivery reviews,* vol. 54, pp. 715-758, 2002.

[172] Z. Dai, T. Gjetting, M. A. Mattebjerg, C. Wu, and T. L. Andresen, "Elucidating the interplay between DNA-condensing and free polycations in gene transfection through a mechanistic study of linear and branched PEI," *Biomaterials,* vol. 32, pp. 8626-8634, 2011.

[173] A. E. Altyar, A. El-Sayed, A. Abdeen, M. Piscopo, S. A. Mousa, A. Najda*, et al.*, "Future regenerative medicine developments and their therapeutic applications," *Biomedicine & Pharmacotherapy,* vol. 158, p. 114131, 2023.

[174] A. Acun and P. Zorlutuna, "CRISPR/Cas9 edited induced pluripotent stem cell-based vascular tissues to model aging and disease-dependent impairment," *Tissue Engineering Part A,* vol. 25, pp. 759-772, 2019.

[175] K. Elkhoury, M. Morsink, L. Sanchez-Gonzalez, C. Kahn, A. Tamayol, and E. Arab-Tehrany, "Biofabrication of natural hydrogels for cardiac, neural, and bone Tissue engineering Applications," *Bioactive materials,* vol. 6, pp. 3904-3923, 2021.

[176] M. V. Giraudo, D. Di Francesco, M. C. Catoira, D. Cotella, L. Fusaro, and F. Boccafoschi, "Angiogenic potential in biological hydrogels," *Biomedicines,* vol. 8, p. 436, 2020.

[177] X. Du, L. Hong, L. Sun, H. Sang, A. Qian, W. Li*, et al.*, "miR-21 induces endothelial progenitor cells proliferation and angiogenesis via targeting FASLG and is a potential prognostic marker in deep venous thrombosis," *Journal of translational medicine,* vol. 17, pp. 1-13, 2019.

[178] O. Oliviero, M. Ventre, and P. A. Netti, "Functional porous hydrogels to study angiogenesis under the effect of controlled release of vascular endothelial growth factor," *Acta biomaterialia,* vol. 8, pp. 3294-3301, 2012.

[179] C. Kuehlbach, S. Hensler, and M. M. Mueller, "Recapitulating the angiogenic switch in a hydrogel-based 3D in vitro tumor-stroma model," *Bioengineering,* vol. 8, p. 186, 2021.

APPENDICES

A. SDS-PAGE BUFFERS AND SOLUTIONS

10 mL Stock 30% Acrylamide:

3 g Acrylamide in 10 mL dH_2O

10 mL Stock 1% Bisacrylamide:

0,1 g Bisacrylamide in 10 mL dH_2O

5 mL Stock 20% SDS:

1 g SDS in 5 mL dH_2O

1.5 M Tris, pH 8.7 – 8.8:

18.15 g Tris-base in 80 mL dH_2O

pH to 8.7 – 8.8 by using 6N HCL

Final volume to 100 mL

0.5 M Tris, pH 6.7 – 6.8:

6 g Tris-base in 80 mL dH_2O

pH to 6.7 – 6.8 by using 6N HCL

Final volume to 100 mL

500 uL, 10% APS:

50 mg APS in 500 uL dH_2O

Laemmli Sample Loading Buffer (4x), (50 mL):

1.514 g Tris-base in 10 mL dH_2O (0.125 M Tris, pH 6.8)

pH to 6.8 by using 6N HCL

20 mL Glycerol (20%)

4 g SDS (4%)

200 mg Bromophenol blue (0.004%)

10 mL 2-mercaptoethanol (10%)

* Storage in -20ºC in aliquots.

*Avoid direct light.

*Dilution ratio is 1:3 (Laemmli:Sample)

*Working volume is 20 uL

10X Running Buffer (500 mL) pH 8.3:

15.1 g Tris-base

72.1 g Glycine

10 g SDS (2%)

In 500 mL dH_2O

*Dilution to 1X as fresh before running.

*70 mL 10X Stock + 630 mL dH_2O

*Working volume is 700 mL

Gel Staining Solution:

0.25 g Coomassie Bright Blue R250 in 125 mL iso-propanol

325 mL dH_2O

50 mL Glacial Acetic Acid

*Incubation for 30 min – 1 hour for gel staining

Fixing & De-Staining Solution (300 mL):

10% Iso-propanol

5% Acetic Acid

*30 mL iso-propanol in 255 mL dH_2O, and 15 mL Acetic Acid

*Alternative de-staining is microwaving for 30 secs in dH_2O

B. PLASMID ISOLATION BUFFERS AND SOLUTIONS

Solution I - Resuspension Buffer:

25 mM Tris-HCl (pH 8.0)

50 mM Glucose

10 mM EDTA

*Storage at 4°C

Solution II - Denaturing Solution:

0.2 N NaOH

1.0% SDS

*Storage at room temperature

Solution III - Renaturing Solution (Potassium Acetate):

120 mL 5M Potassium acetate

23 mL glacial acetic acid

57 mL of dH_2O

*Storage at 4°C

C. CALIBRATION CURVE OF THE BCA ASSAY

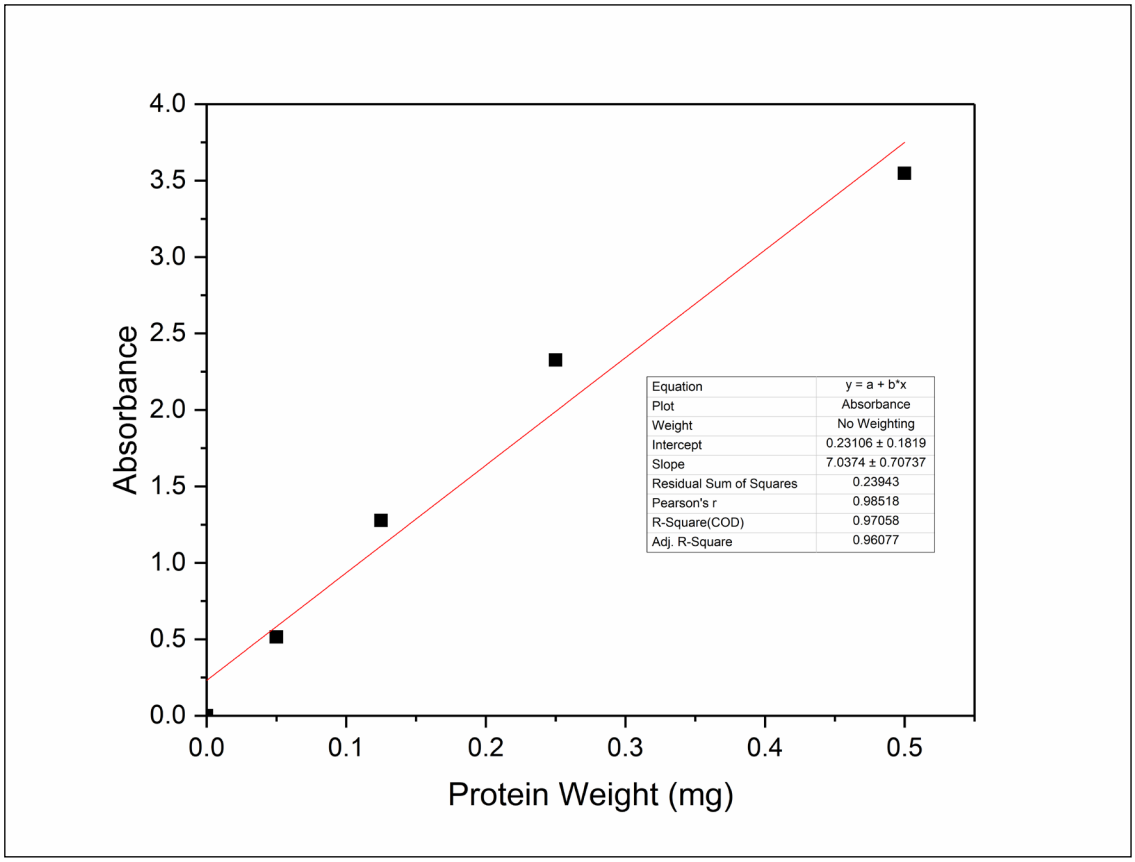

$$y = 7.04x + 0.23 \quad (1)$$